Priscila da Costa Gonçalves

DRY SLIDING BEHAVIOR OF FILLED PDC COATINGS APPLIED ONTO SURFACE MODIFIED SINTERED STEEL

Dissertação submetida ao Programa de Pós-Graduação em Ciência e Engenharia de Materiais da Universidade Federal de Santa Catarina para obtenção do grau de Mestre em Ciência e Engenharia de Materiais.
Orientador: Prof. Aloisio Nelmo Klein, Dr. Ing.
Coorientador: Prof. José Daniel Biasoli de Mello, Doc. Ing.

Florianópolis

2016

Ficha de identificação da obra elaborada pelo autor através do Programa de Geração Automática da Biblioteca Universitária da UFSC.

Gonçalves, Priscila da Costa
Dry sliding behavior of filled PDC coatings applied onto surface modified sintered steel / Priscila da Costa Gonçalves ; orientador, Aloisio Nelmo Klein ; coorientador, José Daniel Biasoli de Mello. - Florianópolis, SC, 2016.
118 p.

Dissertação (mestrado) - Universidade Federal de Santa Catarina, Centro Tecnológico. Programa de Pós-Graduação em Ciência e Engenharia de Materiais.

Inclui referências

1. Ciência e Engenharia de Materiais. 2. Precursores poliorganosilazanos. 3. Revestimentos PDC. 4. Modificações de superfície assistidas por plasma. 5. Compósitos tribológicos. I. Klein, Aloisio Nelmo. II. Biasoli de Mello, José Daniel. III. Universidade Federal de Santa Catarina. Programa de Pós-Graduação em Ciência e Engenharia de Materiais. IV. Título.

DRY SLIDING BEHAVIOR OF FILLED PDC COATINGS APPLIED ONTO SURFACE MODIFIED SINTERED STEEL

Esta Dissertação foi julgada adequada para obtenção do Título de "Mestre em Ciência e Engenharia de Materiais" e aprovada em sua forma final pelo Programa de Pós-Graduação em Ciência e Engenharia de Materiais.

Florianópolis, 17 de novembro de 2016.

_____

Prof. Dr. Guilherme Mariz de Oliveira Barra
Coordenador do Programa de Pós-Graduação

_____ _____

Prof. Dr. Ing. Aloisio Nelmo Klein
Orientador

Prof. Doc. Ing. José Daniel Biasoli de Mello - Coorientador

Banca Examinadora:

_____ _____

Prof. Dr. Eng. Henrique Cezar Pavanati Instituto Federal de Santa Catarina *IFSC*

Prof. Dr. Eng. João Batista Rodrigues Neto
UFSC

_____

Prof. Dr. Eng. Washington Martins da Silva Jr.
Universidade Federal de Uberlândia - UFU

For all ethical people around the world, who strive intellectually and collectively to build a better life in society.

ACKNOWLEDGEMENTS

Ao povo brasileiro, que por meio de impostos financiou a realização deste trabalho, através das agências de fomento CAPES e BNDES;

Aos professores do programa de pós-graduação pelo compartilhamento de tantos conhecimentos, além dos inúmeros questionamentos que tantas vezes me levaram a refletir sobre a ciência e a vida;

Aos orientadores, Professor Aloisio e Professor Daniel pelas orientações científicas, mas principalmente pelas valorosas contribuições para o desenvolvimento de meu pensamento crítico;

Aos professores da banca avaliadora, pelo aceite e pela dedicação demonstrada com as contribuições de diferentes áreas do conhecimento com o desenvolvimento deste;

Aos servidores das universidades no Brasil e na Alemanha pela prestatividade no atendimento das inúmeras solicitações durante a realização do mestrado sanduíche;

À equipe Bragecrim em ambos países pela experiência única proporcionada, ao Dr. rer. nat Günter Motz pela oportunidade de estágio em seu grupo de pesquisa na UBT, e ao Dr. Martin Seifert pelas contribuições;

Aos colegas de laboratório no LabMat e no IMA pelos aprendizados diários, tão importantes em meu desenvolvimento;

Às queridas Patrícia, Deise e Tatiana, sempre tão dispostas a esclarecer as minhas “quase sem fim” dúvidas relacionada a caracterização de materiais;

À querida amiga Kaline, por causa da paixão pela ciência em comum, pela didática, por incontáveis arquivos/modelos/artigos/procedimentos compartilhados, trocas de ideias acaloradas. Mas principalmente pela confiança depositada desde sempre nos projetos em parceria;

Aos colegas pesquisadores “sem medo de pensar fora das caixas” Davut, Rafaela, Nicolás e Thiago por compartilharem seus questionamentos, suas análises críticas e suas soluções criativas neste período;

Ao Daniel e à Alessandra pela grande ajuda com a produção das amostras antes da viagem para a Alemanha;

Aos amigos, minha família de coração, por acreditarem tanto em mim e pelo apoio de sempre;

Ao meu grande amor por compartilhar uma visão de mundo tão única, obrigada pela compreensão e pelo companheirismo, afinal de contas só “eu que sei”;

Á minha família, por ter feito tudo da maneira como o fez, o que me permitiu chegar até aqui. Obrigada pelo amor incondicional;

A todos que colaboraram direta ou indiretamente para a realização deste trabalho.

Obrigada! Vielen Dank! Gracias!

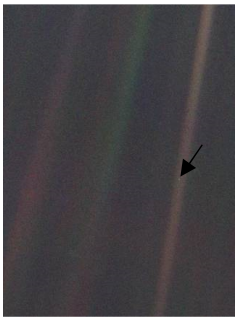

Source: NASA/JPL-Caltech

"There is perhaps no better demonstration of the folly of human conceits than this distant image of our tiny world. To me, it underscores our responsibility to deal more kindly with one another, and to preserve and cherish the pale blue dot, the only home we've ever known."
Carl Sagan, Pale Blue Dot: A Vision of the Human Future in Space.

RESUMO

A transformação direta de polímeros precursores em cerâmicas covalentes, via termólise no estado sólido, foi proposta há mais de 30 anos e desde então permitiu avanços tecnológicos significativos na ciência e tecnologia cerâmica. Entre eles, a redução do coeficiente de atrito (μ) de substratos metálicos e cerâmicos com o uso de revestimentos amorfos de carbonitreto de silício (SiCN), produzidos por meio de cerâmicas derivadas de polímeros (PDC). Porém, através de rotas de processamento tecnologicamente sofisticadas, enquanto neste trabalho a viabilidade de processamento desses revestimentos sobre um aço baixa liga sinterizado, por pulverização de suspensões e pirólise em forno, foi explorada. Para compensar a retração do polímero precursor, evitar a formação de trincas e produzir revestimentos auto-lubrificantes para avaliações tribológicas de deslizamento alternado a seco, cargas inertes foram adicionadas a solução do poli(organo)silazano, especificamente nitreto de silício (Si_3N_4, 30 ou 65% em volume) e nitreto de boro hexagonal (h-BN, 9% em volume). O Si_3N_4 em pó foi utilizado para reforçar a matriz (SiCN) e reduzir o desgaste, pela formação de uma rede agregada pela fase do ligante precursor e, h-BN para gerar um efeito lubrificante na interface reduzindo o atrito, o desgaste e o aquecimento por atrito. A fim de acomodar as diferenças de propriedades, originadas pela natureza das ligações químicas do substrato metálico e revestimento cerâmico, a tecnologia de plasma de corrente contínua (DC) foi utilizada para modificar as superfícies do aço sinterizado. A nitretação ou o enriquecimento de superfície com Mo seguido de nitretação, tinham o intuito de gerar uma camada de compostos na superfície do substrato com uma zona de difusão gradiente abaixo, de modo a aumentar o suporte de carga e evitar a fratura do revestimento pelo carregamento do contra corpo. A nitretação resultou em um aumento na dureza da superfície (600HV) do aço por precipitação de nitretos de ferro metaestáveis, enquanto o enriquecimento com Mo resultou em carbetos (Fe_3Mo_3C) dispersos na superfície do substrato. Os últimos, durante a nitretação evoluem para uma camada descontínua de carbonitreto ($Fe_3Mo_3(C,N)$), que contribuíram para o aumento da dureza na superfície (800HV). Foi possível produzir revestimentos PDC em amostras sinterizadas com espessura de até 10μm e com adequado preenchimento dos poros na superfície, independente dos teores de carga avaliada (39 ou 74 vol.%). Além disso, a combinação de 65% em volume de Si_3N_4 e 9% em volume de h-BN resultou em revestimentos cerâmicos homogêneos, sem macro trincas ou falhas coesivas após o processamento sobre o aço sinterizado,

independente das modificações de superfície. Conforme projetado para o estudo, após o tratamento térmico de pirólise os precipitados $Fe_3Mo_3(C,N)$ não foram totalmente decompostos como os nitretos de ferro, apesar da ausência do endurecimento de superfície. O controle da microestrutura e composição química finais são vantagens inerentes aos processos de manufatura utilizados e foram explorados para projetar a microestrutura final dos compósitos. Porém, apesar da utilização de um teor aumentado de cargas passivas ter possibilitado a obtenção de revestimentos cerâmicos sem trincas sobre substratos sinterizados, os compósitos não apresentaram uma resposta tribológica satisfatória, quando avaliados nas condições testadas. No regime permanente, o coeficiente de atrito médio (0,4 a 0,5) dos compósitos permaneceu acima do regime de lubricidade ($\mu<0,2$), independente da composição do revestimento ou modificação de superfície. A pressão máxima de contato (0,53GPa) causou a falha dos revestimentos, que foram sequencialmente deformados, cominuídos e oxidados pelo substrato e contra corpo durante o deslizamento, revelando um desgaste de caráter tribo-químico. A principal contribuição para o comportamento do coeficiente de atrito foi do substrato, mas controlado pela tribocamada formada, composta de oxigênio e elementos químicos do substrato, revestimentos e contra corpo. A presença dessa tribocamada, indiretamente indicada pela resistência elétrica de contato, aumentou a taxa de desgaste dos compósitos (1,5 a $4,2x10^{-4}.mm^3.N^{-1}.m^{-1}$) e contra corpos (7,0 a $8,7x10^{-5}.mm^3.N^{-1}.m^{-1}$) em relação ao aço sinterizado e sem revestimento (1 e $0,1x10^{-4}.mm^3.N^{-1}.m^{-1}$ respectivamente) ensaiado nas mesmas condições. As taxas de desgaste dos compósitos foram ainda aumentadas com o aumento do teor de Si_3N_4 na composição do revestimento e com a presença de carbonitretos ternários e duros na superfície do substrato.

Palavras chave: precursores poliorganosilazanos, revestimento PDC, modificações de superfície assistidas por plasma, compósitos tribológicos

ABSTRACT

The directly transformation of organosilicon polymers into covalent ceramics, via solid-state thermolysis, was proposed over 30 years ago, and since then enabled significant technological breakthroughs in ceramic science and technology. Among them, the friction coefficient (μ) reduction of metallic and ceramic substrates with use of amorphous silicon carbonitride (SiCN) coatings, produced by the polymer derived ceramic route (PDC). Nevertheless, technologically sophisticated processing steps are used to produce them, while in this work, the possibility to process such coatings onto sintered low alloy steel samples by simple spraying of poly(organo)silazane suspensions and oven pyrolysis was explored. In order to compensate the precursor shrinkage, avoid crack formation and produce hard and self-lubricating coatings for reciprocating dry sliding evaluations, inert fillers namely silicon nitride (30 or 65 vol.%) and hexagonal-boron nitride (9 vol.%) were added to the polymer precursor. Powdered Si_3N_4 was used to strengthen the matrix and reduce wear, by formation of a network aggregated by the precursor binder phase, and h-BN to generate a lubricating effect on the interface reducing friction, wear and friction heating. To accommodate dissimilarities of properties, originated from different chemical bonds of the metallic substrate and ceramic coating, the direct current (DC) plasma technology was utilized to modify the surface of the sintered steel. Nitriding or surface enrichment with Mo followed by nitriding was expected to generate a compound layer at the surface of the substrate with a gradient diffusion region below, in order to increase the load support and avoid coating fracture from the counterface load. Nitriding led to an increase in surface hardness of steel (600HV) due to precipitation of metastable iron nitrides, while surface enrichment resulted in dispersed carbides (Fe_3Mo_3C) onto the substrate surface. The latter evolved to a discontinuous carbonitride layer ($Fe_3Mo_3(C,N)$) during nitriding, which increased the surface hardness (800HV). It was possible to produce PDC coatings with thickness below 10μm and with proper filling into substrate surface pores, regardless of total filler amount evaluated (39 or 74 vol.%). Moreover, the combination of 65 vol.% of Si_3N_4 and 9vol% of h-BN resulted in homogeneous ceramic coatings, free of macro cracks and cohesive failure after processing onto sintered substrates, independent of surface modification. As desired for evaluating, after pyrolysis the $Fe_3Mo_3(C,N)$ precipitates were not totally decomposed as the iron nitrides, despite the surface hardening absence. The high control of final microstructure and chemical composition are competitive advantages

inherent to cited manufacturing processes, explored to project the final microstructures of the steel, interfaces and ceramic coatings involved. However; despite the use of an increased amount of filler (74 vol.%) allowed the successful obtainment of homogeneous and crack-free ceramic coatings, the composites did not presented a satisfactory tribological response when evaluated under tested conditions. The average steady state friction coefficient of composites (0.4 to 0.5) were above the lubricious regime (μ<0.2), regardless of coating composition or surface modification. The maximum contact pressure (0.53GPa) caused failure of coatings, which were in sequence deformed, comminuted and oxidized by substrate and counter-body during sliding, revealing a tribo-chemical wear character. The major contribution to the friction coefficient behavior was from the substrate but controlled by the formed third-body, composed of oxygen and chemical elements from substrate, coatings and counter-body. The third-body presence, indirectly indicated by the contact electrical resistance, increased the wear rates of composites (1.5 to $4.2x10^{-4}.mm^3.N^{-1}.m^{-1}$) and counter-bodies (7.0 to $8.7x10^{-5}.mm^3.N^{-1}.m^{-1}$) in relation to the sintered steel tested under same conditions (1 and $0.1x10^{-4}.mm^3.N^{-1}.m^{-1}$ respectively). The wear rates of composites were further increased with the raise of Si_3N_4 amount in the coating composition, and with the presence of hard ternary carbonitrides at the substrate surface.

Keywords: polyorganosilazanes precursors, PDC coatings, plasma assisted surface modifications, tribological composites

FIGURES

TABLES

ABBREVIATIONS, ACRONYMS AND SYMBOLS

ABSE – bis(dichloromehyl)silylethane

Al_2O_3 – Aluminum oxide or alumina

Bragecrim – Brazilian-German collaborative initiative in advanced manufacturing

BET – **B**runauer, **E**mmett e **T**eller – Specific surface area analysis through determination of gas volume physically adsorbed in the sample surface

BSE – Backscattered electrons

CAPES – Coordenação de Aperfeiçoamento de Pessoal de Nível Superior

c-BN – Cubic boron nitride

CME – Ceramic Material Engineering Department

CTE – Coefficient of thermal expansion

CV – Chemical vapor deposition

cv – Coefficient of variation

DC – Direct current

DCP – Dicumyl peroxide

DFG – Deutsche Forschungsgemeinschaft

EDX – Energy dispersive X-ray spectroscopy

EDX – Energy dispersive X-ray spectrometer

F_N – Normal force

F – Friction force

HB – Brinell hardness

h-BN – Hexagonal boron nitride

HIP – Hot isostatic pressing

HRTEM – High-resolution transmission electron microscopy

HV – Vickers hardness

IBAD – Ion beam-assisted deposition

K_{1C} – Plain strain fracture toughness

kV – 10^3 electron Volt

L – Total sliding distance

LabMat – Interdisciplinary Materials Laboratory

m – meter

Me-Al_2O_4 - Spinel metal aluminate

MEMS – Microelectromechanical systems

MoS_2 – Molybdenum bisulfide

OM – Optical microscope

PCSZ – Poly(carbo)silazane

PDC – Polymer-derived ceramic

PECVD – Plasma-enhanced chemical vapor deposition
PHPS – (Perhydro)polysilazane
PMMA – Poly(methyl)methacrylate
PSZ – Polysilazane
PTFE – Polytetrafluorethylene
PUMVS – Poly(ureamethylvinyl)silazane
PVD – Physical vapor deposition
RH – Relative humidity
Rq – Root mean squared parameter of roughness
S – Sintered interface
SN – Nitrided interface
SEN – Enriched with molybdenum and nitrided interface
SE – Secondary electrons
SEM – Scanning electron microscopy
SEM – Scanning electron microscope
SEM-FEG – Field emission gun scanning electron microscope
SiC – Silicon carbide
Si_3N_4 – Silicon nitride
TGA – Thermogravimetric analysis
UBT – University of Bayreuth
UFSC – Federal University of Santa Catarina
UV – Ultraviolet
YSZ – Yttria-stabilized zirconia
W – Applied normal load
WD – Working distance
ZrO_2 – Zirconia

α – Ferrite crystalline phase
ε-$Fe_{(2-3)}N$ – Hexagonal iron nitride
γ – Austenite crystalline phase
γ´-Fe_4N – Cubic iron nitride
μ - Friction coefficient
ΔV – Volume loss of tested specimen
ΔT –Temperature rise

CONTENTS

1. INTRODUCTION

Friction is a dissipative phenomenon and one of the most significant source of irreversibility in thermodynamic processes. It is not a material property, as commonly thought, but a system response with important practical consequences in daily life and industrial applications. Friction allow several and fundamental activities as walking, writing, picking objects, using automobile tires on a roadway, the manufacturing process of machine components, among others in which resistance to motion is desired.

However, as a source of irreversibility, friction in combination with wear are responsible for energy and material losses estimated to cost up to 7% of gross national product in the most industrialized nations (ERDEMIR; MARTIN, 2007). In addition to the energy wasted, heat generated by friction affects negatively the performance of mechanical systems and is responsible by hazardous emissions to our environment (HOLMBERG; ANDERSSON; ERDEMIR, 2012). Many achievements were already reached in the development of components less susceptible to friction and wear, but still optimized energetic efficiency is pursued by scientific and industrial communities (BHUSHAN, 2000).

In a recent review, concerning the last forty years of Polymer Derived Ceramics (PDCs) developments, a few scientific issues were highlighted for advanced PDCs research, and, among them the discussion and presentation of possible real-life application of special characteristics of such materials (COLOMBO et al., 2010). Aimed to join in a synergic way existing knowledge and infrastructure of the Ceramic Material Engineering group (CME) from the Bayreuth University (UBT), and the Interdisciplinary Materials Laboratory team (LabMat) located at UFSC, the research groups became partners within a Brazilian-German collaborative initiative in manufacturing, called Bragecrim[1]. Within this framework, the research groups initiated in 2013 a project entitled *Development of wear resistant and dry self-lubricating coatings on sintered steels from polymer-derived ceramics*.

It is possible to conclude from literature that polymer derived ceramic coatings, namely SiCN films from poly(organo)silazanes, can serve to improve tribological properties of metallic and ceramic substrates. Nevertheless, high technological processing routes, which include steps of UV exposure, hot isostatic crosslinking and pyrolysis, surface finishing, among others were developed to produce them. The

[1] More information in Appendix

primary interest in this work was the investigation of processing such films on sintered low alloy steel samples, for dry sliding evaluations, by simple spraying and oven pyrolysis.

To compensate polymer shrinkage and avoid crack formation the use of inert fillers, added to the precursor (HTTS) synthetized from a commercial liquid precursor (Durazane 1800, Merck), was an interesting alternative, since a suitable combination could provide tailored tribological properties for coatings during application (GREIL, 2012). Aiming to produce hard and self-lubricating coatings, based on previously developed composites (BARROSO et al., 2016; CARRAPICHANO; GOMES; SILVA, 2002; CHEN et al., 2010), silicon nitride was used to strengthen the matrix (GREIL, 2000, 2003) and reduce wear, by formation of a network aggregated by the precursor binder phase. While hexagonal boron nitride, due to layered structure and low shear strength, added to generate a lubricating effect on the interface reducing friction, wear and friction heating (ERDEMIR, 2000).

The high performance and low environmental impact of direct current (DC) plasma technology, specifically when applied to powder metallurgy (PM) parts (KLEIN et al., 2013), became suitable for generating interfaces by surface modifications. Namely, surface enrichment and nitriding, capable of accommodating dissimilarities between metallic substrate and ceramic coatings. Additional reductions in wear and friction of the composite were expected due to surface hardness enhance of the sintered steel, which due to increased load support, avoid fracture of the brittle coating from the counterface load (HOLMBERG; MATTHEWS; RONKAINEN, 1998).

Given the context, this work present the outcomes of an exploratory development of graded composites, produced in sequence through powder metallurgy, plasma surface modifications and polymer derived ceramics, tailored for dry-sliding tribological applications. The high control of final microstructure and chemical composition are competitive advantages inherent to cited manufacturing processes and were used to compare the tribological response of different interfaces (sintered, nitrided and enriched with Mo and nitrided surface) between steel and coating, and two coating composition (with 39 and 74 vol.% of passive fillers) of graded composites.

2. LITERATURE BACKGROUND

2.1. WHAT ARE POLYMER-DERIVED CERAMICS (PDCs)?

Silicon-based PDCs are advanced ceramic materials, in which the transformation of molecular precursor into ceramic occurs via solid-state thermolysis (RIEDEL et al., 2006). The directly transformation of polymers into covalent, oxide or nonoxide ceramics by proper thermal treatment of organosilicon polymers (curing and thermolysis), was proposed over 30 years ago and since then, enabled significant technological breakthroughs in ceramic science and technology (COLOMBO et al., 2010).

The technique allows unique design of ceramic materials properties by tailoring its chemical composition and microstructure, not possible hitherto by conventional processing routes, such as sintering or casting. Which in turn, explains the increasingly attention for commercial developments of coatings, fibers, complex shaped components, tapes, as binder of advanced ceramic components and infiltrated porous media in the fields of chemical engineering, energy, environmental, transportation and communication technology (GREIL, 2000).

2.1.1. A novel processing technique, the PDC route

In general, manufacturing from polymer precursor systems comprises the polymer synthesis from precursor compounds, shaping of product in desired geometries, crosslinking of the polymer into a non-meltable thermoset and pyrolysis under controlled atmospheres, where between 400 and 800°C the organic-inorganic transitions occur. The commonly involved processing temperatures are indicated in Figure 1.

The complete processing of such inorganic materials are divided into major steps namely polymerization, or synthesis of suitable monomers to form polymer macromolecules, crosslinking, in which such precursors are transformed into preceramic networks at moderate temperatures, and thermolysis or pyrolysis that convert the network into a covalent ceramic. The concept behind the process relies on generating preferred structural characteristics during polymerization of organometallic precursors, transforming them into ceramics by retention of initially building blocks and release of organic groups (WEINMANN et al., 2013).

Figure 1: Polymer to ceramic transformation of PDCs.

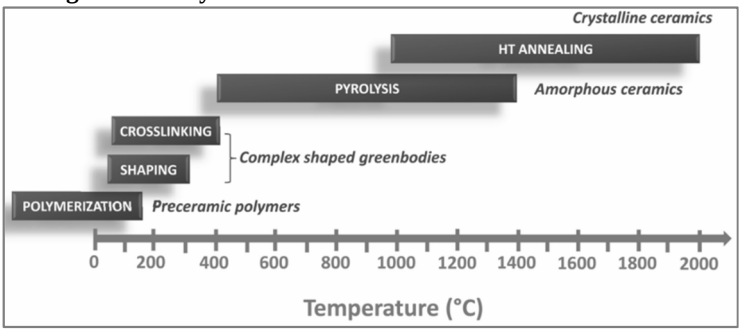

Source: (IONESCU; RIEDEL, 2012)

A schema of aforementioned steps, in Figure 2, aim to facilitate comprehension of molecular and microstructural transitions during ceramic manufacturing from a polymer or preceramic precursor. The most know classes of such materials are the binary to quaternary systems Si_3N_4, SiC, BN, AlN, SiCN, SiCO, BCN, SiCNO, SiBCN, SiBCO, SiAlCN, and SiAlCO, stable up to 2000°C concerning decomposition, crystallization, phase separation and creep (COLOMBO et al., 2010).

Figure 2: Polymer to ceramic conversion of a chloro-organosilicon starting compound.

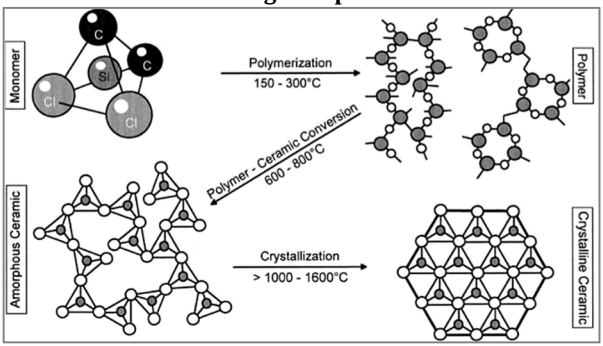

Source: (GREIL, 2000)

The production of engineering components by the PDC route present notorious advantages in comparison with ceramic conventional processing or other molecular routes. Firstly, the preceramic precursor is a polymer when is shaped, therefore, can appropriately make use of versatile polymer forming techniques, such as casting, injection

moulding, pressing, tape casting, fiber drawing, coating, rapid prototyping, among others. Furthermore, do not present the drying difficulties, long processing times nor the need to use flammable solvents, such as sol gel techniques.

In comparison with classical ceramic powder technology, in which the presence of sintering additives is mandatory due to low atomic mobility, final composition and microstructure of PDCs are additive free and present enhanced thermochemical properties, as exceptional oxidation and corrosion stability. Besides dispensing additives, which constrain technical application, the significantly lower processing temperatures are of economic interest. Covalent Si_3N_4 and SiC-based ceramics commonly sintered at 1700-2000°C can be synthetized by the PDC route between 1000 and 1300°C, moreover, there is no other approach, so far, to produce SiCN and SiCO based ceramics (COLOMBO et al., 2010; GREIL, 2000; IONESCU; RIEDEL, 2012; RIEDEL et al., 2006; WEINMANN et al., 2013)

Final composition and microstructure of such ceramic materials, relies directly on the molecular structure of polymer precursors, therefore, PDCs macroscopic chemical and physical properties can be modified by the design of composition and structure of these materials.

Polymer precursors

Organosilicon polymer materials are imperatively present in our daily life, due to properties combination of low weight, mechanical strength and processability (RICHTER et al., 1997). Widespread used as ceramic precursor, with oversimplified general formula presented in Figure 3, those hybrid materials can have both groups, X of the backbone and organic substituents R^1 and R^2 attached to silicon, modified to design physical and chemical properties.

Figure 3: Organosilicon polymer suitable as polymer precursor.

Source:(COLOMBO et al., 2010)

Different backbone groups result in several classes of Si-based polymers, while variation of functional groups modify chemical and thermal stability, solubility, beyond electronic, optical and rheological properties of the polymer. Latter is of particularly importance, as a

function of temperature, for the following processing steps of PDCs. The main classes of organosilicon precursor systems for PDC production are represented schematically in Figure 4, among them polysilanes, polycarbosilanes, polysiloxanes, polysilazanes (PSZ) and polysilylcarbodiimides are the most investigated as preceramic precursors (WEINMANN et al., 2013).

Figure 4: Most representative classes of polymer precursors.

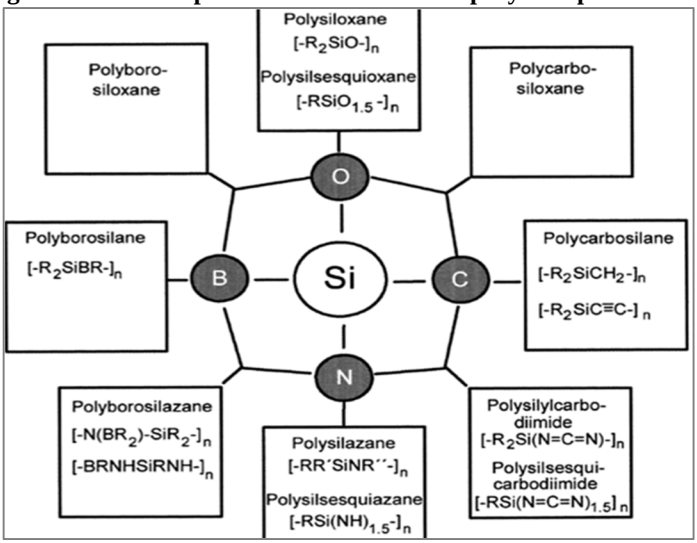

Source:(GREIL, 2003)

Poly(organo)silazanes, are a class of polysilazanes and typically have carbon containing groups appended to silicon and nitrogen atoms within the polymer chain. The also called poly(carbo)silazanes (PCSZ) offer combination of properties such as high hardness, oxidation and corrosion resistance, high temperature and UV stability. Moreover, adhere tenaciously to a wide range of substrates, including ferrous and non-ferrous alloys, therefore, quite used in protective coating formulations with wide utility in the clear-coat market segment.

Additionally, such raw materials possess properties for joining chemically, microstructurally and structurally dissimilar materials, including metals and ceramics. For this reason, may also be used as binders of, among others, ceramic fillers for fabricating composite materials (GREIL, 2000; KROKE et al., 2000; RIEDEL et al., 2006). The impediments of it use in some markets, due to lack of availability and

price, has been increasingly overcome with the commercial availability of reasonably priced large volumes of polysilazanes (LUKACS, 2007).

Polymer to ceramic conversion

After shaping, the crosslinking, which takes place typically below 200°C, is accomplished mainly to retain shape of usually low viscous polymer precursors during the ceramic conversion. The use of catalysts can further lower this temperature and increase the ceramic yield, by avoiding evaporation of oligomers and formation of bubbles. Above 400°C, radical reactions and rearrangements lead to cleavage of chemical bonding and detachment of non-functional groups from the main polymer chain, macroscopically observed as gas release.

Amorphous $Si_xC_yN_z$ ceramics can be obtained after conversion of poly(organo)silazanes, commonly by oven pyrolysis under flowing atmosphere to remove gaseous products (KROKE et al., 2000). The organic to inorganic transition, accompanied by a shrinkage over fifty percent in volume, mass loss and pronounced density increase, is completed at 800-1000ºC, as indicated in Figure 5. Consequently, unless dimension stand under a few hundred micrometers, final microstructure may present large defects as pores and cracks, deleterious for mechanical properties. To overcome such drawback, to load the polymer with the use of fillers, has been the main strategy (COLOMBO et al., 2010).

Figure 5: Weight and density changes of polymer precursors, during thermal decomposition in inert atmosphere.

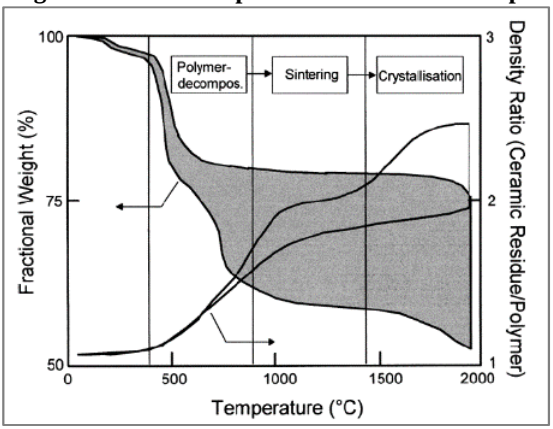

Source: (GREIL, 2000)

Fillers addition

Inert or active fillers, with various shapes and dimensions, are used to reduce shrinkage, eliminate cracks and large pores, as can be visually observed in Figure 6. In addition to tailor final composition, improving mechanical, electrical, tribological and magnetic properties of polymer derived ceramics or composites. In general, PDC processing occurs within the routes presented in Figure 7.

Figure 6: Top view of SiCN coatings pyrolyzed at 1100°C under inert atmosphere, without filler (a), containing 4.2 vol.% of Al_2O_3 (b) and 50 vol.% of Al_2O_3 (c).

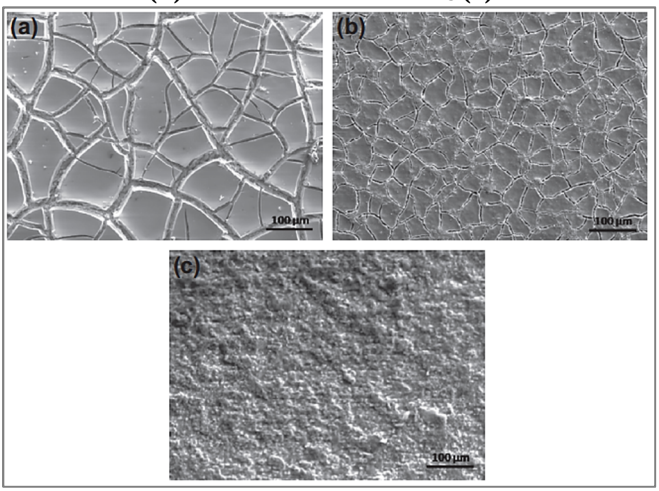

Source: (WEINMANN et al., 2013)

Figure 7: Methods of processing preceramic precursors.

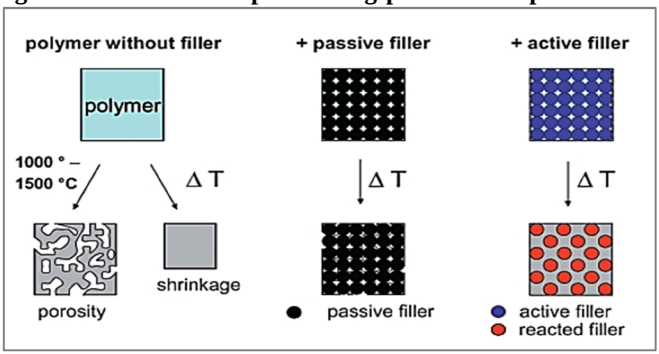

Source:(RIEDEL et al., 2006)

Metals, intermetallic and ceramics, used as active fillers react with solid or gaseous residues from polymer precursor and heating atmosphere. Alternatively, inert fillers, commonly metal carbides, oxides or nitrides, do not react but provide means of escape for the gaseous products derived from thermolysis. The latter decrease volume shrinkage according to the decrease of polymer fraction, while active generate new phases with increased specific volume.

A representation of polymer and fillers interaction during pyrolysis is presented in Figure 8. Diffusion bonding by expansion of active fillers can create a rigid network, while passive fillers with reactive surface create primary bonds with the preceramic matrix. Despite the physical bonding depend on residual stresses, resultant from polymer conversion and thermal expansion mismatches, inert fillers are a convenient solution to reduce dimensional scattering, maintaining original properties of added fillers (GREIL, 1995, 2003).

Polymer-derived amorphous ceramics generally present low matrix toughness ($K_{1C} \ll 2MPa\sqrt{m}$) and, similar to most porous ceramic materials, directly depend on porosity presence. Beyond, molecular precursor structure and processing parameters, the final properties of PDCs loaded with fillers are also determined by the interactions among networks and dispersed phases present in the composite. For example, mechanical properties increase with filler volume amount up to critical threshold at 40-50%, while higher values lead to formation of large filler cluster and excessive porosity for a variety of filler containing polysiloxane (GREIL, 2000).

Figure 8: Filler and polysiloxane precursor interactions.

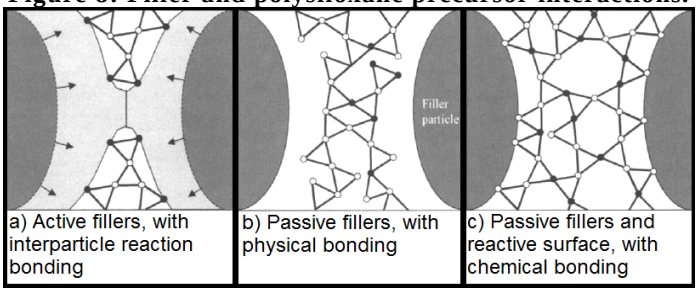

Source: Adapted from (GREIL, 2003)

The combination of functional fillers, which provide specific properties in combination with increased mechanical properties, has an increasingly appeal for transfer into product developments and industrial

processes, summarized in Figure 9. Amorphous and crystalline PDC coatings are of particular interest for protecting surfaces, since several manufacturing processes based on liquid or vapor phase of filled polymer suspensions, can provide versatile chemical and structural compositions (GREIL, 2012).

Figure 9: Emerging fields for PDC ceramics and composites.

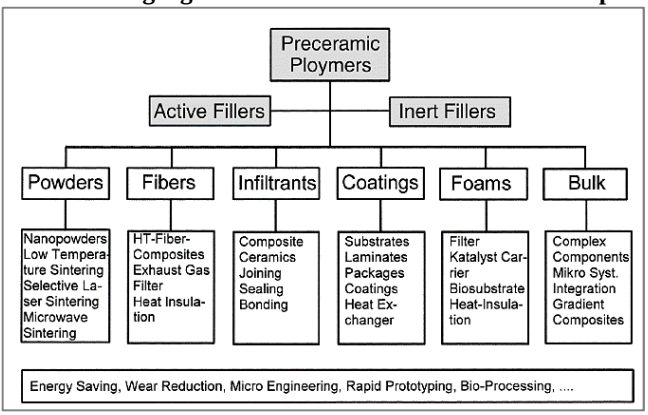

Source: (GREIL, 2000)

2.1.2. PDC coatings

Obviously, due to exorbitant energy consumption and associated costs worldwide (HAYS, 2010; HOLMBERG et al., 2014; HOLMBERG; ANDERSSON; ERDEMIR, 2012), there is a strong interest in developments of low cost and effective ways of protecting metal surfaces against oxidation, corrosion and wear. Coatings are the most promising area for polymer-derived ceramics, since polymer precursor can be deposited onto different substrates by low cost techniques, such as dip or spray coating, in comparison to CVD and PVD methods (COLOMBO et al., 2010).

Polysiloxanes (TORREY; BORDIA, 2008a, 2008b), polycarbosilanes (COLOMBO; PAULSON; PANTANO, 1997; KRAUS et al., 2009) or polysilazanes (GREIL, 2000) are the commonly precursors used for this purpose. Furthermore, the loading of preceramic precursor with fillers allows modifying desired properties and the increase of coating thickness without cracks presence. Particularly SiCN films, produced from poly(organo)silazane precursor, have potential application as protective coating formulations in ceramic and metal matrix

composites, in situations where high temperature stability, corrosion resistance or long term durability need to be considered (RIEDEL et al., 2006).

Filler loaded polysilazane-based coatings

Motz and coworkers have demonstrated that polysilazane coatings, processed by dip coating and oven thermolysis, are suitable to protect steel from oxidation up to 1000ºC. Coatings of synthesized poly(carbo)silazane (ABSE) and (perhydro)polysilazane (PHPS, NN120-20) solutions in solvent were reported to wet very well the substrates, with excellent adhesion (>38N/mm^2), attributed to chemical bonds formed between substrate and coatings (metal-O-Si). Nevertheless, the absence of fillers restricted coatings thickness up to 1.5μm for applications without high tribological solicitation (GÜNTHNER et al., 2009a).

Environmental barrier coatings, applied on low alloy (AISI A182) and stainless (AISI 304) steels, composed of an inorganic bond coat layer (PHPS) and poly(organo)silazane (HTT1800[2], Clariant Advanced Materials) composites, were successfully developed for medium temperatures (700ºC) working conditions (GÜNTHNER et al., 2011). The critical thickness of polysilazane-based coatings (GÜNTHNER et al., 2009b; KRAUS et al., 2009) was increased up to 100 μm by the addition of ZrO_2 and a glass system as fillers. Such materials, also characterized as protective against abrasive wear, withstood with negligible surface damage, the effect of a scratch applied by a tipped diamond (radius 0.2mm) using a load of 5N (SCHÜTZ et al., 2012).

Using the same approach of a PHPS layer between substrate and composite, a top coating was developed for low thermal conductivity by combination of passive (YSZ) and active (Zr_2O) fillers on a poly(organo)silazane (Durazane 1800, Merck Group) matrix. Despite the porosity (27%vol), the achievement of a system with superior results was possible by adjustment of thermal expansion coefficient (CTE) of composite coating onto the steel substrate (AISI441) (BARROSO; KRENKEL; MOTZ, 2015).

On the other hand, without the presence of bond-coat layers, organic-inorganic PMMA/polysilazane coatings applied on AISI1006 steel, revealed enhanced substrate corrosion protection, beyond increase of hydrophobic coating aspect and adhesion by the increase of HTT1800 amount (COAN et al., 2015).

[2] Presently named Durazane 1800, owned commercially by the Merck Group.

2.2. TRIBOLOGY, THE MODERN NAME OF AN ANCIENT ISSUE

The term was introduced exactly 50 years ago, announced in a report by the UK Department of Education and Science, and back then defined as *the science and technology of interacting surfaces in relative motion and associated practices*. During these five decades tribology has gained global interest and even a new definition, *the physical science-based generic technology of friction*, however, the report conclusions remain relevant nowadays (“50 years of the Jost Report”, 2016).

Friction is a dissipative phenomenon and one of the most significant source of irreversibility in thermodynamic processes. It is not a material property, as commonly thought, but a system response with important practical consequences in daily life and industrial applications. Friction allow several and fundamental activities as walking, writing, picking objects, using automobile tires on a roadway, the manufacturing process of machine components, among others in which resistance to motion is desired.

However, as a source of irreversibility, one-third of the world's energy resources is estimated to be spent to overcome friction by several approaches. Friction is also the main cause of wear, major origin of materials wastage and loses in mechanical performance. (STACHOWIAK; BATCHELOR, 2014). In addition to the energy wasted, heat generated by friction affects negatively the performance of mechanical systems and is responsible by hazardous emissions to our environment (HOLMBERG; ANDERSSON; ERDEMIR, 2012).

Many achievements were already reached in the development of components less susceptible to friction and wear, but still optimized energetic efficiency is pursued by scientific and industrial communities (BHUSHAN, 2000).

2.2.1. Solid lubricants

Despite liquid lubrication being traditionally used to reduce friction and wear, under severe service conditions where oils and greases may decompose, oxidize, solidify, evaporate or act as contaminants like in food and pharmaceutical-production machinery, dry lubrication may be the only feasible solution (BUSCH, 2007; ERDEMIR, 2000). The use of solid lubricants is not new, but the lubricant deposition method, critical to the efficiency of the lubricating film, have been greatly extended by new technologies to deposit solid films on wearing surfaces, as summarized in Figure 10.

Figure 10: Historical development of tribological coatings and solid lubricant films.

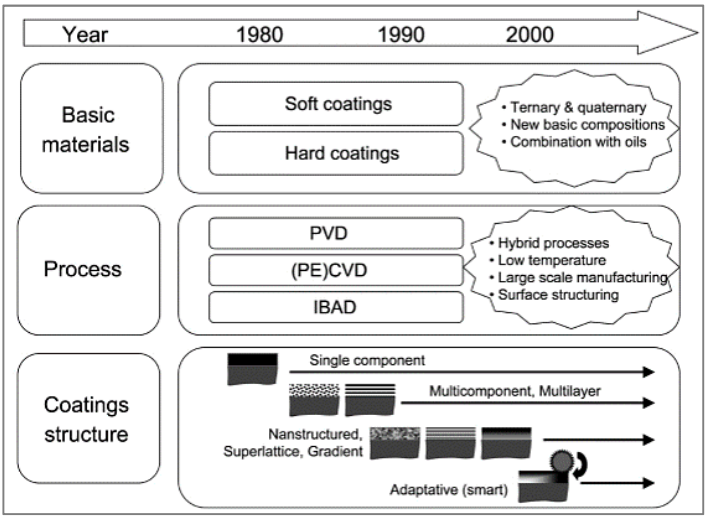

Source: (DONNET; ERDEMIR, 2004)

As others lamellar solid lubricants, hexagonal boron nitride (h-BN) present a layered crystal structure, weakly bonded between the layers and with atoms on the same layer strongly bonded. Which in turn, enables the formation of a low shear strength film between sliding surfaces and might reduce friction. Like graphite, h-BN is well known for its improved lubricity effect when in atmospheres with moisture and other condensable vapors. In addition, h-BN particularly exceeds the performance of other solid lubricants with regard to thermal and chemical stability, graphite and MoS_2 lubricity persist up to 400°C while h-BN can withstand temperatures up to 1000°C (LANCASTER, 1990; MARTIN et al., 1992).

2.2.2. Coatings

Most solid lubricants are produced as thin films by modern deposition methods, which depend on the properties of plasma in a moderate vacuum to produce a lubricant film of high quality. However, are also used as additives to a mechanically stronger material, forming self-lubricating composite coatings, tailored in a way that one phase is responsible for lubrication and another for the scuffing resistance of the tribological system. In general, the formation and transfer of a low shear film at sliding surfaces is responsible for the decrease in friction

coefficient and long wear lives of solid lubricated interfaces (ERDEMIR, 2000).

The durability of such coatings relies directly on the adhesion with the substrate, which is linked to the chemical composition, deposition method and resulting microstructure of composite materials (ERDEMIR, 2000, 2005; STACHOWIAK, 2014). Concerning the vitreous aspect of PDCs and the inherent surface porosity of sintered substrates, despite considering a possible mechanical bonding (physical adhesion) (WACHTMAN; HABER, 1993), factors as chemical affinity, elastic modulus differences and Poisson's ratio should be also considered. In order to enhance adhesion, surface engineering techniques enable the production of substrates with graded compositions and properties, improving the match of materials.

The presence of porosity in a sintered substrate reduces namely strength and ductility of the material (BOCHINNI, 1986), but the actual effect of porosity on the wear behavior of such materials is not clearly understood (DUBRUJEAUD; VARDAVOULIAS; JEANDIN, 1994). Mechanical properties and the load bearing capacity are reduced by the presence of pores, generally detrimental to the wear resistance (DE MELLO; HUTCHINGS, 2001). But under some conditions, can also have a beneficial effect in prevent degradation of the material (CHEN; LI; COOK, 2009). Porosity affect the stress distribution and the metal deformation of subsurface layers during dry sliding, and can act as generator and debris sink, removing wear particles from sliding interfaces (DUBRUJEAUD; VARDAVOULIAS; JEANDIN, 1994; SIMCHI; DANNINGER, 2004). Moreover, pores are reported to act as lubricant reservoirs that can be released during the tribological solicitation (HAMMES et al., 2014b).

2.2.3. Surface modifications

Concerning coated surfaces, additional reductions in wear and friction can be achieved by enhancing the hardness of the substrate surface. Which in turn, difficult the deformation of substrate beneath the coating from the counterface load, and avoid fracture of the brittle coating, thus, increasing the load support (HOLMBERG; MATTHEWS; RONKAINEN, 1998).

Surface modifications involve alteration of chemical composition and/or properties of the surface (BUNSHAH, 1994). To improve the tribological performance of ferrous-alloys components, surface treatment processes commonly used to increase surface hardness can improve not

only the wear resistance, but also fatigue and corrosive resistance. Thermochemical processes, in which the composition of the surface is locally modified, produce a near-surface region with properties differing from those of the bulk material (HUTCHINGS, 1992).

2.2.4. Plasma assisted nitriding

Plasma nitriding is a well investigated and widely used ferritic thermochemical treatment based on the diffusion of nitrogen for surface hardening and corrosion resistance of steels, cast irons as well as refractory metals (PYE, 2003).

The concept of the process, in contrast to nitriding in conventional furnaces, is based on the ionization of molecular nitrogen to generate very reactive nascent nitrogen at low temperatures and pressures. During the plasma discharge species like fast neutrals or high energetic electrons and ions are generated, which, enable the formation of customized nitride layers at comparatively short processing times with reduced gas consumption, very low environmental impact and high process reproducibility (ALVES JUNIOR, 2011; CHAPMAN, 1980; PYE, 2003).

To obtain even superior results when nitriding sintered steels, a surface enrichment with high nitrogen affinity elements, as Mo and Cr, can be realized concomitant with plasma assisted sintering. The high performance of DC plasma technology became suitable for surface enrichment and nitriding of substrates. Generating interfaces between substrate bulk and coating, presumably capable of accommodating dissimilarities between metallic substrate and PDC, beyond reducing surface porosity and increasing hardness in the same region (KLEIN et al., 2013).

2.3. TRIBOLOGY OF SICN PRODUCED FROM THE PDC ROUTE

The first report about friction and wear behavior of bulk and thin films of SiCN, processed from a poly(organo)silazane by the PDC route (CROSS; PRASAD; RAJ, 2005), aimed further developments of high temperature MEMS devices (CROSS et al., 2002; LIEW et al., 2001, 2002). In which, bulk 10mm squared samples were produced by photopolymerization of a poly(urea-methyl-vinyl)silazane (PUMVS, KiON). Solid polymers were obtained by adding a photo initiator to the precursor followed by UV photolithographic patterning (CROSS et al., 2002), hot isostatic crosslinking and pyrolysis.

To obtain thin films, dilute solutions of the precursor were spun cast onto Si and synthetic sapphire (Me-Al_2O_4) substrates, UV cured in air, crosslinked and pyrolyzed inside a conventional furnace. Crosslinking and pyrolysis atmosphere (N_2 and NH_3), temperature (260/400°C and 900/1000°C), time (1 and 1.5hr) beyond heating rates, were systematically varied to evaluate friction coefficient and wear through reciprocate Si_3N_4 ball-on-disk linear tests, varying contact pressures, environment and humidity. The friction behavior under nitrogen atmosphere and contact pressure of 0.44GPa is reproduced in Figure 11.

Figure 11: Friction coefficient of bulk and films of SiCN.

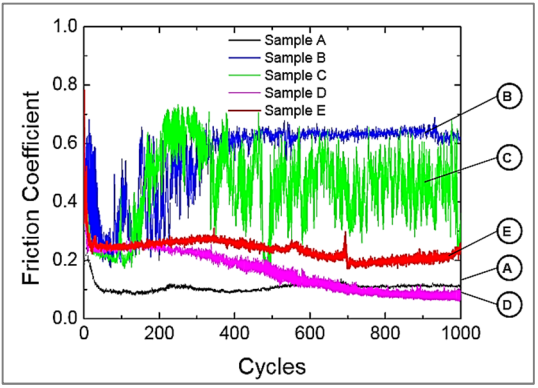

Source: (CROSS; PRASAD; RAJ, 2005)

Bulk SiCN (A), accordingly to authors, consisting of graphitic nanoclusters surrounded by complex Si, O, C and N bonding, presented low μ values (0.13-0.2) and minimal wear. Pyrolysis of thin films under N_2 resulted in highly ordered graphitic phases within a Si-O matrix, while under NH_3, led to less ordered graphene phases in a Si-N network, probably due to increased nitrogen availability. The friction coefficient was directly affected by such structures, higher (0.6) for nitrogen-pyrolyzed films (B and C) and decreased when films were pyrolyzed under ammonia (D and E). The smallest value (0.13) was achieved for films deposited onto silicon (D), and, cylindrical rolls were found on wear track and counterface of NH_3 pyrolyzed films.

Right after these first results, a comprehensive tribological investigation (KLAFFKE et al., 2006) was published describing friction and wear of fully dense homogeneous SiCN ceramics, within a range of structures and prepared by a casting technique also from PUMVS

(Ceraset, KiON). Ceramic discs, with 10-12mm diameter and 0.4-0.5mm thickness, were obtained by casting and sealing the precursor inside a PTFE mold, thermal cross-linking at 260°C during 5h and pyrolysis under argon at temperatures from 800 to 1100°C.

Characterization of such materials, described elsewhere (JANAKIRAMAN; ALDINGER, 2009), revealed an open network structure of mixed $SiC_{(4-x)}N_x$ tetrahedra, containing methyl or hydrogen terminations, beyond oxygen and moisture contamination during samples handling in air. The increase in pyrolysis temperature led to further depletion of hydrogen, higher network connectivity among $SiC_{(4-x)}N_x$ units and consequently raise of density, elastic modulus and hardness of final material. Furthermore, aggregation of sp^2-carbon into graphitic clusters detected in all fully amorphous ceramics, presented amount, distribution and organization dependent upon pyrolysis temperature.

The oscillating (20Hz) sliding (0.2mm) tribological evaluations were carried under air, with an AISI52100 ball applying 10N of normal force on the surface of polished discs glued on a coin. After samples pyrolysis at progressively higher temperatures, fretting tests under medium relative humidity exhibited a significant decrease (150 to $6x10^{-6}mm^3/Nm$) of wear rate and steady state μ (>0.4 to 0.1), presented in Figure 12. Such results were dependent on contact adhesion, contact fatigue and tribo-oxidation mechanisms, furthermore, densification, mechanical properties and stiffness of such materials increases with pyrolysis temperature, as its resistance against contact damage.

Large fractions of remaining organic groups for the 800°C pyrolyzed samples together with wear scar analysis, serrated aspect of friction curve and high wear rate, suggested adhesive wear and tribo-oxidation. Specimens processed 100°C above, also indicated formation of an unstable tribo-oxidation layer (friction curve with oscillations regularly spaced), but, followed by a stabilization of wear evolution. Steady state friction coefficient decreased slightly with the further increase of pyrolysis temperature.

Wear scars comparison revealed a smooth surface and appreciably smaller wear of ceramics pyrolyzed at 1100ºC, qualitatively indicating a better deformability of debris, spread and shoved to the scar edges. In addition to Raman and HRTEM analysis, authors assume that graphite was formed in situ during sliding of such samples, facilitated from the clusters in the amorphous matrix, and forming an interface of low shear resistance between surfaces reducing friction and wear.

Figure 12: Evolution of friction in tests of SiCN in normal air.

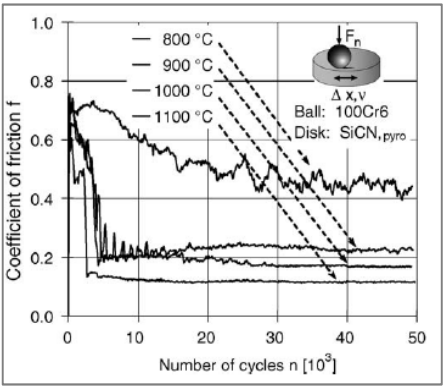

Source: (KLAFFKE et al., 2006)

Relative humidity indicated a major influence on the behavior of studied tribo-systems, since plays an important role in the formation of low friction carbon films on the interface. Dry test atmospheres resulted in higher friction coefficients (0.8-0.6) and wear rates, as indicated in Figure 13. Further enhances in pyrolysis temperature (1000-1100°C) did not influenced friction and slightly decreased wear in dry test environments, while in moist air, steady state μ achieved 0.1 after a short running period and wear was reduced by nearly one order of magnitude.

Figure 13: Friction and wear of samples pyrolyzed at 1000°C.

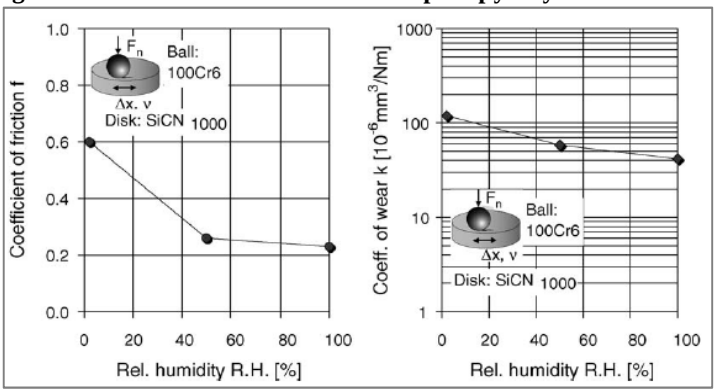

Source: (KLAFFKE et al., 2006)

Moreover, the evolution of μ and wear of SiCN pyrolyzed at 1000°C tested against an Al_2O_3 counter-body revealed similar trends with

moisture presence, however, smaller wear and friction coefficient (0.28-0.1) than against the steel ball. In all cases, the wear of counter-bodies were much smaller than the samples tested.

The high carbon content of investigated PDCs, which can approach one third molar, raised their tribological behavior interest since these initial studies. But, concerning the fact that materials in the SiCN system produced by the PDC route nearly always contain oxygen, another study (CROSS et al., 2006) indicated the significance of the nitrogen/oxygen molar ratio on tribological properties of called $SiC_xO_yN_z$ compounds.

For the discussion of results, the understanding of structures in polymer-derived SiCN, previously modelled as a cellular network of graphene sheets filled with nanodomains of SiC and Si_3N_4 anchored by mixed bonds of Si, C, N and O (MERA et al., 2010; SAHA et al., 2005; SAHA; RAJ; WILLIAMSON, 2006), is schematically presented with their typical compositions in Figure 14.

Figure 14: Composition regimes for SiOC and SiCN PDCs.

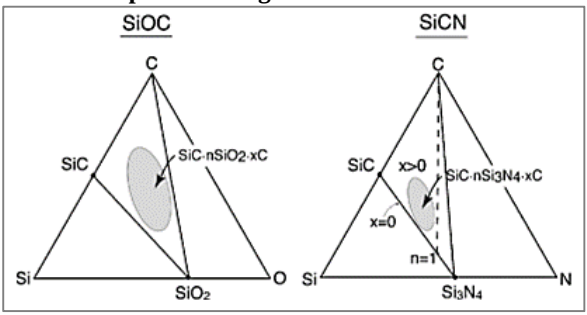

Source:(CROSS et al., 2006)

Specimen production, also from PUMVS, was initiated by UV polymerization as already described in the first presented work. Thermal cross-linking (400ºC, 340min), pyrolysis (700ºC, 180min) and annealing (800(A)-1400ºC(E), 500min) steps were carried under nitrogen overpressure (HIP). For tribological evaluation samples were polished (Rq=3nm), and sliding (3.3mm/s) of a Si_3N_4 ball over a track distance of 1.6mm during 1000 cycles occurred under varying relative humidity (RH:0-80%) and Hertzian contact stresses (0.29-1.02GPa).

The increase in the density of amorphous materials with annealing temperature was linked to higher N/O ratios, and strongly influenced hardness and elastic modulus. Estimated K_1c was 2.56 $MPa.m^{1/2}$ after pyrolysis at 1000ºC, but a relation with temperature was not statistically

possible to report. Friction behavior under dry atmosphere for distinct pyrolysis temperatures, presented in Figure 15, revealed two regimes. One with low friction and negligible wear and another with high friction and wear (average of $3.7x10^{-4}mm^3(N.m)^{-1}$ at 0.97GPa).

Figure 15: Typical plots of u versus sliding distance, and wear track of sample D after test in both type of regimes.

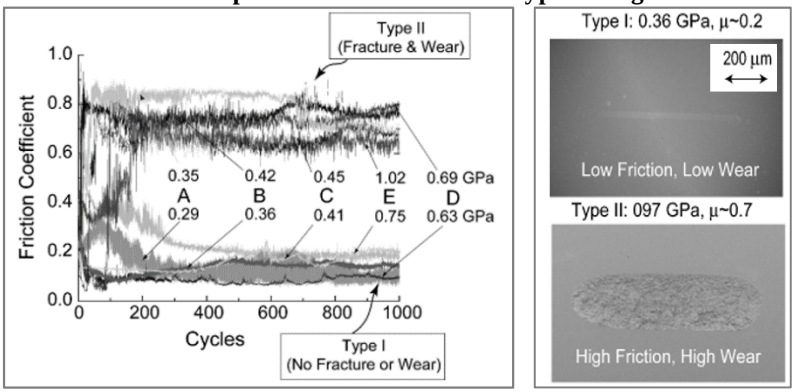

Source:(CROSS et al., 2006)

All samples presented a sharp transition, which moves systematically from the lower (A) to the higher annealing temperature (E) when the contact stress was slightly increased, e.g. friction coefficient of condition C abruptly changed from 0.2 to 0.7 by increasing the contact stress in 0.04GPa. In contrast, when tested in humid air and despite contact stress, only low friction coefficient (~0.2) and negligible wear were observed. Further results indicated that friction coefficient remains independent of RH under constant contact stress, and, independent of contact stress for experiments conducted at 50%RH.

Authors suggest a critical applied stress for the fracture initiation of PDCs, and an increase in work to fracture the PDC with presence of water molecules in the crack tip, providing a crack-bridging effect. The fracture delay seemed to increase such critical load beyond the range of cited experiments, which were limited to a contact stress of about 1GPa.

A conceptual model was presented to explain such tribological results, in which the composition of nanodomain is responsible for the elastic modulus and critical stress for fracture or for the load support, while surrounding graphene sheets reduce friction. In this model, presented in Figure 16, Si-N-O domains and graphene form an interface by mixed bond of Si-C-O-N. In comparison with presented results,

authors suggest that higher friction values and wear rates reported by Klaffke, discussed previously, were result of tests conducted above the threshold stress for fracture.

Figure 16: Schematic of interrelation among tribological properties and nanostructure of polymer derived ceramics.

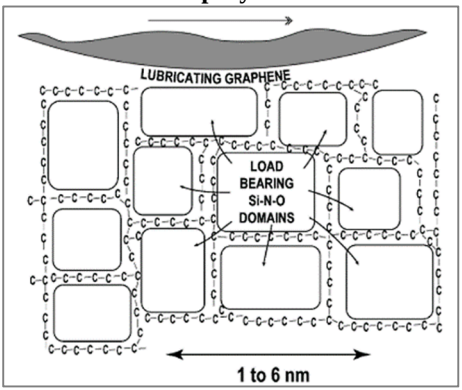

Source:(CROSS et al., 2006)

To understand the role of carbon in the SiCN composition with respect to strength, friction and wear, an interesting study (BAKUMOV et al., 2012) produced ceramic discs (0.2mm thickness) from polysilazane (Ceraset 20) and/or poly(carbo)silane precursor, with an additional source of non-crystalline carbon (tri-phenyl-vinyl-silane, TPVS). Discs and counter-bodies with hemisphere form were produced by casting, after degassing, into previously produced poly(di-methyl)siloxane forms and applying drops directly on PTFE support, crosslinked (175ºC, overnight) and pyrolyzed in furnace under flowing nitrogen or argon (1130-1370ºC, 2h).

In comparison with pure polysilazane, introduction of cited additives lead to more ordered "free" carbon species, predominantly sp^2-form in nano-crystalline graphite clusters, within a covalent SiCN matrix. The poly(carbo)silane presence resulted in SiC enriched samples, and carbon enriched SiC in standing atmospheres, due to expelled hydrocarbons during pyrolysis. Microstructures after pyrolysis of precursors mixture (~6:4wt %), resulted in β-SiC nano-crystallites in a mixed matrix of amorphous and turbostratic graphite. Addition of carbon by TPVS, led to increase in number of β-SiC crystallites beyond additional tiny soft inclusions of graphitic carbon into the matrix, significantly improving tribological properties of materials ($\mu < 0.1$).

Tribological evaluation, by application of normal load (1N) and with sliding velocity of 5mm/s, revealed lower friction coefficients for PDC counter-bodies in comparison with alumina. Pronounced with increasing load (5N), such behavior was attributed to higher carbon amount on the contact zone and/or reduced Hertzian contact stress, due to Young´s Modulus differences of counter-bodies. SiC-enriched samples presented lower friction coefficient, explained in terms of faster heat dissipation by the SiC crystallites. Decrease of μ was achieved by both increase of carbon and SiC phases in final microstrucures, moreover, absence of soft graphite and the excellent lubricating properties of such amorphous carbon were highlighted.

Lastly and very recently, the development of polysilazane-based coatings using inert fillers was reported within the context (BARROSO et al., 2016). Suspensions, homogenized by stirring sequences, were produced by adding h-BN or c-BN fillers and poly(carbo)silazane (ABSE) precursor in solvent. In sequence, applied by dip coating on AISI 304 substrates and pyrolyzed in a chamber furnace (800ºC-1h) under air. After pyrolysis, the coatings containing solid lubricant fillers consisted of 67% h-BN and 33% of the amorphous SiCNO ceramic phase, with average thickness of 8μm and increased porosity of approximately 10%, in comparison with 3% achieved by the ABSE/c-BN composition.

Adhesion of coatings, analyzed by the cross-cut tape test, was characterized in the best class and explained by substrate-O-Si bonds formed between polysilazane and steel (AMOUZOU et al., 2014; GÜNTHNER et al., 2009a). However, the ABSE/h-BN coating was completely removed after less than 50 cycles, while ABSE/c-BN coating initiated substrate exposure only after 750 cycles during abrasion tests (ASTM D 4060), carried with force of 5N and rubber/Al_2O_3 wheels. Results, reproduced in Figure 17, were explained in terms of fillers hardness and coatings porosity, which decreases mechanical stability of such materials.

Figure 17: ABSE based coatings on steel after Taber Abraser Test.

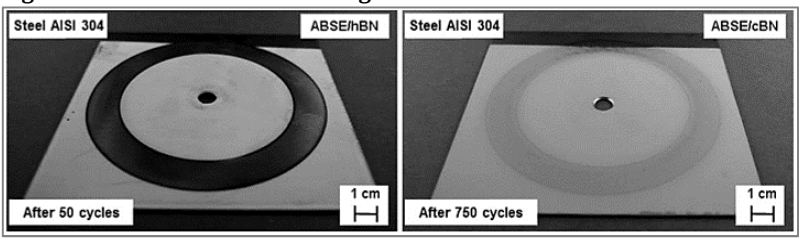

Source:(BARROSO et al., 2016)

Friction analysis, by ring-on-disk configuration and a SiC counter-body, performed under ambient temperature and air moisture of 30%, investigated the pressure (0.05 and 0.4 MPa) and velocity (1 and 5 $m.s^{-1}$) influence. The ABSE/h-BN performed poorly and withstood only 600m before failure, at lower pressure and velocity, in which friction coefficient varied between 0.1 and 0.35. The superior performance of ABSE/c-BN coating confirmed the major influence of pressure in performance change, presented in Figure 18, in which μ increased abruptly before failure (glide path).

Figure 18: Results of tribological tests of ABSE/c-BN coatings applied on AISI 304 steel.

Test	Parameters	Glide path [m]	COF
(a)	0.05 MPa and 1 m s^{-1}	35 000	< 0.18
(b)	0.4 MPa and 1 m s^{-1}	1 300	0.1–0.3
(c)	0.05 MPa and 5 m s^{-1}	27 500	< 0.18
(d)	0.4 MPa and 5 m s^{-1}	1 200	0.2–0.3

Source:(BARROSO et al., 2016)

In addition to SiC counter bodies analysis, authors conclude that coatings performed well until debris, from body and counter-body, lead to μ increase and coating failure. Moreover, suggest that polysilazane-based coating containing c-BN and small amounts h-BN may present improved tribological performance, due to combination of fillers hardness and lubricating properties.

2.3.1. Filled SiCN coatings applied onto surface modified sintered steel: the proposed study

Given the context, in this work, novel composites consisting of sintered low-alloy steel with surface properties modified by plasma and coated with amorphous SiCN coatings filled with h-BN and Si_3N_4, were tailored and produced for unlubricated tribological sliding evaluations and discussion.

The substrate, prepared with mass proportions of 97.4%(Fe1.5%Mo) + 2%Ni + 0.6%C, was designed to provide the load bearing capacity of the composite and was shaped via powder metallurgy (PM), an economic and high volume production technique largely used for producing ferrous net-shape mechanical parts from a mass of dry

powders (THÜMMLER; OBERACKER, 1993). Low alloy steels present up to 5 wt.% of alloying elements and are used mainly for processing components in which the mechanical support is the main factor to be considered, supporting medium to high mechanical stresses when in work, without excessive deformation or rupture during its lifetime of use (SOUZA, 1989).

Molybdenum alloyed steels with elemental additions of Ni provides sintered steels that are used in structural parts requiring strength, wear resistance, and impact toughness (GRAHAM et al., 1997; YOUSEFFI; WRIGHT; JEYACHEYA, 2000). Both alloying elements promote hardenability in PM parts and ferrous materials with sufficient hardenability may develop microstructures, during cooling, containing significant percentages of martensite without need for a secondary quenching operation. The so called sinter-hardening offers good manufacturing economy by providing a one step process and a unique combination of strength, toughness, and hardness (JAMES, 1998; RUTZ; GRAHAM; DAVALA, 1997).

High performance and low environmental impact of DC plasma technology, specifically when applied to PM parts (KLEIN et al., 2013), became suitable for generating interfaces between substrate and coatings. Presumably capable to accommodate dissimilarities of properties, originated from different chemical bonds on metallic substrate and ceramic coating, mainly thermal expansion coefficient and elastic modulus, which might result in residual stress or even micro cracks in the interfacial region.

The sintered substrates were plasma assisted nitrided after the sintering step on samples with and without surface enrichment with Mo, sputtered from a molybdenum cathode inside the same plasma reactor during the sintering thermal cycle. The modified chemical composition of the enriched surface was expected to form more hard and stable compounds, such as mixed nitrides, carbides, or carbonitrides by subsequent nitriding (BENDO et al., 2014, 2016; PAVANATI et al., 2006), contributing to withstand loads exerted in tribological systems (HOLMBERG; MATTHEWS; RONKAINEN, 1998).

Filled-coatings were prepared through production of suspensions, followed by application over sintered steels and oven thermal treatment, for cross-linking and pyrolysis. The poly(organo)silazane HTTS used for the coatings production is synthetized (RICHTER et al., 2014) from crosslinking of a commercially available liquid precursor (Durazane1800, Merck), with simplified chemical structure presented in Figure 19. The

PCSZ synthesis, not in the scope of this work, can be understood in details elsewhere (FLORES et al., 2013; FLORES; HEYMANN; MOTZ, 2015).

Figure 19: Basic chemical structure of Durazane1800.

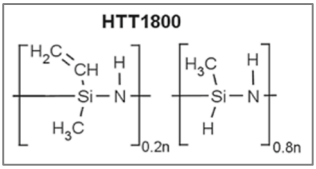

Source: (FLORES; HEYMANN; MOTZ, 2015)

The incorporation of fillers in PDC coatings, overcome crack formation due to polymer shrinkage and allows additional functionalities, as tailored tribological properties. Aiming to produce hard and self-lubricating coatings, based on previously developed composites (BARROSO et al., 2016; CARRAPICHANO; GOMES; SILVA, 2002; CHEN et al., 2010), silicon nitride was used to strengthen the matrix (GREIL, 2000, 2003) and reduce wear, by formation of a network aggregated by the precursor binder phase. While hexagonal boron nitride, due to layered structure and low shear strength, added to generate a lubricating effect on the interface reducing friction, wear and friction heating (ERDEMIR, 2000).

Particulate hard fillers can nonetheless, lead to less tough composites due to decrease of coating continuity, promoting wear by fatigue and abrasion. Thus, two compositions were compared to point the influence of precursor amount on final coating microstructure, one with 39 vol.% of total fillers amount and another with 74 vol.%, for both compositions the h-BN amount was fixed at 9 vol.%. The high control of final microstructure and chemical composition are competitive advantages inherent to cited manufacturing processes. Such benefits were explored to project the final microstructures of the steel, interfaces and ceramic coatings involved, through the selection of raw materials and processing parameters, described in details sequentially.

3. EXPERIMENTAL PROCEDURE

3.1. COMPOSITES PRODUCTION

Novel composites, consisting of sintered low-alloy steel with surface properties modified by plasma and coated with an amorphous SiCN coating filled with h-BN and Si_3N_4, were tailored and produced at facilities in both universities UFSC and UBT. Figure 20 summarizes the processing sequences, which enabled such materials production for unlubricated tribological sliding evaluations and discussion.

Figure 20: Flowchart of composites production.

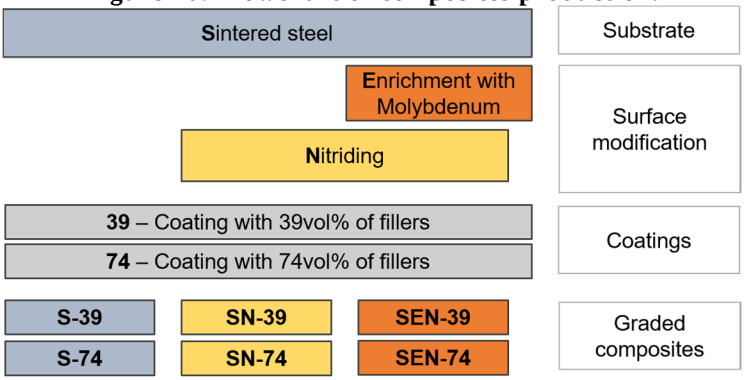

Source: Own authorship

The substrate was designed to provide the load bearing capacity of the composite and was shaped via powder metallurgy, an economic and high volume production technique largely used for producing ferrous net-shape mechanical parts. Interfaces between substrate and coatings were produced by plasma assisted surface modifications of the steel to accommodate dissimilarities of properties, originated from different chemical bonds on metallic substrate and ceramic coating. Nitriding or surface enrichment with Mo followed by nitriding was expected to generate a compound layer at the surface of the substrate with a gradient diffusion region below.

And coatings were produced from a poly(organo)silazane precursor (HTTS) with the use of fillers to provide tailored tribological properties, using the PDC route. Silicon nitride to strengthen the matrix and reduce wear, by formation of a network aggregated by the precursor binder phase, while hexagonal boron nitride, due to layered structure and

low shear strength, added to generate a lubricating effect on the interface reducing friction, wear and friction heating.

In the first processing path, sintered samples were coated with one or another coating composition and pyrolyzed, generating the samples condition named S-39 and S-74, or sintered samples coated with the coating containing 39 or 74 vol.%. of fillers respectively. Alternatively, the sintered substrates were nitrided before coating application and pyrolysis, producing the group of samples SN-39 and SN-74. Finally, samples were surface enriched with Mo during sintering, nitrided, coated and pyrolyzed, generating the third group of samples named SEN-39 and SEN-74.

3.1.1. Substrate produced by powder metallurgy

Molybdenum alloyed steels with elemental additions of Ni provides sintered steels that are used in structural parts requiring strength, wear resistance, and impact toughness. The properties of these materials, like all PM steels, are dependent on density, microstructure and composition (GRAHAM et al., 1997; YOUSEFFI; WRIGHT; JEYACHEYA, 2000).

By using the conventional route of powder metallurgy, cylindrical specimens (Ø 20 per 5mm) were produced from powder mixtures with mass proportions of 97.4% pre-alloyed Fe1.5Mo wt.% (Astaloy Mo, Höganäs), 2.0% elementary nickel (d50=6.06, Epson Atmix) and 0.6% graphite (d50=9.88, Nacional de Grafite). Moreover, 0.8% of amide wax (Acrawax C, Lonza) was added to assist during the pressing stage. After homogenization in a Y-type mixer during 45 minutes, such mixtures were uniaxial cold pressed at 600 MPa using floating die and stationary lower punch, providing a double-sided densification (THÜMMLER; OBERACKER, 1993).

To ensure samples debinding before sintering, a thermal step of 5ºC/min up to 500ºC during 0.5h was realized under flowing ($7.5x10^{-6} m^3/s$) atmosphere of 95%Ar and 5%H_2. Sintering occurred sequentially, using twice the heating rate and same atmosphere, at 1150ºC during 1 hour. Cooling after sintering was carried within the tubular oven with an average rate of 25ºC/min up to 430ºC, as presented in Figure 21, where cooling rates were separated at the end of low alloy steel austenitic transformation, previously determined by sintering tests in dilatometer (JUSTUS, 2016).

Figure 21: Linear trendlines and R-squared values presented beside cooling curve, acquired from 907 up to 136°C.

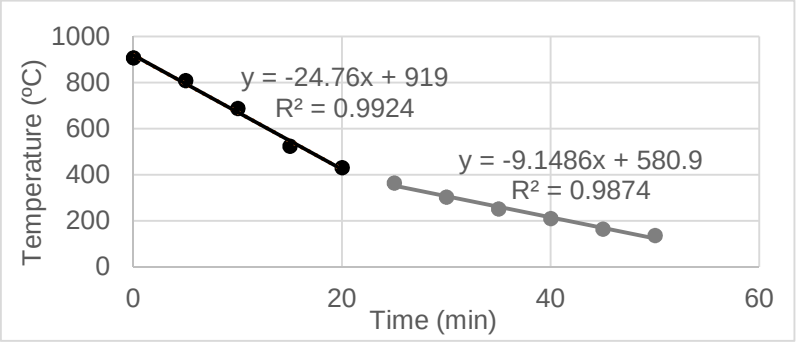

Source: Own authorship

3.1.2. Interfaces generated by plasma treatments

Beyond sintered two other surface conditions, regarded as the common boundary between substrate and coatings or interfaces, were obtained through nitriding of sintered and molybdenum-enriched samples. For producing the second ones (enriched and nitrided samples), shaped specimens were sintered and surface enriched simultaneously, inside the reactor using the same sintering cycle described above. In order to facilitate comprehension of results during discussion, the three conditions were named S (sintered), SN (sintered and nitrided) and SEN (sintered, Mo-enriched and nitrided).

Both thermochemical treatments were performed in a hybrid plasma reactor (BINDER et al., 2009; MACHADO et al., 2006), containing a grounded anode and a cathode connected to the negative voltage output, besides a resistive heating system inside the vacuum chamber. A potential difference was applied between the electrodes through a square waveform DC pulsed power source (SCFP002-SDS Plasma), under flowing gaseous mixtures restrained by mass flow controllers (1179A-MKS) and pressure by a capacitance manometer (626C Baratron-MKS). Electron current measured on cathode and other processing parameters of the treatments are detailed in Table 1.

This configuration based on previous works (BENDO et al., 2014; KLEIN et al., 2013; MALISKA, 1995; PAVANATI et al., 2007), led to the generation of an abnormal glow discharge, suitable for processing materials since voltage and current rise following certain degree of proportionality, which, enable discharge control and completely

surrounds the cathode allowing a homogeneous treatment (CHAPMAN, 1980; PYE, 2003).

Table 1: Processing parameters of thermochemical treatments.

	Sintering/Mo enrichment	Nitriding
Electrode material	TZM (Plansee)	AISI304
Electrodes distance	0.015m	0.040m
Cathode dimensions	16.3x11.4cm	14.5x10cm
Potential difference	600V	500V
Atmosphere	80%Ar+20%H_2	90%H_2+10%N_2
Pressure	2Torricelli	3Torricelli
Gas flow rate	$2.5x10^{-6}m^3/s$	
Current	(1.3±0.1)A	(0.5±0.1)A
Heating rate	5ºC/min	
Temperature	1150ºC	540ºC
Time	1hour	2hours
Samples position	Anode/floating potential	Cathode

Source: Own authorship

The use of a pulsed voltage source was employed mainly to avoid a shift from abnormal glow to arc discharge regime, which can lead to instabilities in generated plasma. The pulse length (Ton) set as 180 µs in combination with pulse repetition time of 250µs (Ton+Toff) leads to a plasma duty cycle (Ton/(Ton+Toff)) of 72% for both thermochemical treatments, utilized to increase the period of energetic species collision. For sintering and enrichment with Mo, shaped specimens were placed over Al_2O_3 plates in anode to avoid diffusion and bonding between samples and electrode. Otherwise, during nitriding samples were positioned directly on cathode, as exhibited in Figure 22.

Temperature was measured using a chromel–alumel thermocouple (type K) coated with Inconel, electrically insulated and inserted into a molybdenum or low carbon steel reference sample, symmetrically positioned with the treatment samples. Samples were cooled after treatments inside the reactor chamber, with plasma reduced duty cycle of 6% and using 1 Torricelli of gaseous mixture pressure, with average cooling curves exhibited in Figure 23.

Figure 22: Schematic electrodes configuration during sintering/Mo enrichment (a) and nitriding (b).

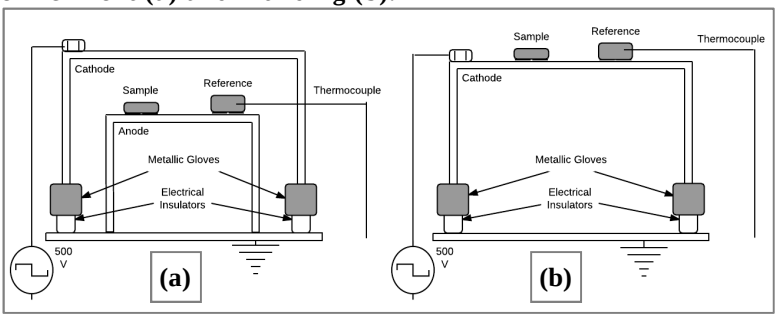

Source: (SEIFERT et al., 2016)

Figure 23: Cooling curves obtained after enrichment and nitriding.

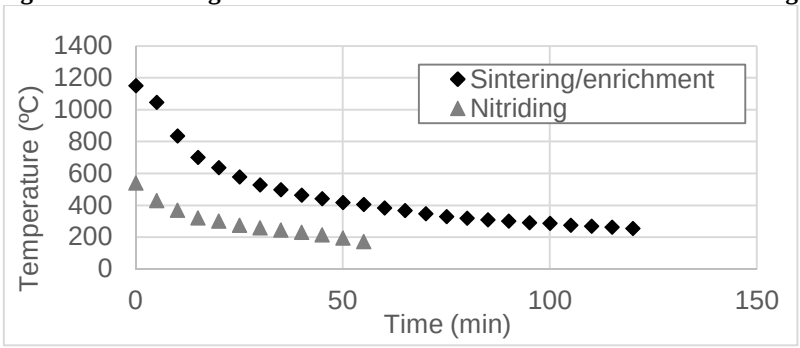

Source: Own authorship

3.1.3. Coatings prepared by the PDC route

Filled-coatings were prepared through production of suspensions, followed by application over sintered steels and oven thermal treatment, for cross-linking and pyrolysis. The poly(organo)silazane HTTS used for the coatings production is synthetized (RICHTER et al., 2014) from crosslinking of a commercially available liquid precursor (FLORES et al., 2013; FLORES; HEYMANN; MOTZ, 2015). Based in recent works of the partner institute (BARROSO et al., 2016; GÜNTHNER et al., 2011, 2012, SEIFERT et al., 2014, 2016), the used raw materials and processing parameters are described in sequence.

Sequentially, solutions of di-n-butyl-ether (Alfa Aesar) and a dispersant agent (Disperbyk-2070, BYK) were mixed during 15 minutes in a magnetic stirrer, before the addition of h-BN and Si_3N_4 particles. The

dispersion of ceramic fillers was assisted with the use of ZrO_2 spheres (Ø=1mm), through five sequences of stirring (15min) and ultrasonic agitation (5min). Lastly, the precursor HTTS and 3 wt.% of a radical initiator (dicumyl peroxide, Aldrich), used to accelerate cross-linking, were added and stirred during at least 2 hours.

Based in previous developments with the precursor, the total amount of passive fillers, described in Table 2, was set between 30 and 80 percentage in volume. The hexagonal boron nitride content was set in 9 vol.%, since a sufficient amount of low shear fillers is necessary to provide lubrication between interfaces, and the presence above approximately 10 vol.% cause a drastic decrease of mechanical properties regardless of material matrix (CARRAPICHANO; GOMES; SILVA, 2002; HAMMES et al., 2014a).

Table 2: Coating architecture after pyrolysis.

Total filler amount vol.%	α-Si_3N_4 vol.%	h-BN vol.%	SiCN vol.%
(A) 39	30%	9%	61%
(B) 74	65%	9%	26%

Source: Own authorship

Beyond further compensate polymer shrinkage after pyrolysis, different amounts of Si_3N_4, further detailed in Table 3, were planned to change the phase distribution of composite coatings. One, tailored to present an amorphous SiCN matrix containing dispersed Si_3N_4(A), and other Si_3N_4 particles joined by the SiCN binder phase (B), both with the same amount of h-BN particles that act as solid lubricant.

Table 3: Passive fillers information from product datasheet.

	α-Si_3N_4	h-BN
Manufacturer	H.C. Starck	Henze BN products
Trade name	Alpha-Silicon Nitride Grade B7	HeBoFill® 410
Particle size (d50)	0.9 – 1.3µm	1.0µm
Specific surface (BET)	$4m^2/g$	$20m^2/g$

Source: Own authorship

Before coating, the edges of the substrates were grinded to avoid border effects and samples immersed in acetone for cleaning in an ultrasonic bath during 15 minutes. For application of the suspensions on the substrates, the spray technique was choose concerning the samples

geometry. The spray gun (Mignon 3, Krautzberger), presented inside the painting cabin in Figure 24, was used with air pressure of 1.5 bar, nozzle width of ¾ and 5 opening rounds for suspension flow control. The distance between samples and spray gun was set in 12cm, to process coatings with maximum thickness of 10μm covering mainly plateaus over the surface, parameters based in a previous work (JUSTUS, 2016).

Figure 24: Painting cabin.

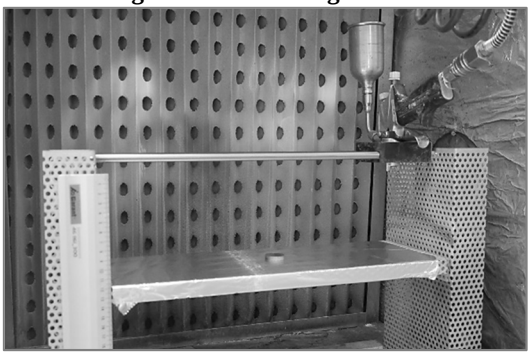

Source: Own authorship

The conversion of the coatings was carried in a tubular furnace (RO10/100, Heraeus), with a heating rate of 3K/min up to 1000ºC maintained during one hour. Performed under flowing nitrogen atmosphere (purity 5.0), pyrolysis of pure HTTS provides a ceramic yield of ~80%, and the behavior during cited thermal treatment is well investigated in the literature (SEIFERT et al., 2016). Cooling was carried inside the oven, with cooling rate of approximately 3K/min under flowing nitrogen.

3.2. CHARACTERIZATION

3.2.1. Substrate

Dimensions and weight of all samples, acquired after sintering using micrometer and a digital scale, were used to calculate the geometrical density. At least one sample per batch was analyzed, for microstructural characterization, with optical (OM - BX60, Olympus) and scanning electron microscopes (SEM - JSM-6390LV, Jeol), equipped with an energy dispersive X-ray spectrometer (6733a, ThermoScientific).

Samples were cross-sectioned using a diamond containing disc in a cutting machine (Isomet4000, Buehler), before embedding in bakelite resin. The metallographic preparation (ASTM E3-11) consisted in grinding sequences with abrasive paper (SiC) followed by polishing with Al_2O_3 suspensions, interleaved with ultrasonic cleaning of samples in ethanol (99.99% purity). Etching of samples, by immersion in a solution containing ethanol and 2% of nitric acid (Nital 2%) revealed the steel microstructure. Micro hardness of phases was determined by measuring the diagonals of at least ten indentations per phase in three samples, after applying loads from 0.1 to 1.0N during 10 seconds, accordingly to MPIF Standard 51.

3.2.2. Interfaces

Before the application of coatings and pyrolysis, as produced samples (one per batch - S, SN and SEN) were cleaned in acetone with ultrasonic agitation. Surface morphology was analyzed by SEM (1540ESB, Zeiss) equipped with field emission cathode, and elemental composition with EDX (Thermo Noran System 6, Thermo Fischer Scientific).

The crystalline structures of the surfaces were investigated by X-ray diffraction technique (AXS D8, Bruker AXS), using monochromatic CuKα radiation. For data acquisition, parameters were set in angular step size of 0.01°/2θ with 2θ varying from 20° to 120°, angular step time of 0.5 seconds, applied voltage of 40kV, 40mA of current and sample spinning (15 rotations per minute). The acquired data was evaluated with the third version of software Diffrac.Eva software, and the phases identified using PDF-4+ 2012 structural database.

For the cross section analyses, samples were cold mounted (EpoFix, Struers) one day before sectioning with a diamond wire (Ebner 6800, Well), in order to retain the modified surfaces. After metallographic preparation, carried as already described, investigations of layers microstructures and effective case depth (MPIF Standard 52), with at least three samples of each condition, were conducted using SEM (Vega 3, Tescan) equipped with EDX (X act, Oxford), beyond microscopes and micro-hardness tester described in section 3.2.1.

3.2.3. Coatings

A field emission gun scanning electron microscope (JSM-6701F, Jeol) was used for fillers aspect characterization, using acceleration of

10kV and 6mm of working distance. Thermogravimetric analysis (Júpiter F3, Netzsch) of pure and filled precursor were carried, under flowing N_2, using a heating rate of 3K/min up to 1000ºC and maintained during 1 hour, in order to accompany pyrolysis behavior and mass loss of coatings.

After pyrolysis, all coatings were investigated regarding homogeneity, cracks or pores presence by visual and light microscope evaluations (Axiotech 100, Zeiss). Thickness characterization of all samples was realized by magnetic induction, using a Dualscope FMP40 (Helmut Fischer) through a standard method for nonmagnetic coatings on magnetic basis metal (ASTM B499-09).

Crystalline structures of composites surface after pyrolysis were also investigated by X-ray diffraction (Philipps X´Pert), with parameters previously described, evaluated using the software X´Pert Highscore Plus 2.0 and PDF-2+ 2004 structural database. Cross section analyses were carried as explained in section 3.2.2., and coatings linear coefficient of thermal expansion estimated by the rule of mixtures.

3.2.4. Tribological characterization

The tribological behavior of graded composites was investigated under air by reciprocating linear, pin-on-flat test geometry (BHUSHAN, 2013), schematically presented in Figure 25, using a CETR-UMT 4 tribometer. In order to isolate the lubrication effect of h-BN, experiments were conducted without the use of lubricants and under room relative humidity (44-52%).

Figure 25: Schema of performed reciprocating linear sliding tests.

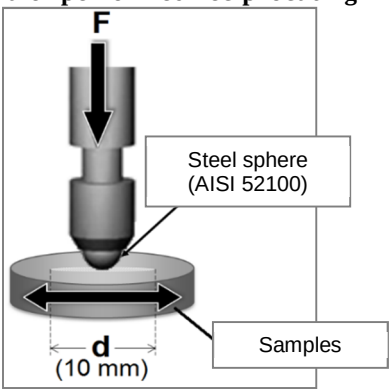

Source: (FURLAN, 2016)

Surface regions to be tested, were aligned with the counter-body sphere (AISI 52100 - Ø10mm) in order to maintain certain parallelism of surfaces during the reciprocating test (2Hz). While a constant load of 4N, controlled with a load cell (100N), was applied in the sphere holder against composite, the friction coefficient of system was obtained during sliding by monitoring normal and tangential forces (software version 1.136257.F05). The electric resistance, through the tribological pair, was simultaneously acquired to indicate coating failure or the formation of an electrically isolating tribo-layer between surfaces.

Both mean friction coefficient and electrical resistance were calculated using data acquired (averaging filter width of 100 samples) during the steady state sliding, indicated in Figure 26, set experimentally in this work as the sliding distance from 30 to 48 meters (criteria based on the stabilization of the electrical resistance). At least three samples of each condition, concerning coating composition and interface were tested with maximum of three analysis per specimen. For comparison, non-coated sintered samples were also evaluated.

Figure 26:Friction coefficient behavior and eletric resistance during sliding test.

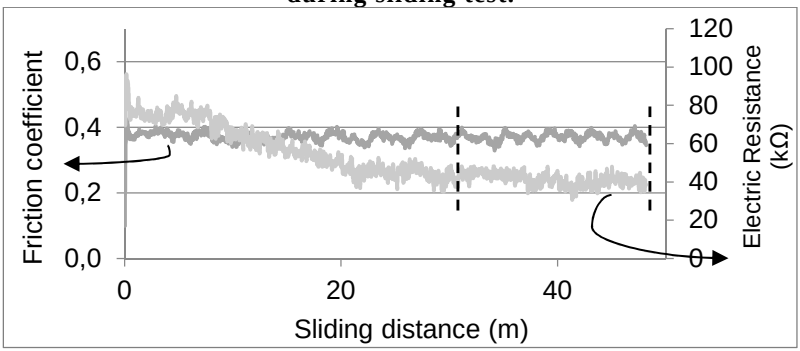

Source: Own authorship

$$Q = \frac{\Delta V}{L F_N} \qquad \textbf{Equation 1}$$

After testing, bodies and counter-bodies were cleaned in acetone and ultrasonic bath during 15 minutes. Specific wear rates (Q) were calculated accordingly to Equation 1, from the standard method test for linearly reciprocating ball-on-flat sliding wear (ASTM G133-05). In

which, ΔV is the volume loss of the tested specimen, L the total sliding distance (48m) and F_N the normal load (4N) applied to the samples.

The volume loss of counter-bodies was characterized as the volume of worn spherical cap, Equation 2, schematically presented in Figure 27. Both diameters were measured, using light microscopy (200x), with half of the mean value considered the radius of spherical cap.

Figure 27: Schema for volume loss evaluation of counter-bodies

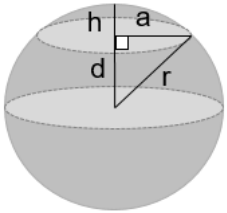

$$h = (r - d)$$

$$d = \sqrt{(r^2 - a^2)}$$

Source: Own authorship

$$\Delta V = \frac{\pi h}{6}(3a^2 + h^2) \qquad \textbf{Equation 2}$$

All composites wear tracks were analyzed using white light interferometry (Zygo NewView 7200), acquiring topographic data at least three times per wear track by a stitch function (20% overlap), as detailed in Table 4.

Table 4: Parameters of data acquisition.

Software	Scan lenght	Camera mode	Objective	Zoom
MetroPro	150µm	640x480 pixels-210Hz	5x	0.5

Source: Own authorship

The software Mountains Map Universal (3.0.11) was used to treat acquired data, initially to fill non-measured points, based in a smooth shape calculated from surrounding data. In sequence to level the surface and to select the region containing the wear but excluding initial and final edges of the track (7mm height per 1.5mm width). After obtainment and treatment, such surface was converted into series of 2D profiles by extracting west-east profiles, from which it was possible to obtain an average profile, as presented in Figure 28. Then, the worn volume could be calculated by multiplying the average worn area per track distance.

After tribological sliding evaluations, the worn surface of a representative sample for each condition, was investigated by SEM (JSM-

6390LV, Jeol) using secondary and backscattered electrons signals (sample inclined 30°), beyond EDX microanalysis (6733a, ThermoScientific).

Figure 28: Average profile of the worn track of a S-39% sample.

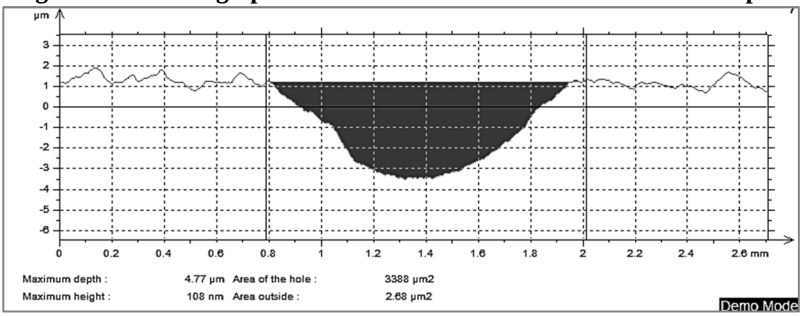

Source: Own authorship

3.2.5. Statistical analyses

A statistical two-stage analysis was adopted to evaluate differences among mean values of friction coefficient, electrical resistance, wear rates and other measured properties, using the Origin software. Assuming normal distribution and same variance, ANOVA (analysis of variance) indicated if means were equal, if unequal, then Tukey's test indicated by how much (MONTGOMERY; RUNGER, 2003).

4. RESULTS AND DISCUSSION

4.1. SINTERED SUBSTRATE

The sintered steel, common substrate among the academic works developed within the project context, was already characterized and the outcomes (JUSTUS, 2016) briefly summarized in sequence. The low alloy steel presented an average density of 7.06±0.03g/cm^3 with low dispersion (cv<1%) of results among batches. The average value represent 89.6% of the theoretical density, or, approximately 10% of porosity calculated by the rule of mixtures, presented qualitatively in Figure 29.

Figure 29: Non-etched cross section of the sintered sample under observed under OM (right), and surface top view under SEM (SE).

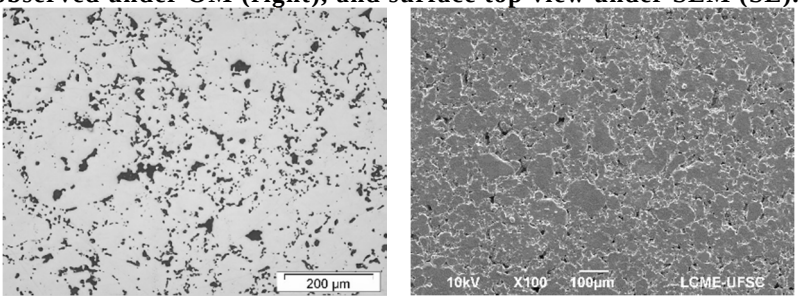

Source: Own authorship

As expected, due to use of pre-alloyed and elementary powders, the sintered steel presented a heterogeneous microstructure, regions identified as original Fe1.5Mo particles, original nickel particles and an interdiffusion region among them. Such distribution, presented in Figure 30, resulted in regions with micro constituents of bainite (B) and perlite (P) at original Fe1.5Mo particles and interdiffusion regions, moreover austenite (A) and martensite (M) at original and surrounding location of nickel particles.

The steel composition is estimated to present properties of approximately 500MPa of Yield strength and 675MPa of ultimate tensile strength (HOGANÄS, 1999). The linear coefficient of thermal expansion (CTE) of sintered steel does not depend on porosity since is an intensive property, data from wrought steels could be assumed concerning some slightly composition differences (DANNINGER; GIERL-MAYER, 2013; THÜMMLER; OBERACKER, 1993). For this work, the α value

$12.8x10^{-6}$/K (GALE; TOTEMEIER, 1992) was assumed as the average linear coefficient of thermal expansion.

Figure 30:Typical microstructures observed, with martensite regions indicated in higher magnification (15kV-15mmWD-SE).

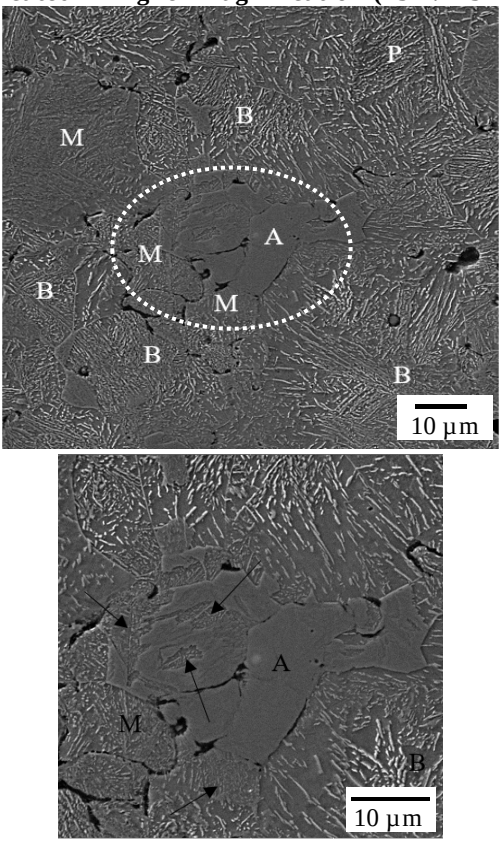

Source: (JUSTUS, 2016)

4.2. PLASMA MODIFIED SURFACES

When observed under optical microscope, the produced surfaces for subsequent coating presented a metallic shine after sintering, modified to a matte appearance after thermochemical treatments. Top view surfaces analysis revealed neck formation among adjacent particles and pore rounding, indicated in Figure 31(a). Neck formation and pore rounding are known stages from the sintering process, from a particle agglomerate

to a coherent body, in which the driving force is to minimize the free surface enthalpy (ΔG surface<0) (THÜMMLER; OBERACKER, 1993; UPADHYAYA, 1997).

After nitriding, Figure 31(b), despite the presence of fine granular precipitates on the surface of sintered particles and into the pores, it was still possible to identify the original sintered network. However, after the double thermochemical treatment of enrichment and nitriding (c), the morphology evolved to a coalesced crystals aspect, related mainly to the simultaneous Mo enrichment during sintering of a steel containing carbon, explained in sequence.

Figure 31:As produced sintered-S (a), nitrided-SN (b), enriched and nitrided-SEN (c) surfaces, revealed in details for the regions indicated (SEM-15kV-15mmWD-SE).

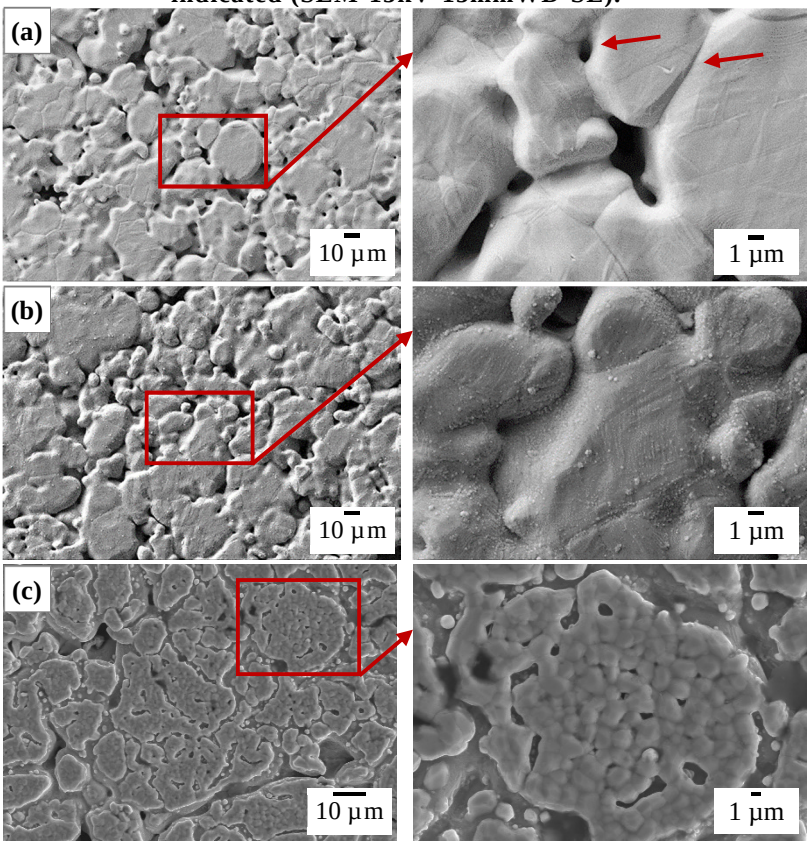

Source: Own authorship

In accordance, X-ray analyses revealed the presence of different precipitates on samples after surface modification processes, indicated in Figure 32. Ferrite was identified for all conditions, as the single structure after sintering and with reduced peak intensity after nitriding, due to precipitation of γ´-Fe_4N and ε-$Fe_{(2-3)}N$, as also concluded by other author, when plasma nitriding a sintered Fe1.5Mo wt.% alloy (PEREIRA et al., 1995). However, the presence of carbon as an alloying element into the substrate, led to identification of the second pattern as an ε-$Fe_{(2-3)}$(C,N), with prevalence of the γ´-phase, as reported by other authors using treatment atmospheres with increased nitrogen ratios.(MOLINARI et al., 1993; PINASCO et al., 1995).

Figure 32: Diffraction patterns of surface modifications.

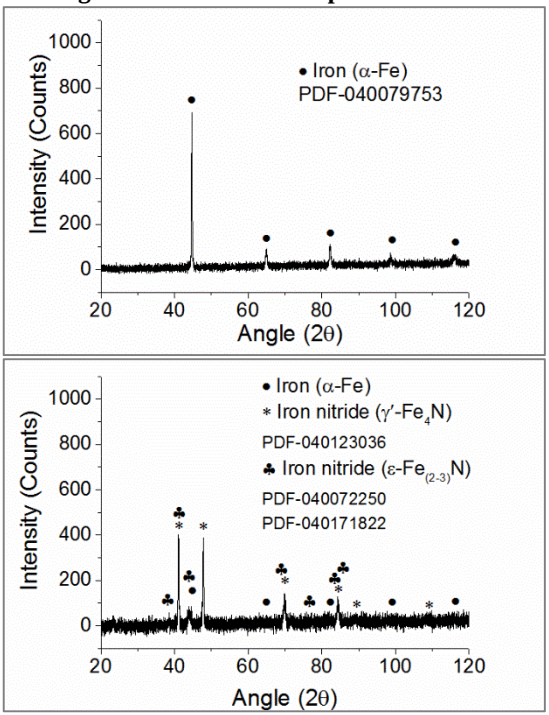

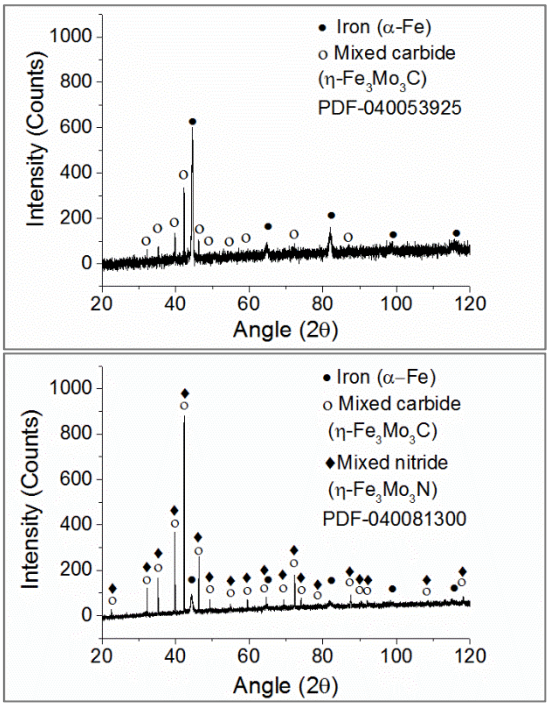

Sintered and enriched condition (SE)

Sintered, enriched and nitrided condition (SEN)

Source: Own authorship

During sintering and enrichment, Mo atoms are sputtered from the cathode due to ion and neutral atoms bombardment, which diffuse to the atmosphere and sample, promoting the surface enrichment. Due to atoms preference for concave surfaces, because of the reduced vapor pressure in relation to a non-tensioned plane surface, the simultaneous treatment is reported to reduce presence of smaller surface porosity also due to stabilization of alpha iron phase (PAVANATI et al., 2007).

The concomitant treatment in the low alloy steel used in this work, resulted in the precipitation of a bimetallic carbide (Fe_3Mo_3C), reported in the literature to be distributed as precipitates or as a pure surface layer, depending on the carbon amount into the iron matrix (PAVANATI et al., 2006). SEM and EDS analysis, shown in Figure 33, revealed the angular morphology of agglomerated carbides on SE surfaces. With increased amount of Mo and reduced Fe content in relation to the matrix in which were precipitated, accordingly to stoichiometry of characterized phase.

Figure 33: Color mapping of precipitates on the surface of SE samples, (SEM-20kV-13mmWD-BSE).

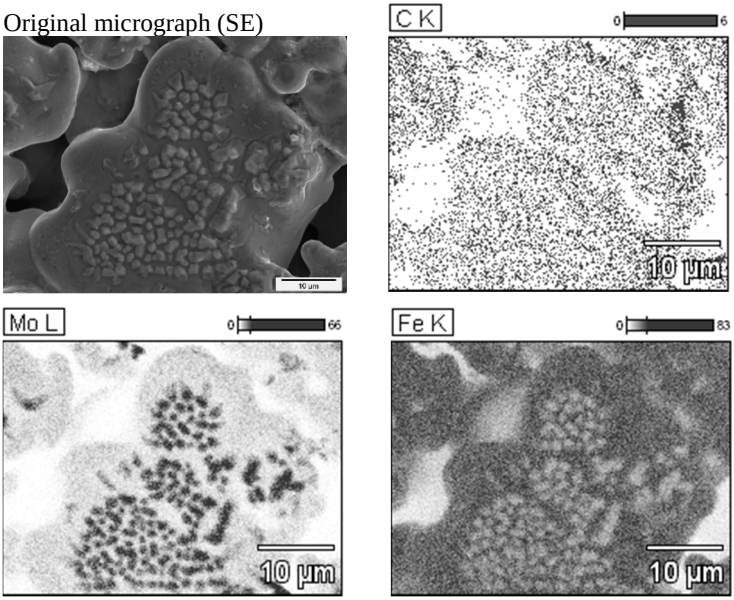

Source: Own authorship

Subsequent nitriding of these samples (SEN) led to a layer outgrowth, assumed to evolve from Fe_3Mo_3C precipitates, which hindered visualization of grain boundaries and penetrated into the pores, as presented in Figure 34. Furthermore, in accordance with the decreased ferrite peak intensity when compared to the (SE) condition in Figure 32, the phase was characterized by diffraction patterns as Fe_3Mo_3C or Fe_3Mo_3N, given the treatment to which the samples were submitted.

Based on reported topotactic synthesis of ternary (η-$Fe_3Mo_3(C,N)$) interstitial carbides and nitrides (ALCONCHEL et al., 1998; ALCONCHEL; SAPINA; MARTINEZ, 2004). In which, nitrogen and carbon atoms exchange their interstitial positions, while the structure of metallic atoms remains unaffected during reactions, between oxide or nitrided precursors and flowing gaseous mixtures. Moreover, considering that solid solution of Mo enhances the solubility of nitrogen into the ferrite matrix and interferes on nitrides precipitation (BENDO et al., 2014, 2016), it is believed that a mixture of $Fe_3Mo_3(N,C)$ was formed during nitriding from carbides agglomerates. However, further analyses are required to confirm the hypothesis.

Figure 34: Precipitates in detail, after SE (a) and SEN (b), (SEM-20kV-13mmWD-BSE).

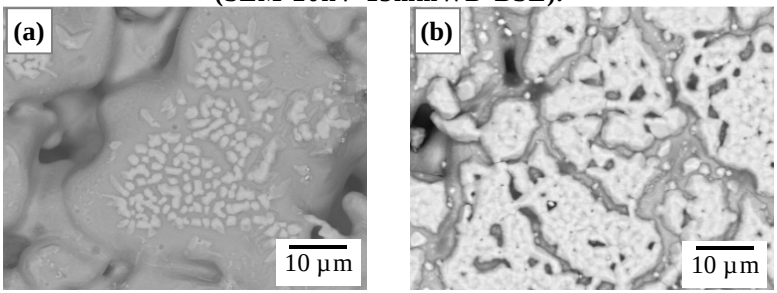

Source: Own authorship

Cross section optical micrographs revealed the microstructure of nitrided samples after sintering (a) and Mo enrichment (b), in distinct surface regions in Figure 35. Both presented a white layer, continuous in (a) and related to the compound layer, while discontinuous in (b) correlated to the surface outgrowth aspect, previously presented in Figure 31(c) and Figure 34(b).

Moreover, two distinct regions can be observed beneath the $Fe_3Mo_3(C,N)$ layer in Figure 35(b). The first (I) probably related to the Mo enrichment that stabilizes the α-Fe, when reaches a certain amount, and results in earlier formation of alpha phase grains (PAVANATI et al., 2007), in which fine nitrides and carbides might be precipitated (PAVANATI et al., 2006). Below the interface, indicated schematically (II) in Figure 35(b), another microstructure was noted, corresponding presumably to bainite, since solid solution of Mo in carbon steels favors such structure formation at the used cooling rates.

The average thickness of discussed regions, obtained by optical micrographs evaluating a minimum of five distinct regions of at least three samples in each condition, revealed layers with low dispersion of measurements as presented in Figure 36. Due to its reduced size, it was not possible to evaluate separately the microhardness of observed carbonitride layers in SEN specimens. However evaluations carried in regions closest to the surface as possible, revealed an increase of microhardness from 584±68 in SN samples to 821±74(HV0.01) for Mo enriched samples. As already expected at this discussion point, due to hardening by precipitation of interstitial bimetallic carbides and nitrides.

Figure 35:Etched cross section of nitrided surfaces, SN(a), SEN(b).

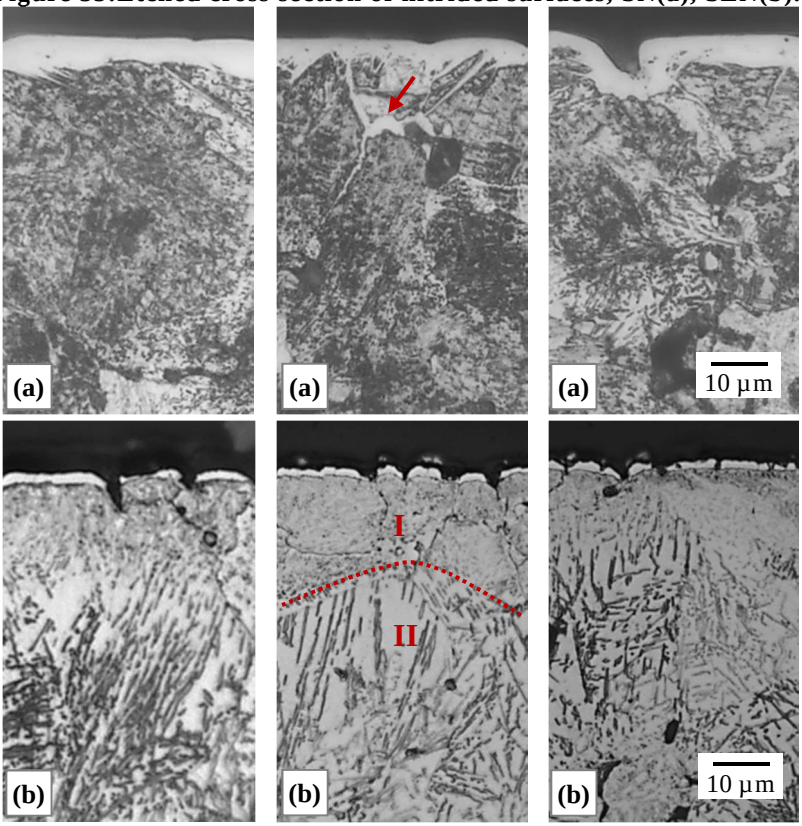

Source: Own authorship

Figure 36: Thickness of produced surface layers.

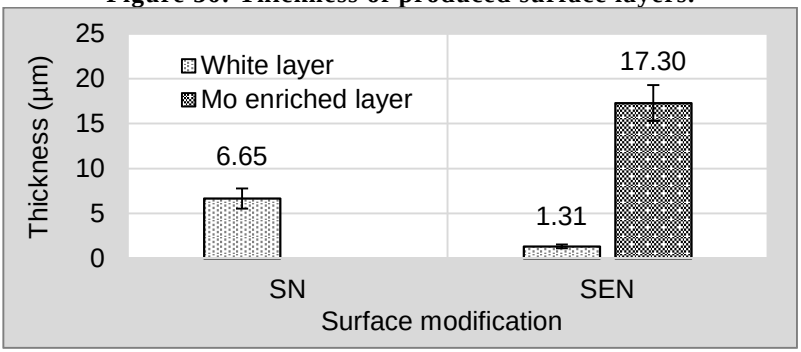

Source: Own authorship

Concerning the presence of Ni, Mo and C as alloying elements, the reduced nitrogen content on used nitriding atmosphere and their influence on the formation of such layers, thickness and microhardness results are in accordance with previously published data (BENDO et al., 2014, 2016; MOLINARI et al., 1993; PAVANATI et al., 2006; PEREIRA et al., 1995; PINASCO et al., 1995).

4.3. FILLED PDC COATINGS

Fillers were observed under SEM with field emission gun (FEG) before coating production, the angular aspect of silicon nitride, as well as the lamellar characteristic and increased specific surface area of hexagonal boron nitride, are presented in Figure 37. Passive fillers do not react with polymer, gaseous products or pyrolysis atmosphere during set thermal treatment, thus, maintaining original mass and material properties indicated in Table 5.

Figure 37: Passive fillers, α-Si_3N_4 (a) and h-BN (b).

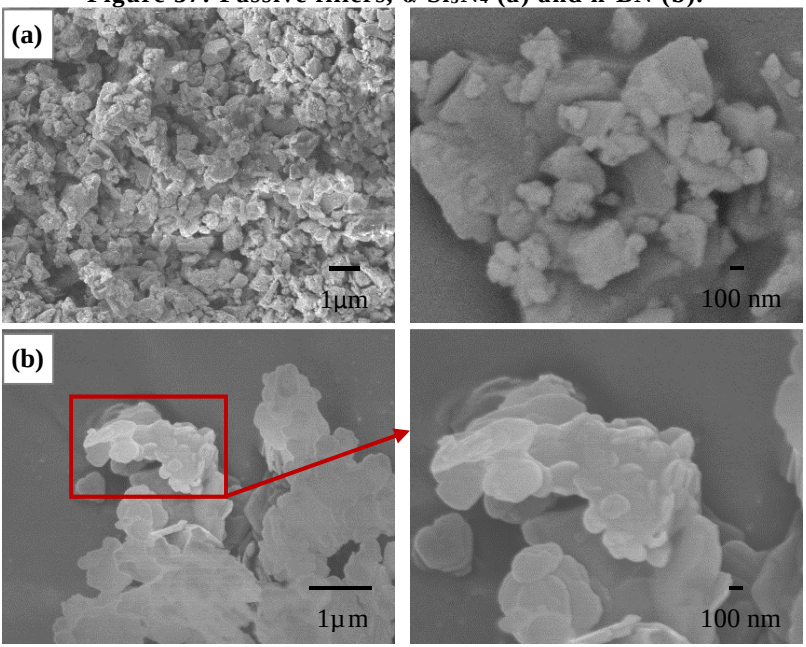

Source: Own authorship

Table 5: Comparison of CTE and density of selected materials.

	α-Si_3N_4	h-BN	SiCN(O)	Coating with 39% of fillers	Coating with 74% of fillers
CTE α (10^{-6}/K)	2.5 – 3.5	3.5 – 4.0	3.0 – 4.0	2.9 – 3.3	3.9 – 4.0
Density (g/cm^3)	3.2	2.3	2.4	2.6	2.4

Source: (BARROSO et al., 2016; BARROSO; KRENKEL; MOTZ, 2015; COLOMBO et al., 2010; GÜNTHNER et al., 2011)

Linear CTE values of pure materials were used to estimate the coefficient for the produced coatings, but the differences between them were considerably smaller if compared with the assumed value for the substrate. For this reason, no inferences about the thermal compatibility behavior of coatings over produced surfaces were possible.

The pyrolysis behavior of pure precursor (HTTS) and filled coatings, occurs into well-defined steps, and were characterized by TGA analysis. The slight mass loss from about 110 up to 300ºC, observed more pronouncedly for the HTTS (solid line) in Figure 38, is related to release of non-crosslinked oligomers and ammonia during thermoplastic-thermoset precursor evolution (FLORES; HEYMANN; MOTZ, 2015). In comparison with literature, the decreased initial cross-linking temperatures are explained due to the presence of dicumyl peroxide, the radical initiator used to accelerate the cross-linking of filled coatings (SEIFERT et al., 2014).

The largest mass shrinkage occurred up to approximately 700ºC, due to conversion of used precursor into an amorphous SiCN ceramic by degradation and release of organic substituents, mainly volatile hydrocarbons (CH_4), decomposition products containing Si, H_2 and NH_3. (FLORES et al., 2013) As expected, the mass loss is almost complete at 700ºC, and, the increase of filler amount monotonically decreased the mass loss of composite coatings to the values presented in Figure 39. The obtained ceramic yield of about 80% for the pure precursor is in accordance with reported values for HTTS pyrolyzed in nitrogen (FLORES et al., 2013).

Figure 38: Comparative thermogravimetric analyses among pure precursor and with the presence of passives fillers.

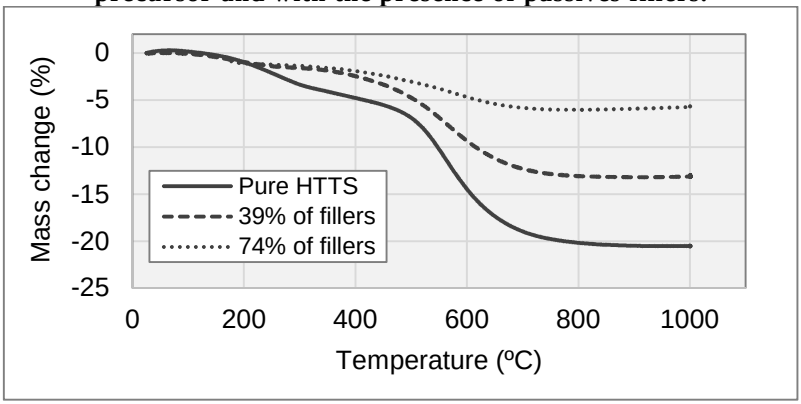

Source: Own authorship

Figure 39: Mass loss after pyrolysis at 1000°C during 1 hour (N_2).

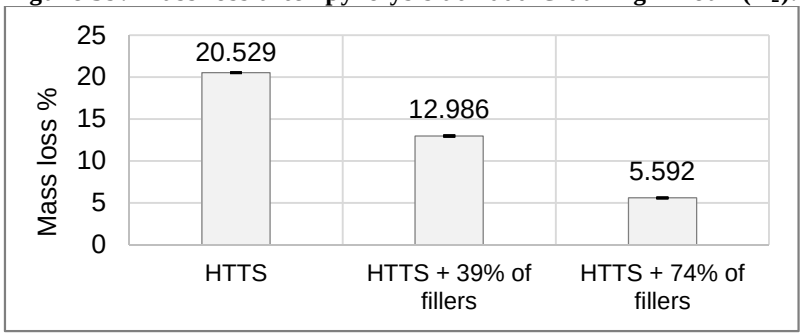

Source: Own authorship

4.4. COMPOSITES

4.4.1. Coatings and interfaces after pyrolysis

Visually, the increase of filler amount decreased coatings heterogeneity, specifically the border effect observed in samples before and after thermal treatment, presented in Figure 40, regardless of substrate modification. Additionally, avoided spalling of coatings in such regions as occurred with the composition containing less fillers, observed as bright points inside the dark border of pyrolyzed specimens in Figure 40(a), zoomed and presented in Figure 41.

Figure 40: Samples (SN) with coating containing 39 (a) and 74% of fillers (b) before and after pyrolysis.

Before pyrolysis | After pyrolysis

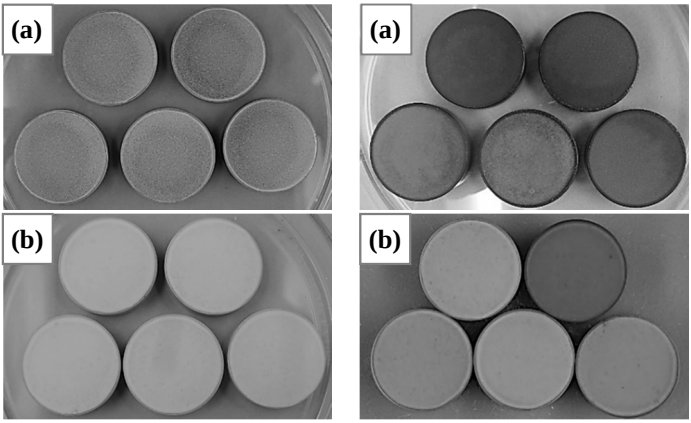

Source: Own authorship

Figure 41: Detail of coating spalling after pyrolysis, sample SN-39.

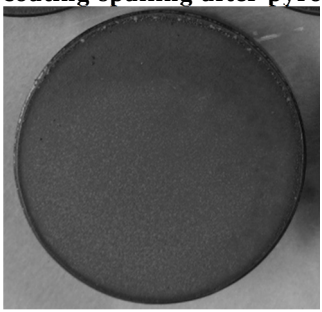

Source: Own authorship

Processing parameters used in the PDC route led to coating thicknesses below 10µm, as presented graphically in Figure 42. Averages were not considered statistically different at a 95% level of confidence.

Top view light microscopy evaluations, supported the correlation between filler amount and coating homogeneity, as shown in Figure 43. Furthermore, revealed the presence of pores (indicated by arrows) independent on surface modification or coating composition, beyond the presence of macro-cracks (dotted circle) in less filled coatings. Additionally, the increase of Si_3N_4 filler amount visually indicated smaller and rounder pores.

Figure 42: Average coating thickness of produced coatings over sintered (S) and modified surfaces (SN and SEN).

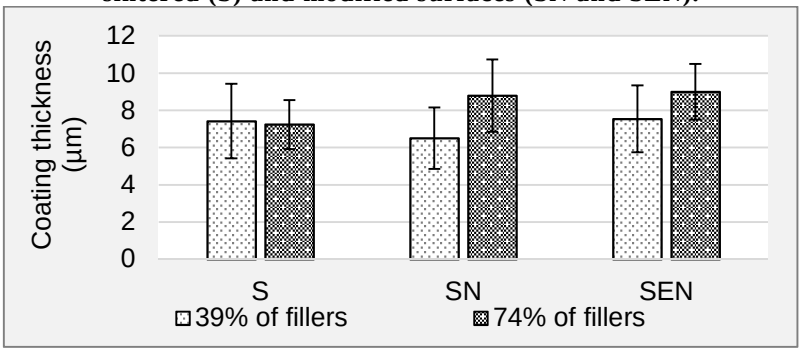

Source: Own authorship

Figure 43: Pores and crack, indicated in pyrolyzed coatings.

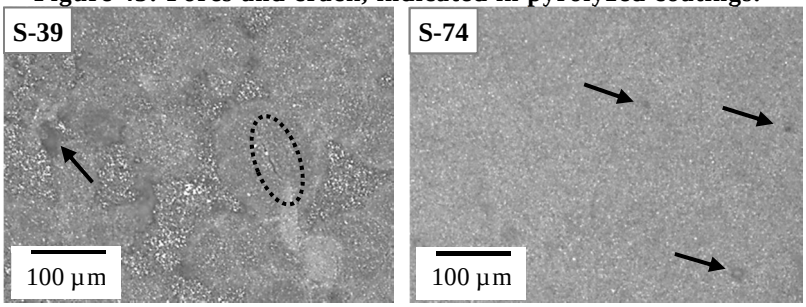

Source: Own authorship

The fulfillment of cracks with mounting resin, of coatings cross section analysis as in Figure 44, confirmed it was not a defect produced during the metallographic preparation. Regions containing deeper surface porosity, purposely presented, revealed a few unfilled spots for both coatings compositions at the bottom of larger pores. Due to elimination of gaseous products formed during coating pyrolysis, and absence of further processing steps to produce dense ceramics, pores were already expected. However, cracks indicated that the filler amount of 39 vol.% was not sufficient to compensate the precursor shrinkage, or, produce a crack-free PDC coating over the sintered steel and modified surfaces using the presented processing route.

The coating with only 26 vol.% of SiCN (or 74 vol.% of fillers) visually presented a proper filling into substrate, regardless of interface, as observed in Figure 45 at different magnifications. No cohesive cracks,

large pores, filler agglomeration nor interface failure were observed, suggesting a successful obtainment of homogeneous, and free of macro cracks, ceramic coatings over sintered substrates.

Figure 44: Micrographs comparison of filled coatings, arrows indicate cracks or unfilled spots (SEM-15kV-10-13mmWD-BSE).

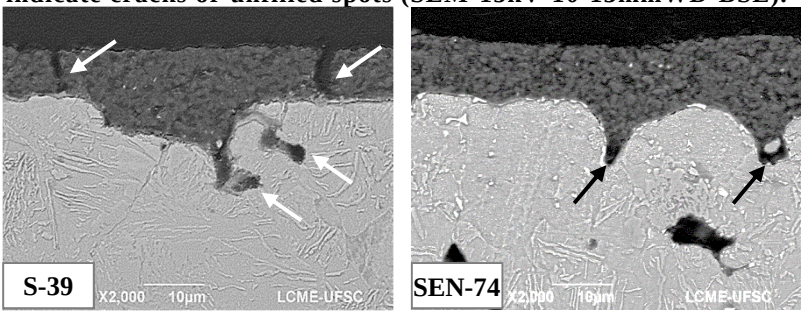

Source: Own authorship

Figure 45: Coatings with 74% of fillers, applied over different interfaces, afer pyrolysis (SEM-15kV-10-24mmWD-SE).

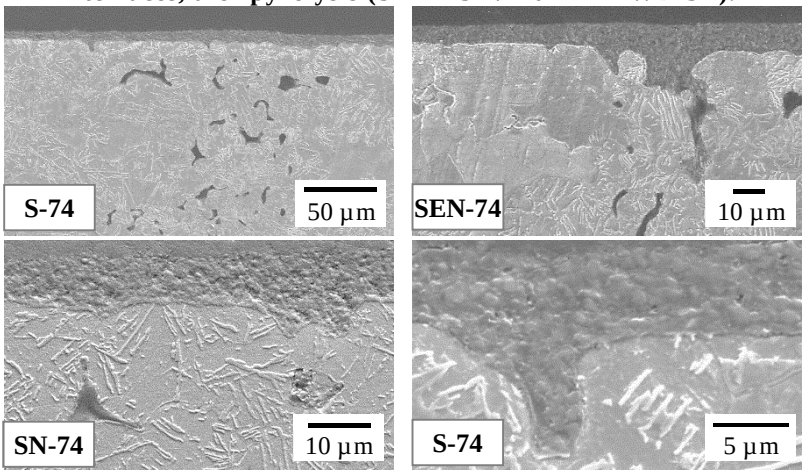

Source: Own authorship

After pyrolysis of carbon rich PCSZ precursor systems like HTTS, the derived ceramics are generally amorphous, composed of mixed SiC_xN_y (x+y=4) tetrahedral and SiC_4 units (GREGORI et al., 2005; SEIFERT et al., 2016; TRASS et al., 2000). Beyond a free carbon phase,

which amount strongly depends upon molecular precursor architecture (TRASSL et al., 2002).

Nevertheless, X-ray diffraction analysis of pyrolyzed coatings did not revealed the typical halo, with one or two broad maxima expected from amorphous structures (CULLITY, 1978), as presented comparatively in Figure 46. Presumably, due to thickness and reduced precursor amount of produced coatings, however, an increased background noise noted up to approximately 50º (2θ) might be associated to the SiCN amorphous phase.

Figure 46: Diffraction patterns of coated samples after pyrolisis.

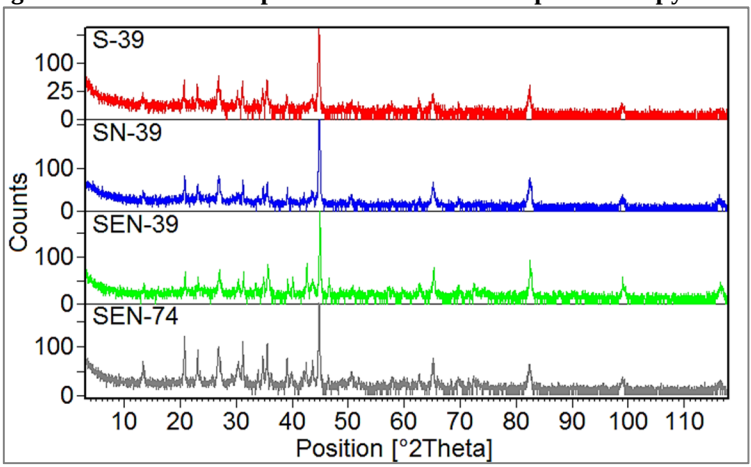

Source: Own authorship

The peaks, characterized in Figure 47, originate from added fillers, hexagonal boron and silicon nitride, beyond body centered cubic iron from substrate. Observed small variations of peak intensity among composites were correlated with filler amount and coating thickness variations, e.g., in Figure 46 increased peaks up to 50º of SEN-74 sample (9.45±0.83μm) in comparison with the SEN-39 sample (6.18±1.11μm).

Regarding surface modifications, no significant differences were observed in diffraction patterns between sintered and nitrided interfaces, indicating the decomposition (diffusion of nitrogen into substrate and or coating) of previously characterized nitrides γ´-Fe_4N and ε-$Fe_{2-3}N$ during pyrolysis. Results in accordance with literature that indicates, at temperatures above 580ºC, an evolution of ε-nitride into γ´-phase with

thermal stability up to 650ºC (ALVES JUNIOR, 2011; FIGUEIREDO, R., 1991).

Figure 47:Diffraction pattern of SEN-74 composite, after pyrolysis.

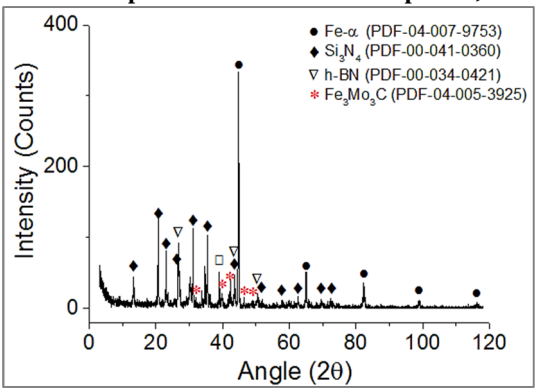

Source: Own authorship

Notwithstanding, interfaces containing mixed carbonitrides revealed maintenance of phase (Fe_3Mo_3C and/or Fe_3Mo_3N), characterized mainly due to exclusive peaks presence in the region around 40º, when compared with SN or S interfaces, region zoomed in Figure 48.

Figure 48: Peaks of carbonitrides indicated on SEN interfaces.

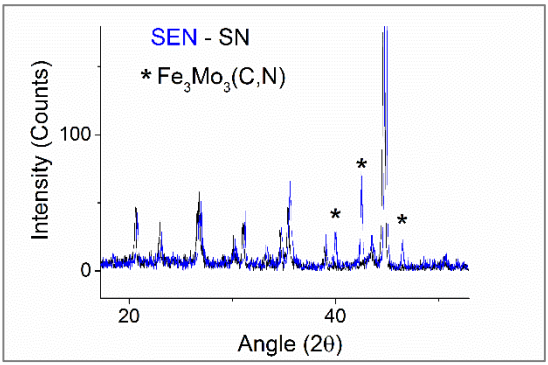

Source: Own authorship

Cross section analysis under SEM corroborated such results, revealing the presence of Mo-rich precipitates in a small depth below the coatings of SEN samples, indicated in Figure 49, regardless of coating

composition. Due to its reduced size, it was not possible to determine the microhardness of the discussed phase, constituted mainly by iron (~50wt.%), molybdenum (~30wt.%) and carbon (~20wt.%) accordingly to EDS results.

Figure 49: Micrographs comparison of interfaces after pyrolysis, (SEM-10-15mmWD-SE on left and BSE on right side).

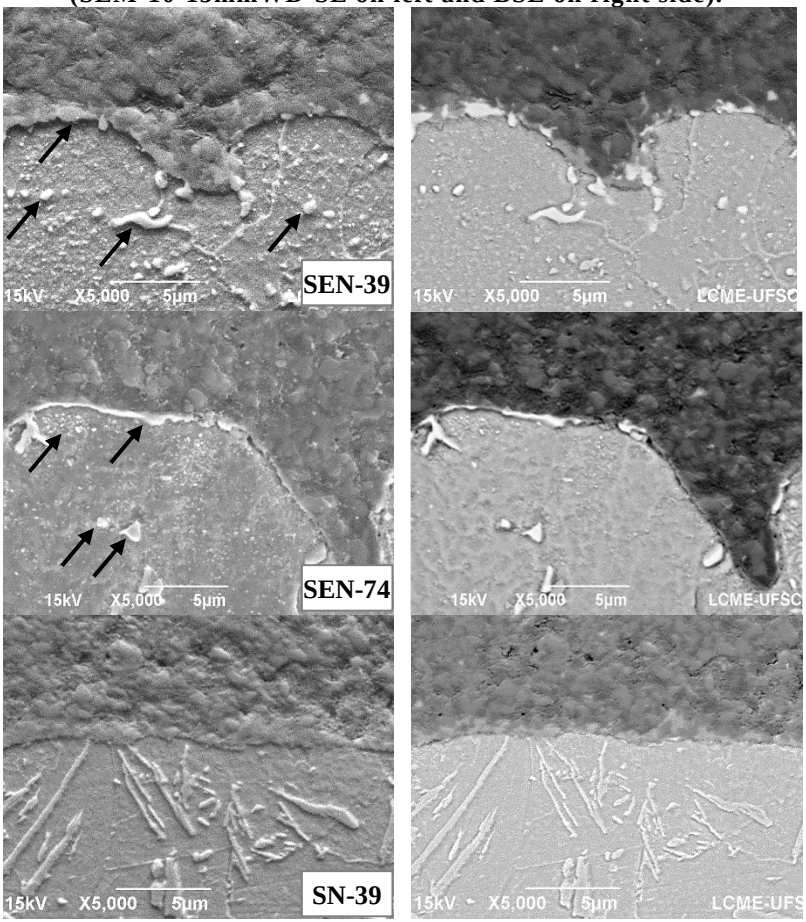

Source: Own authorship

Chemical analysis, carried by EDS on coatings of all composites, identified essentially silicon, carbon, nitrogen and oxygen. The first were expected from coating and fillers chemical composition beyond

suggesting oxygen incorporation, as reported in literature due to processing handling (SEIFERT et al., 2016).

Aforementioned results, corroborated by comparative elemental maps of coatings[3], suggest that after pyrolysis no considerably diffusion of elements from substrate and surface modifications occurred to coatings and vice versa. The nitrogen distribution, pointed out the absence of previously observed nitrided layer on SN composites, in accordance with already discussed X-ray diffraction results after pyrolysis

Also revealed a micro constituent evidenced by the oxygen distribution, clearly observed for sintered and nitrided interfaces (S and SN) and presented in Figure 50, indicating a concentration between coating and substrate. The trend can be related to a possible iron oxide formation at the surface during pyrolysis, due to its high negative Gibbs energy (GALE; TOTEMEIER, 1992), also observed on interfaces between coatings and substrates in Figure 44(S-39) and Figure 49(SN-39) previously presented.

Figure 50: Comparative of all coating elements on composites, SN-74 and SEN-74, after pyrolysis (SEM-20kV-15mmWD-SE).

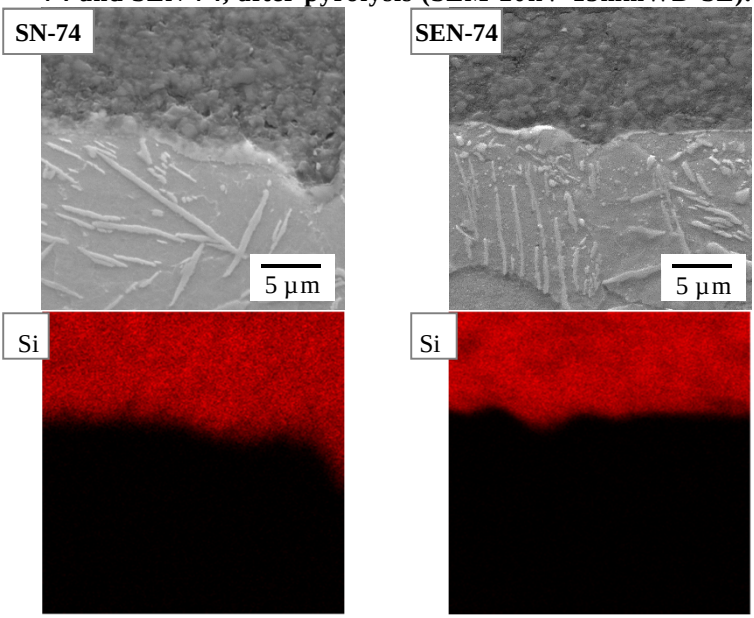

[3] Presented in detail in Appendix, Figure 71 to 73.

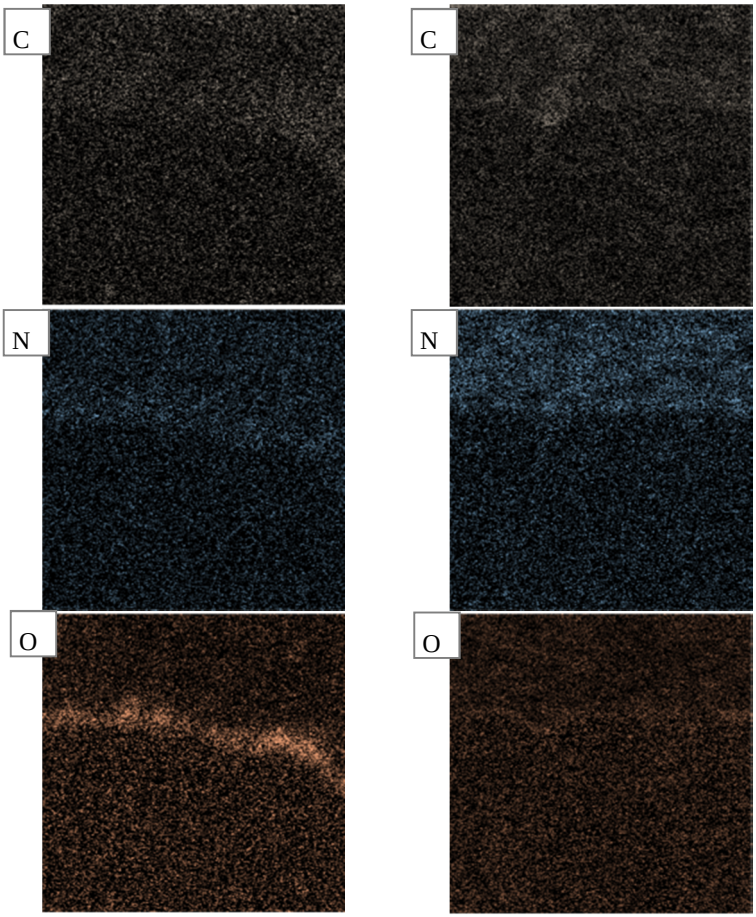

Source: Own authorship

Similar analyses concerning the substrate, presented in Figure 51, revealed a good homogenization of substrate alloy elements (Fe, Ni and Mo). Except for enriched and nitrided samples (SEN), which presented concentrated Mo spots inside a distinct surface depth, presumably related to partial conservation of Fe-Mo carbonitrides phase.

Another microstructural feature observed on SEN interfaces after pyrolysis is presented in Figure 52. Presumably, ferrite grains stabilized by Mo, the element was more concentrated above half of the grains and on precipitates, as indicated in Figure 73 in appendix.

Figure 51: Comparative of all interface elements on composites SN-74 and SEN-74 after pyrolysis, (SEM-20kV-15mmWD-SE).

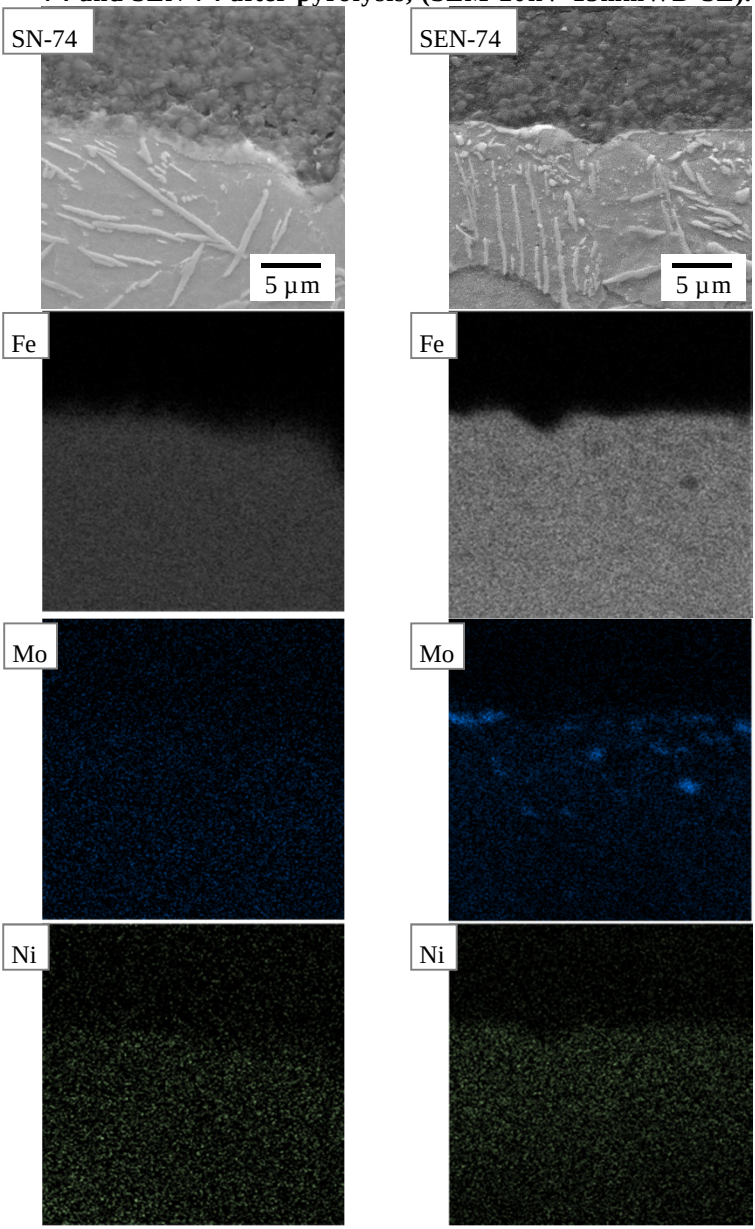

Source: Own authorship

Figure 52: Detail of SEN interfaces after pyrolysis (SEM-20kV-15mmWD-SE).

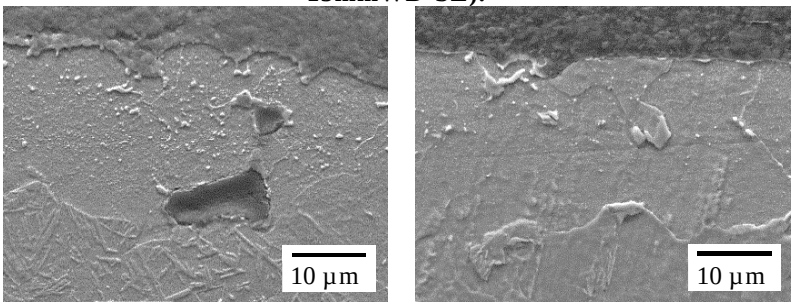

Source: Own authorship

Comparison of microhardness profiles of SN and SEN specimens after pyrolysis suggest absence of the surface hardening effect, plainly observed after thermochemical surface modifications in Figure 53. In accordance with microstructural evolution of the nitrided interface (SN), but not expected for the enriched and nitrided ones (SEN). After pyrolysis, the SEN condition revealed slightly decreased values up to a depth of approximately 10µm, in accordance with microhardness results of ferrite regions enriched with Mo.

Figure 53: Vickers microhardness profiles of SN and SEN samples, as a function of depth from samples surface.

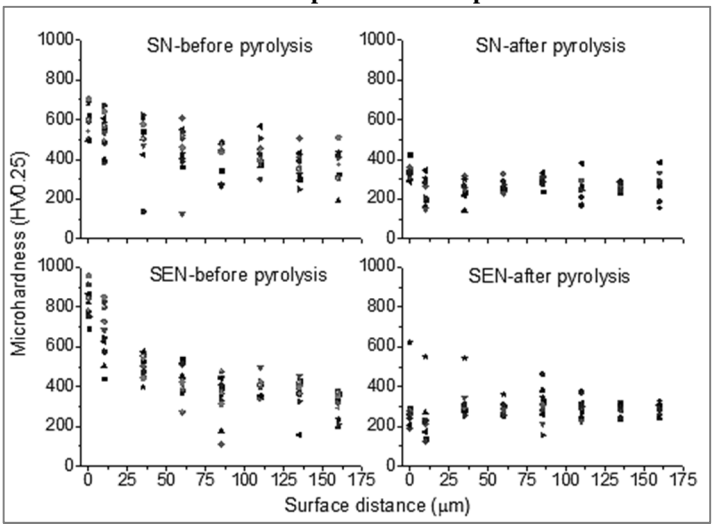

Source: Own authorship

Furthermore, it was not possible to evaluate with used equipment the microhardness of mixed carbides or carbonitrides, present mainly as a top layer of the substrate after pyrolysis, due to its reduced size.

4.4.2. Heat treated substrate

Concerning the material core and not the interfaces, the sequential post sintering treatments (namely surface modifications and pyrolysis) mainly when carried above the austenitic temperature, 679ºC during heating after sintering (JUSTUS, 2016), also led to metallurgical transformations of the substrate, with average final microhardness of 224±17(HV0.10) and hardness of 144±7HB.

The solid solution of Mo and C into iron retards the formation of pearlite and increases the alloy hardenability, respectively. Combined with used pyrolysis cooling rate, presumably allowed the precipitation of upper bainites, non-lamellar aggregates of ferrite and carbides, and some ferrite grains, indicated in Figure 54. Furthermore, nickel remained concentrated around the areas of original Ni particles, due to the low diffusion rate of Ni into iron (GALE; TOTEMEIER, 1992), and since was not previously pre alloyed as the iron molybdenum powder, for comparison.

Figure 54: Cross section of substrates after pyrolysis.

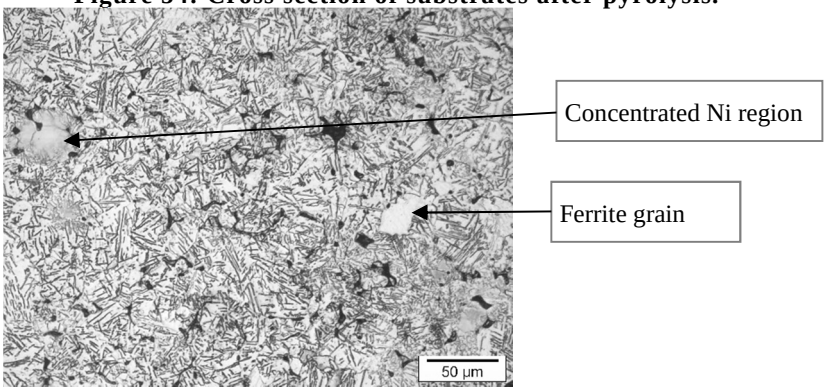

Source: Own authorship

Nickel is a stabilizer of iron austenite, and the carbon present in regions where the amount of nickel is not high enough to form austenite generates small amounts of martensite, even when cooling down rate is not high (HOGANÄS, 1999). A better homogenization of nickel

presumably decreases the austenite and increases the martensite phase amount, which is in accordance with the microhardness raise of such phases from 410±56 to 530±46 (HV0.01) on samples before and after pyrolysis, respectively.

Microhardness profiles of sintered, coated and pyrolyzed samples, presented in Figure 55, revealed a dispersion of results accordingly to the phases characterized on samples substrate after pyrolysis (ferrite, bainite, austenite and martensite). As expected, the coating composition indicates no influence on such results.

Figure 55: Vickers microhardness profiles of sintered samples after pyrolysis, as function of depth from samples surface.

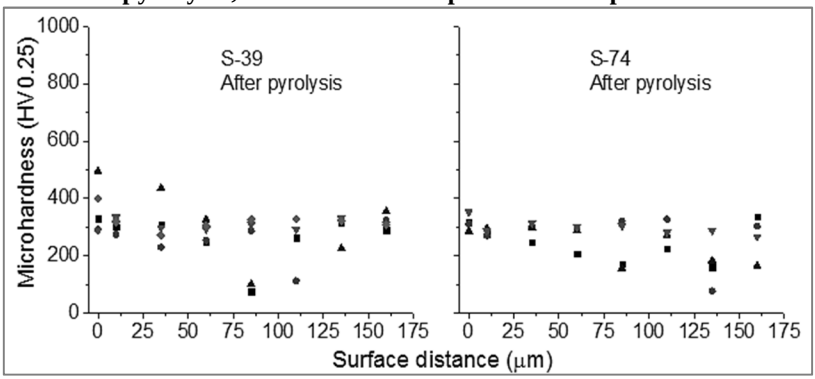

Source: Own authorship

4.4.3. Substrate friction behavior

In order to evaluate friction behavior changes, due to the metallurgical evolving of sintered steel, sliding tests were carried on uncoated substrates after sintering and after a second thermal treatment, which reproduced the pyrolysis parameters. The comparison presented in Figure 56 indicates two distinct sliding regimes, friction increasing in the initial period and ranging around an average value during the steady state regime, regardless of sample processing path.

During initial regime, the slight difference noted was related to the systemic character of surface interactions, nevertheless, the average friction coefficient calculated on the second regime was the same, 0.38±0.01, after sintering and second thermal treatment.

Observed average wear rates of substrates ($1.05\text{-}1.36 \times 10^{-4}$ $mm^3/N.m$) and counter-bodies ($1.15\text{-}1.33 \times 10^{-5}$ $mm^3/N.m$) were not

considered different at a 95% level of confidence. A slight increase of electrical resistance, also observed for both substrate conditions, was associated to the formation of an oxide tribo-layer at the interface of sintered substrate and the AISI52100 counter-body.

Figure 56: Friction coefficient and contact electrical resistance behavior of uncoated sintered samples.

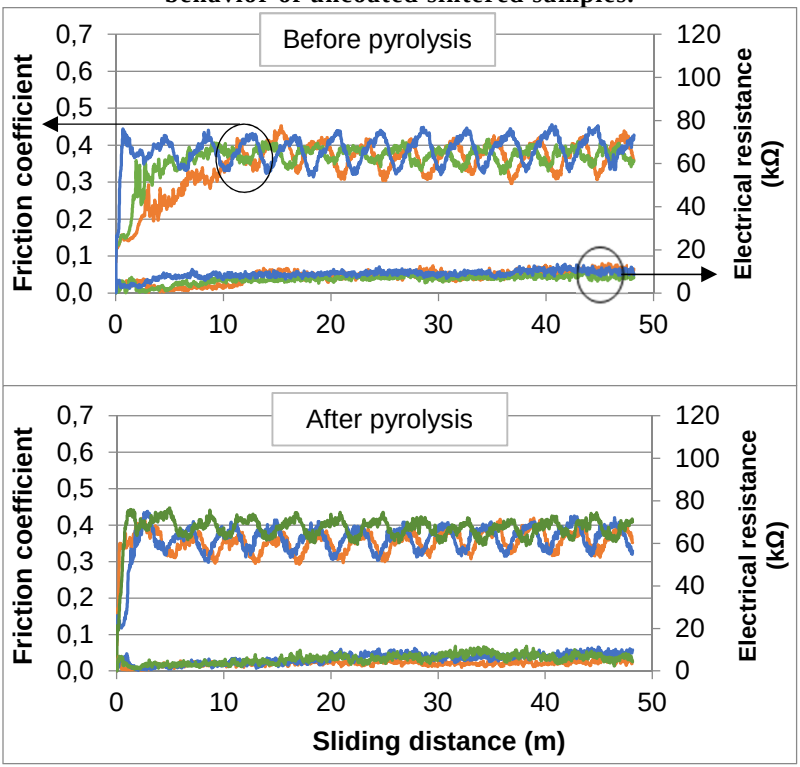

Source: Own authorship

4.4.4. Composites friction behavior

The friction behavior of all composites were very similar under the tested sliding condition and revealed a transition from an initial to a steady state regime. But, with increased averages when compared with the uncoated steel, as presented in Figure 57, where composites with highly loaded coatings (74vol.% of fillers) and modified interfaces are compared with an uncoated sintered steel.

Figure 57: Friction evolution of coated samples, with higher filler amount, as a function of sliding distance.

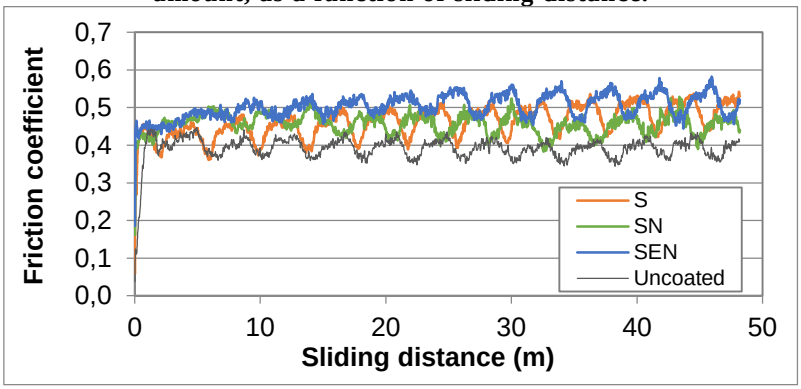

Source: Own authorship

The average steady state friction coefficient of composites and uncoated samples were above the lubricious regime (μ<0.2), despite coating composition or surface modification. Furthermore, the friction averages, presented in Figure 58, when analyzed by Anova tests were not considered different at a 95% level of confidence.

Figure 58: Average friction coefficient, calculated in the steady state regime.

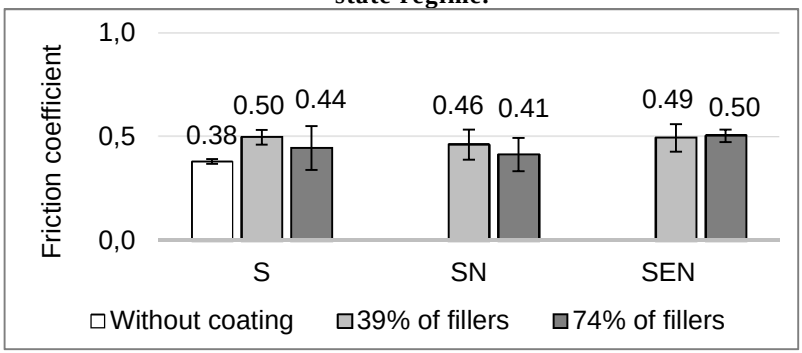

Source: Own authorship

The typical aspect of composites and uncoated steel after sliding tests, in Figure 59, contains an important information to understand the friction results. At the end of the tribological process, a metallic aspect was visually revealed inside all wear tracks. Which in turn, pointed to the

complete wear of both coatings (with 39 and 74 vol.% of fillers), regardless of surface modification.

Therefore, coating failure occurred during the transient regime, caused presumably by loading above a critical threshold value (CROSS et al., 2006), due to repeated surface interactions and surface and subsurface stresses developed at the interface (HOLMBERG; MATTHEWS; RONKAINEN, 1998).

Figure 59: Composites and sintered steel after sliding test.

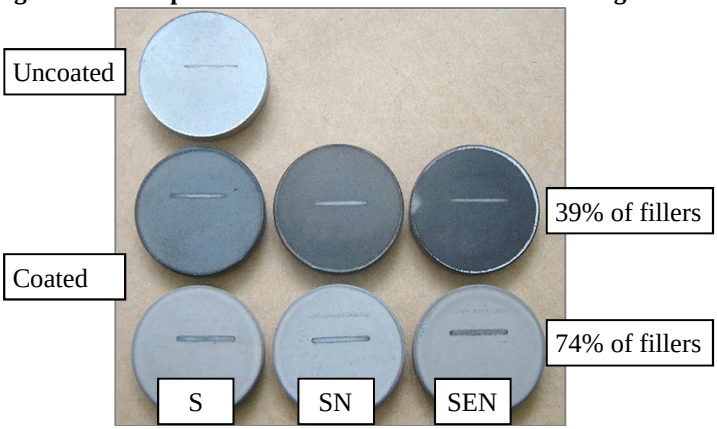

Source: Own authorship

The fracture toughness is an important material property in the friction of such ceramic coatings, with mechanical properties compared to brittle glasses and K_{1C} estimated in 0.7 $MPa.m^{-1/2}$, but dependent upon precursor, processing route and fine microstructure details (ROUXEL, 2010). Similar to most porous ceramic materials, fracture toughness of PDCs directly depend on porosity, and in the present case, also on the adhesion among particulate fillers and the SiCN phase, beyond fillers agglomeration in coatings microstructure, understood as discontinuities in the ceramic matrix.

Properties values of fully dense SiCN ceramics, in Table 6, were used to estimate a maximum contact pressure of 0.53GPa between the plane-sphere sliding geometry (coated surfaces against AISI 52100 sphere). Even considering the differences among atmosphere environments and final microstructures, the value is above the contact stress of 0.45GPa, associated to high friction and severe wear behavior of fully dense SiCN ceramic, pyrolyzed under similar conditions, but tested under N_2 atmosphere (CROSS et al., 2006).

The critical applied stress, achieved during load, presumably resulted in premature coating failure followed by generation, comminution and oxidation of wear particles from body and counter-body during sliding, forming an eventual tribo-layer. Such supposition, explains the similar friction average obtained for all composites, controlled by the substrate in combination with wear particles and environmental parameters.

Table 6: Data used for contact pressure estimation, in http://www.tribology-abc.com/sub10.htm

	Elasticity modulus	Poisson ratio	Radius of body geometry
AISI 52100	207GPa	0.29	5mm
PDC coating	97GPa	0.22	0

Source:(CROSS et al., 2006; JANAKIRAMAN; ALDINGER, 2009; MATWEB)

4.4.5. Contact electrical resistance

Differences on contact electrical resistance are dependent on the real contact area, and related to phenomenological details of contact mechanisms, not evaluated in the scope of this work. Yet, observed trends are presented to complement the discussion of the tribological composites behavior during sliding.

Results showed two distinct behavior directly related to the coating filler amount, indicated in Figure 60. The electrical resistance raised to a maximum value (<100kΩ) before decreasing, during the sliding of less filled coatings (a and b). In addition, started at increased values, before decreasing, when the surface was coated with more fillers (c). In both cases, it was indirectly possible to indicate the formation and/or degradation of a third body, which electrically insulates substrate and counter-body.

The differences observed mainly at the beginning of tests between coating composition, might be attributed to an increased load bearing capacity of the coating with higher filler amount and/or the presence of cracks in the less filled coatings, but as already mentioned, further investigations are necessary to infer causes. However, during the steady state regime, defined by the stabilization of electrical resistance among composites, the averages differences were significant for coated and uncoated samples, indicated in Figure 61.

Figure 60: Friction and electrical resistance evolution of coated samples, S-39(a), SEN-39(b) and SEN-74(c).

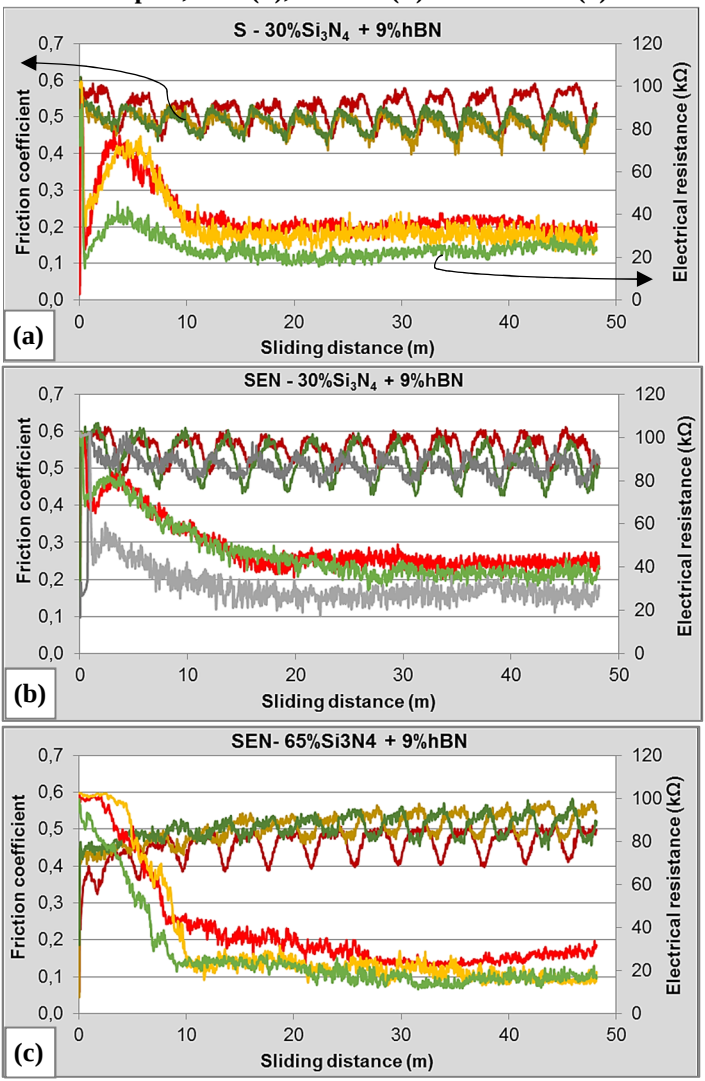

Source: Own authorship

The presence of the coating on surfaces increased the electrical resistance of the contact, presumably due to the presence of a tribo-layer

formed from wear and comminution of insulating coatings by the counter-body against the steel, under the testing atmosphere.

Figure 61: Average contact electrical resistance calculated in the permanent regime.

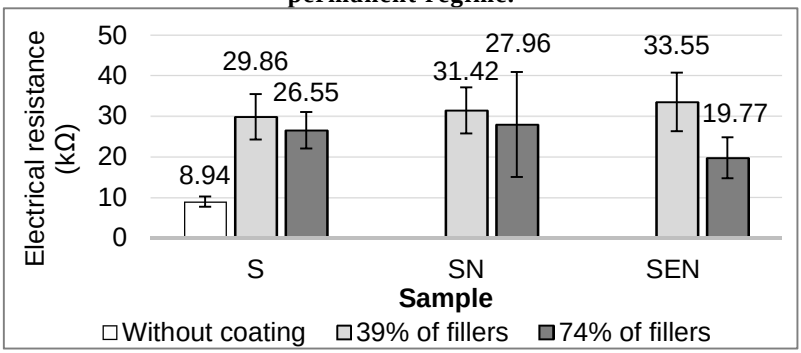

Source: Own authorship

4.4.6. Composites and counter-bodies wear rate

The drawback of precursor-derived ceramics is their brittle nature leading to a deterioration of their mechanical properties. The incorporation of fillers to form composites is an approach to reinforce the brittle ceramics, but in this work, led to an increase of composite wear rate, indicated in Figure 62. Statistically, the averages differences showed significance, when coated and uncoated samples and coating compositions were compared.

The increased wear rate of coated samples is explained by coating failure, accompanied by a third-body formation resultant from the removal and chemical reaction from the surfaces in contact and atmosphere, explained in sequence. The influence of Si_3N_4 amount on coating composites, can be related presumably to the formation of a more abrasive third-body (due to increased amount of abrasive particles). Metallic and nonmetallic wear debris may act abrasively and roughen the contacting surfaces, but formation of protective tribo-layers may lead to smoother surfaces again (ZUM GAHR, 1987).

The wear rate, among surface modifications, revealed average differences only for SEN composites, with higher wear rates, possibly related to the presence of hard carbonitrides or carbides, previously characterized, on the interface.

Figure 62: Average wear rate of composites as function of coatings composition and surface modification.

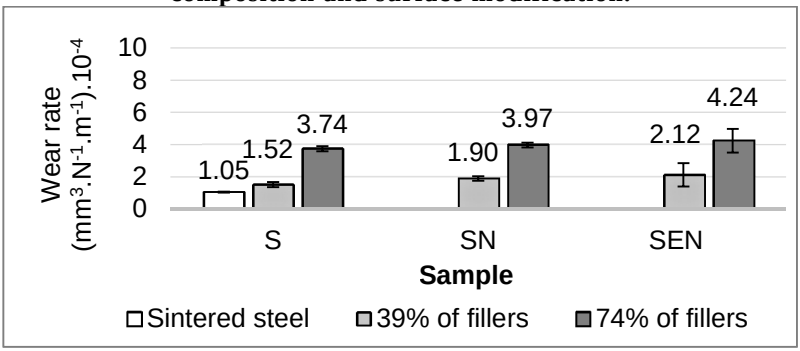

Source: Own authorship

On the other hand, concerning the associated wear of the counter-bodies presented in Figure 63, averages differences where only significant when sintered steel and coated samples were compared. The increased wear rate of the counter-bodies tested against coated samples was explained due to the presence of comminuted coating at the contact, acting as debris during sliding. Furthermore, no statistical influence of the Si_3N_4 coating amount on the wear rate of counter-bodies was observed (for the described tests parameters), presumably due to the higher wear resistance of the AISI52100 when compared to the sintered low alloy steel.

Figure 63: Average wear rate of counter-bodies.

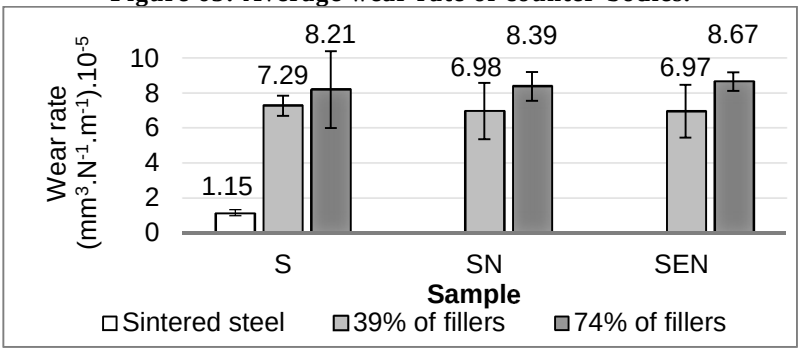

Source: Own authorship

4.4.7. Composites wear tracks investigation

Visually all wear tracks presented similar metallic appearance, suggesting the complete wear of coatings at the end of test. However, further investigation by SEM revealed particularities beyond common features between them. The wear tracks of sintered and uncoated samples, initially observed, are presented in Figure 64.

Figure 64: Wear tracks of sintered sample without coating, SEM-15kV-21mmWD-SE(a) and BSE (b).

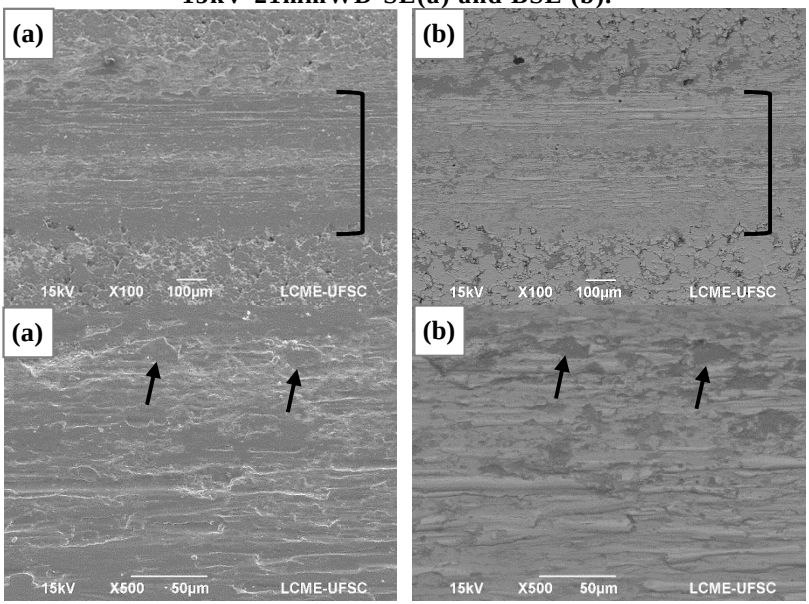

Source: Own authorship

Due to plastic deformation, from contact and relative sliding between body and counter-body delimited by brackets, pore closure and grooves can be observed in the same sphere sliding direction. Higher magnification suggested a material accumulation, indicated by arrows, derived from the plastic flow and counter-body material transfer. EDX microanalysis revealed a high degree of oxidation in these regions, and corroborated the material transfer from counter-body to the wear track, mainly due to detection of Cr from counter-bodies in these regions (Table 8 and 9 in Appendix). Presumably, this tribo-layer was formed from

oxides removal and ploughing of asperities from substrate and sphere, which, during sliding were further comminuted and oxidized.

Typical wear tracks of the composites, at different magnification under SEM, are presented in Figures 65 to 68. Qualitative analysis revealed apparently filled pores inside the wear track, observed as dark or white regions inside the wear track if observed using BSE or SE signals, in contrast to the pore closure on uncoated samples. Furthermore, the tracks observed with backscattered signal in Figure 65, indicated more wide tracks comparative to uncoated samples, in accordance with the wear rate results of composites and counter-bodies.

Figure 65: Wear track comparison of coated samples, as function of filler amount and interface (SEM-15kV-12-21mmWD-BSE).

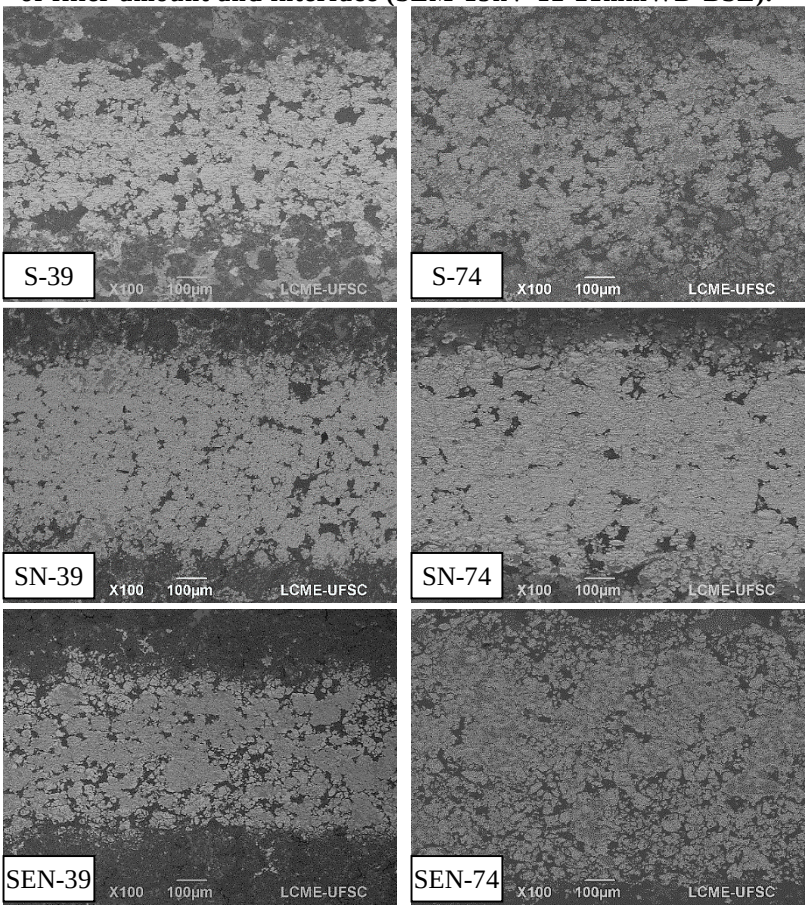

Source: Own authorship

Both surface modifications and coatings composition do not visually modified the smooth aspect of wear or material transfer among the composites, visualized in Figures 66 and 67 respectively.

Figure 66: Wear track details analyzed with secondary electrons signal (SEM-15kV-12-21mmWD).

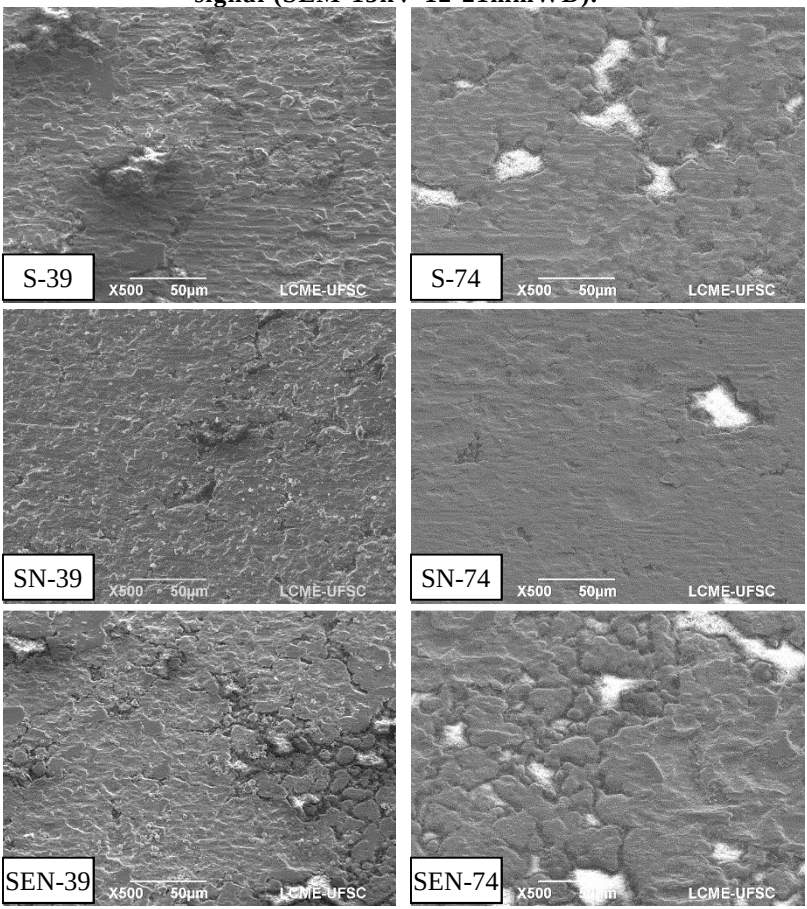

Source: Own authorship

Figure 67: Wear track details analyzed with backscattered electrons signal (SEM-15kV-12-21mmWD).

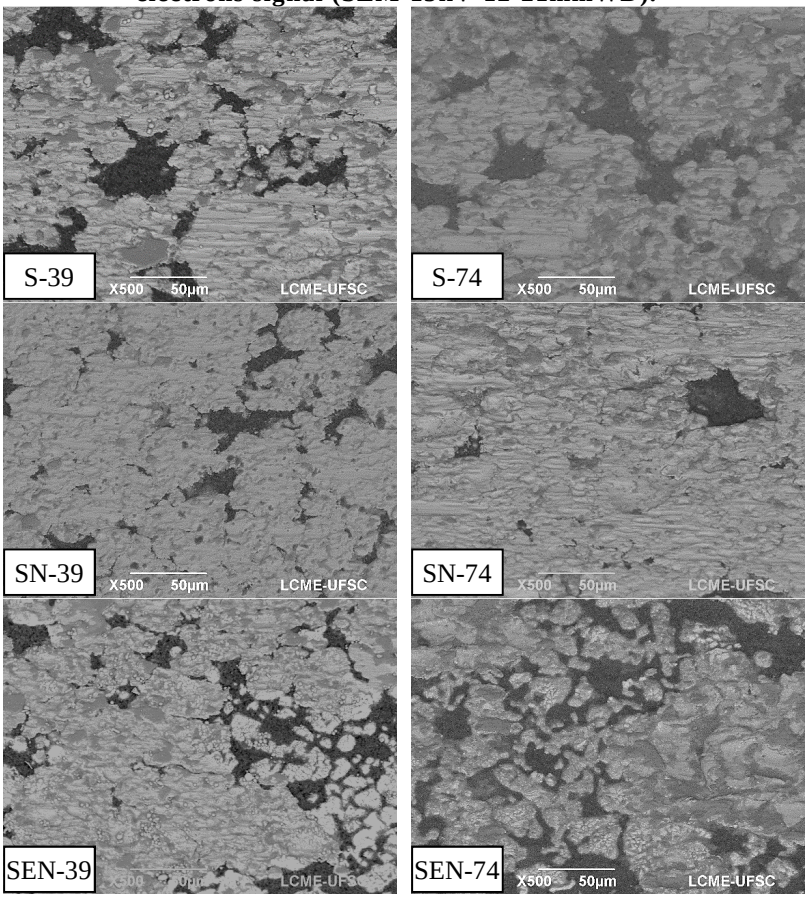

Source: Own authorship

The comparison indicated presence of common regions in the wear tracks of all samples, named A and B, and already discussed for the uncoated substrate. Other, shared only by coated samples, called C, and another exclusive of SEN composites, called D, all identified in Figure 68.

The spherical microstructural feature indicated with arrows, rich in Ni (~67wt.%) and Fe (~14wt.%), was observed only in wear tracks of composites containing the lower amount of Si_3N_4, and further investigations are necessary to clarify its source.

Figure 68: Characteristic regions (A, B C and D) in wear tracks, (SEM-15kV-16-21mmWD-BSE).

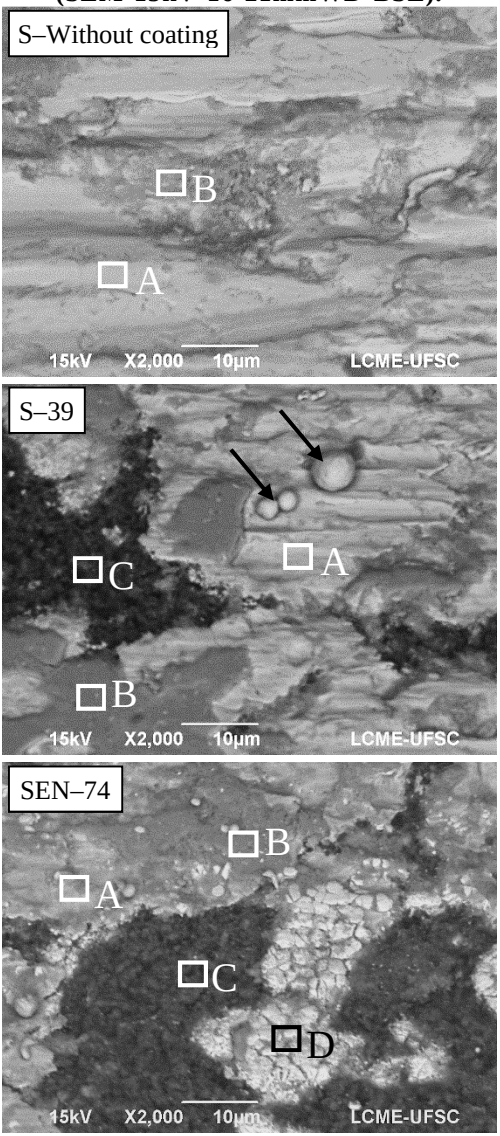

Source: Own authorship

4.4.7.1. Elemental analysis

To understand the observed regions in composites, wear tracks were also analyzed by X-ray microanalysis, comparatively presented in Figure 69. To identify material transfer between body (composite), counter-body (sphere) beyond tribo-chemical reactions (oxidation), the original chemical elements on the tribological pair were identified as presented in Table 7. After analyses, the main chemical elements in each region of every composite, detailed in Table 8 to 11 in Appendix, were classified among elements presented mainly in the substrate, coating or counter-body.

Table 7: Original chemical elements present in the tribological system before sliding.

	Fe	Ni	Mo	Cr	Mn	S	P	Si	C	N	B
Coating								■	■	■	■
Substrate	■	■	■						■		
Sphere	■			■	■	■	■	■	■		

Source: Own authorship

As already described, regions A and B were common to all samples, the first was composed mainly by substrate elements (Fe+Ni+Mo) and oxygen, beyond coating elements (Si+C) for coated samples. Region B presented a combination of elements from substrate (Fe+Ni), sphere (Fe+Cr) and coating (C+Si), with comparatively higher oxygen content. Confirming the hypothesis of a third-body formation from coating failure, comminution and oxidation, which contributed to the increased tribo-chemical wear of composites, in comparison with non-coated samples.

Characterized as original pores filled with coatings, region C was composed of coating elements (Si+N+C) and oxygen. While region D, as the bimetallic carbonitrides or carbides remaining from the sequential thermochemical treatment of Mo enrichment and nitriding, in accordance with X-Ray diffraction results. The increased wear rates of the SEN composites in combination with observed cracks indicated in the $Fe_3Mo_3(C,N)$ regions, indicate that such hard phase contributed to the third body formation, also confirmed by the increased Mo amount in the tribo-layer (region B) of these composites.

Figure 69: Characteristic regions observed in wear tracks of coated samples (SEM-12-21mmWD).

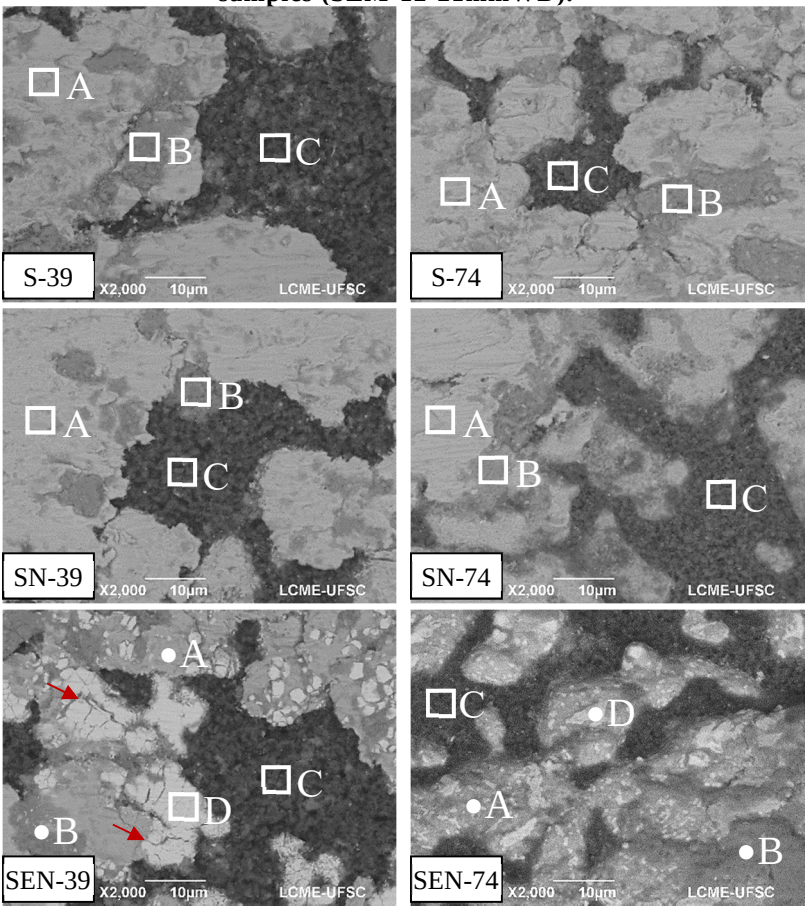

Source: Own authorship

4.4.8. Final tribological considerations

When tribological results of the sintered steel were compared with the composites, it was observed:

- **No influence on the friction coefficient**: For the regime where the averages were calculated the coatings were already worn, and the major contribution to the friction coefficient behavior was from the substrate but controlled by the formed third-body.

- **An increase of wear rate of coated samples and its counter-bodies**: Explained due to the presence of an oxidized mixture of coating, substrate and counter-body, deformed and comminuted at the contact during sliding. The third-body was indirectly indicated by an increase in contact electrical resistance in comparison with the sintered steel, even when calculated during the permanent regime.
- **Maintenance of open porosity inside the wear track fulfilled with coating and wear with tribo-chemical character.**
- **Wear tracks were composed mainly of deformed substrate (A) and a third body (B), composed of oxygen, elements from substrate, coatings and counter-body**: Furthermore, coated samples revealed wear tracks with porosity fulfilled with coating and carbides presence on SEN composites

On the other hand, comparing the tribological response of the composites, it was noted;

- **A decrease of contact electrical resistance, during steady state, with the increase of coating filler amount**: Possibly related to the formation of a more abrasive third-body, which might had increased the real contact between the wear track and the sphere.
- **An increase of composites wear rate, with the raise of Si_3N_4 amount in coating composition**: The increased amount of this filler, after coating fracture, possibly supplied more hard particles to the contact during sliding. However, there were no influence of the Si_3N_4 amount on the counter-bodies wear rate (statistical analysis with 95% of confidence level), certainly due to higher wear resistance of AISI52100 in comparison with the sintered steel.
- **Increased wear rates of SEN interfaces**: Due to the presence of hard ternary carbonitrides or carbides at the interface, acting as another debris source, incorporated to the third-body during sliding, after fracture and comminution against the counter-body.

Therefore; despite the use of an increased amount of filler (74 vol.%) allowed the successful obtainment of homogeneous and crack-free ceramic coatings onto sintered substrates, such coatings did not presented a satisfactory tribological response when evaluated under tested

conditions. The author's perception after the development of this work indicates two possible ways to give research continuity:

a) Development of composite coatings using the same processing route for other applications, loaded poly(organo)silazane coatings might present potential tribological results in situations of lower contact pressure, as in conforming contact applications or even under compression solicitations;
b) In view of the results obtained with the plasma assisted pyrolysis (PAP) technology (SEIFERT et al., 2016), the development of composite coatings for tribological applications with active fillers to promote adhesion among SiCN matrix and fillers, making use of PAP technology for pyrolysis.

5. CONCLUSIONS

About the thermochemical surface modifications of sintered steel:

- Plasma assisted nitriding resulted in the formation of a white layer, with thickness of ~7μm, composed mainly by γ´-Fe_4N and ε-$Fe_{(2-3)}$(C,N) and hardness of approximately 600HV;
- Simultaneous plasma assisted sintering and Mo enrichment resulted in the formation of bimetallic carbides (Fe_3Mo_3C) dispersed on the surface of the substrate;
- Subsequent nitriding of sintered and surface enriched samples led to the formation of a discontinuous carbonitride (Fe_3Mo_3(C,N)) layer (~1 μm), with increased surface hardening effect in comparison with formed iron nitrides (~800HV);
- The iron nitrides were thermally decomposed after pyrolysis, unlike Fe_3Mo_3(C,N) despite the surface hardening absence;

Concerning the coating development and processing over sintered substrates:

- The increase of filler amount monotonically decreased the mass loss of composite coatings, decreased coatings heterogeneity and avoided the spalling
- Processing parameters used in the PDC route led to coating thicknesses below 10μm;
- Both coatings presented pores and a proper filling into the substrate, but the coating with 39 vol.% of fillers presented cracks;
- The increased filler addition allowed the successful obtainment of homogeneous, free of macro and cohesive cracks, ceramic coatings over sintered substrates.

And the tribological evaluation of composites:

- The average steady state friction coefficient of composites were above the lubricious regime ($\mu < 0.2$), despite coating composition or surface modification;
- Sliding tests with maximum contact pressure of 0.53GPa, under dry environment, caused failure of both coatings, which were

deformed and comminuted by substrate and counter-body, while oxidized by atmosphere, during sliding;

- Composites formed tribo-layers during sliding, were composed of oxygen, elements from substrate, coatings and counter-body;
- Formed tribo-layers increased wear rates of composites and counter-bodies in relation to the uncoated sintered steel;
- The interface enriched with molybdenum and nitrided increased the wear rate of composites, by providing carbides or carbonitrides particles, to the contact during sliding.

6. FUTURE WORKS

- Investigation of abrasive resistance of developed composites;
- Tribological investigation of plasma generated carbide and carbonitride layers over the sintered steel;
- Development of composite coating with active filler to promote adhesion among SiCN matrix and fillers, making use of PAP technology (SEIFERT et al., 2016);
- Deposition and pyrolysis of pure polysilazane precursors on metallic surfaces, for tribological evaluations, by the use of plasma technology.

7. REFERENCES

50 years of the Jost Report. Disponível em: <http://explore.tandfonline.com/page/est/50-years-of-the-jost-report>. Acesso em: 20 set. 2016.

ALCONCHEL, S. et al. Chemistry of interstitial molybdenum ternary nitrides MnMo3N (M=Fe, Co, n=3; M=Ni, n=2). **Journal of Materials Chemistry**, v. 8, n. 8, p. 1901–1909, 1998.

ALCONCHEL, S.; SAPINA, F.; MARTINEZ, E. From nitrides to carbides: topotactic synthesis of the [small eta]-carbides Fe3Mo3C and Co3Mo3C. **Dalton Transactions**, n. 16, p. 2463–2468, 2004.

ALVES JUNIOR, C. **Nitretação a plasma: fundamentos e aplicações**. Natal: EDUFRN, 2011.

AMOUZOU, D. et al. Formation of Me–O–Si covalent bonds at the interface between polysilazane and stainless steel. **Applied Surface Science**, v. 320, p. 519–523, 30 nov. 2014.

BAKUMOV, V. et al. Mechanical and tribological properties of polymer-derived Si/C/N sub-millimetre thick miniaturized components fabricated by direct casting. **Journal of the European Ceramic Society**, v. 32, n. 8, p. 1759–1767, jul. 2012.

BARROSO, G. et al. Functional Coatings Based on Preceramic Polymers . **Advanced Engineering Materials**, v. 18, n. 5, p. 746–753, 1 maio 2016.

BARROSO, G. S.; KRENKEL, W.; MOTZ, G. Low thermal conductivity coating system for application up to 1000 °C by simple PDC processing with active and passive fillers. **Journal of the European Ceramic Society**, v. 35, n. 12, p. 3339–3348, out. 2015.

BENDO, T. et al. Nitriding of surface Mo-enriched sintered iron: Structure and morphology of compound layer. **Surface and Coatings Technology**, v. 258, p. 368–373, 15 nov. 2014.

BENDO, T. et al. The effect of Mo on the characteristics of a plasma nitrided layer of sintered iron. **Applied Surface Science**, v. 363, p. 29–36, 15 fev. 2016.

BHUSHAN, B. **Modern Tribology Handbook**. Columbus: CRC Press, 2000.

BHUSHAN, B. **Principles and applications of tribology**. First ed. Columbus: John Wiley & Sons, Ltd., 2013.

BINDER, R. et al. **Plasma process and reactor for treating metallic pieces**WO, 2009.

BOCHINNI, G. F. Influence of Porosity on the Characteristics of Sintered Materials. **International Journal of Powder metallugy**, v. 22, p. 185–202, 1986.

BUNSHAH, R. F. **Handbook of deposition technologies for films and coatings**. 2nd. ed. New Jersey: Noyes Publication, 1994.

BUSCH, C. Solid Lubrication. In: **Lubricants and Lubrication**. Weinheim: Wiley-VCH Verlag GmbH & Co. KGaA, 2007. p. 694–714.

CAPES. **Programa Bragecrim**. Disponível em: <http://www.capes.gov.br/cooperacao-internacional/alemanha/bragecrim>. Acesso em: 18 set. 2016.

CARRAPICHANO, J. M.; GOMES, J. R.; SILVA, R. F. Tribological behaviour of Si3N4–BN ceramic materials for dry sliding applications. **Wear**, v. 253, n. 9–10, p. 1070–1076, nov. 2002.

CHAPMAN, B. **Glow Discharge Processes: Sputtering and Plasma Etching**. New York: Wiley, 1980.

CHEN, Q.; LI, D. Y.; COOK, B. Is porosity always detrimental to the wear resistance of materials?—A computational study on the effect of porosity on erosive wear of TiC/Cu composites. **Wear**, v. 267, n. 5–8, p. 1153–1159, 15 jun. 2009.

CHEN, W. et al. Tribological characteristics of Si3N4–hBN ceramic materials sliding against stainless steel without lubrication. **Wear**, v. 269, n. 3–4, p. 241–248, 18 jun. 2010.

COAN, T. et al. A novel organic-inorganic PMMA/polysilazane hybrid polymer for corrosion protection. **Progress in Organic Coatings**, v. 89, p. 220–230, dez. 2015.

COLOMBO, P. et al. Polymer-Derived Ceramics: 40 Years of Research and Innovation in Advanced Ceramics. **Journal of the American Ceramic Society**, v. 93, n. 7, p. 1805–1837, 2010.

COLOMBO, P.; PAULSON, T. E.; PANTANO, C. G. Synthesis of Silicon Carbide Thin Films with Polycarbosilane (PCS). **Journal of the American Ceramic Society**, v. 80, n. 9, p. 2333–2340, 1 set. 1997.

CROSS, T. et al. **Fabrication process for ultra high aspect ratio polysilazane-derived MEMS**. Technical Digest. MEMS 2002 IEEE International Conference. Fifteenth IEEE International Conference on Micro Electro Mechanical Systems (Cat. No.02CH37266). **Anais**...Las Vegas: IEEE, 2002Disponível em: <http://ieeexplore.ieee.org/lpdocs/epic03/wrapper.htm?arnumber=984232>

CROSS, T. et al. Mechanical and Tribological Behavior of Polymer-Derived Ceramics Constituted from SiCxOyNz. **Journal of the American Ceramic Society**, v. 89, n. 12, p. 3706–3714, 1 dez. 2006.

CROSS, T.; PRASAD, S.; RAJ, R. **Friction and Wear Behavior of Silicon Carbonitride Processed From the Polymer-Derived Ceramic Route**. World Tribology Congress III, Volume 2. **Anais**...Washington, D.C.: ASME, 2005Disponível em: <http://proceedings.asmedigitalcollection.asme.org/proceeding.aspx?articleid=1579143>

CULLITY, B. D. **Elements of X-Ray diffraction**. 2nd. ed. Massachusetts: Addison-Wesley Publishing Company, 1978.

DANNINGER, H.; GIERL-MAYER, C. Advanced powder metallurgy steel alloys. In: **Advances in Powder Metallurgy**. Oxford: Woodhead Publishing, 2013. p. 149–201.

DE MELLO, J. D. B.; HUTCHINGS, I. M. Effect of processing parameters on the surface durability of steam-oxidized sintered iron. **Wear**, v. 250, n. 1–12, p. 435–448, out. 2001.

DFG. **7th Annual Meeting of BRAGECRIM in Porto Alegre and Bento Gonçalves**. [s.l: s.n.]. Disponível em: <http://www.dfg.de/en/dfg_profile/head_office/dfg_abroad/latin_america/reports/2015/151027_bragecrim/index.html>. Acesso em: 18 set. 2016.

DONNET, C.; ERDEMIR, A. Historical developments and new trends in tribological and solid lubricant coatings. **Surface and Coatings Technology**, v. 180–181, p. 76–84, 1 mar. 2004.

DUBRUJEAUD, B.; VARDAVOULIAS, M.; JEANDIN, M. The role of porosity in the dry sliding wear of a sintered ferrous alloy. **Wear**, v. 174, n. 1, p. 155–161, 1994.

ERDEMIR, A. Solid Lubricants and Self-Lubricating Films. In: **Modern Tribology Handbook, Two Volume Set**. Mechanics & Materials Science. Columbus: CRC Press, 2000. p. 787–825.

ERDEMIR, A. Review of engineered tribological interfaces for improved boundary lubrication. **Tribology International**, v. 38, n. 3, p. 249–256, mar. 2005.

ERDEMIR, A.; MARTIN, J.-M. Introduction. In: MARTIN, A. E.-M. B. T.-S. (Ed.). . Amsterdam: Elsevier Science B.V., 2007. p. xvii–xix.

FIGUEIREDO, R., S. **Análise de superfície em aços nitretados por espectroscopia Mossbauer**. [s.l.] Universidade Federal de Santa Catarina, 1991.

FLORES, O. et al. Selective cross-linking of oligosilazanes to tailored meltable polysilazanes for the processing of ceramic SiCN fibres. **Journal of Materials Chemistry A**, v. 1, n. 48, p. 15406–15415, 2013.

FLORES, O.; HEYMANN, L.; MOTZ, G. Rheological behaviour of tailored polysilazane melts for the processing of SiCN ceramics: viscoelastic properties and thermal stability. **Rheologica Acta**, v. 54, n. 6, p. 517–528, 2015.

FURLAN, K. P. **Development of a self-lubricant composite containing MoS2 (In Portuguese)**. [s.l.] Federal University of Santa Catarina, 2016.

GALE, W. F.; TOTEMEIER, T. C. (EDS.). General physical properties. In: **Smithells Metals Reference Book**. 7th. ed. Oxford: Elsevier, 1992. p. 14-1-14–43.

GRAHAM, A. H. . et al. **The effect of nickel content,sintering temperature and density on the properties of a warm compacted 0.85 w/o molybdenum prealloy**. International Conference on Powder Metallurgy & Particulate Materials. **Anais**...Chicago, USA: 1997

GREGORI, G. et al. Microstructure evolution of precursors-derived SiCN ceramics upon thermal treatment between 1000 and 1400 °C. **Journal of Non-Crystalline Solids**, v. 351, n. 16–17, p. 1393–1402, 1 jun. 2005.
GREIL, P. Active-Filler-Controlled Pyrolysis of Preceramic Polymers. **Journal of the American Ceramic Society**, v. 78, n. 4, p. 835–848, 1 abr. 1995.
GREIL, P. Polymer Derived Engineering Ceramics. **Advanced Engineering Materials**, v. 2, n. 6, p. 339–348, 2000.
GREIL, P. Pyrolysis of Active and Passive Filler-loaded Preceramic Polymers. In: ALDINGER, F. et al. (Eds.). . **Handbook of Advanced Ceramics**. Oxford: Elsevier, 2003. p. 369–390.
GREIL, P. Advancements in Polymer-Filler Derived Ceramics. **Journal of the Korean Ceramic Society**, v. 49, n. 4, p. 279–286, 31 jul. 2012.
GÜNTHNER, M. et al. Advanced coatings on the basis of Si(C)N precursors for protection of steel against oxidation. **Journal of the European Ceramic Society**, v. 29, n. 10, p. 2061–2068, 2009a.
GÜNTHNER, M. et al. Particle-Filled PHPS Silazane-Based Coatings on Steel. **International Journal of Applied Ceramic Technology**, v. 6, n. 3, p. 373–380, 1 maio 2009b.
GÜNTHNER, M. et al. High performance environmental barrier coatings, Part I: Passive filler loaded SiCN system for steel. **Journal of the European Ceramic Society**, v. 31, n. 15, p. 3003–3010, dez. 2011.
GÜNTHNER, M. et al. Conversion behaviour and resulting mechanical properties of polysilazane-based coatings. **Journal of the European Ceramic Society**, v. 32, n. 9, p. 1883–1892, jul. 2012.
HAMMES, G. et al. Fe-hBN Composites Produced by Double Pressing and Double Sintering. **Materials Science Forum**, v. 802, p. 311–316, 2014a.
HAMMES, G. et al. Effect of double pressing/double sintering on the sliding wear of self-lubricating sintered composites. **Tribology International**, v. 70, p. 119–127, fev. 2014b.
HAYS, G. F. Now is the time - Corrosion, processes and advanced materials in industry. **Advanced Materials Research**, v. 95, p. 1–2, 2010.
HOGANÄS. Metallography. In: **Höganäs Handbook for Sintered Components**. [s.l.] Höganäs, AB, 1999.
HOLMBERG, K. et al. Global energy consumption due to friction in trucks and buses. **Tribology International**, v. 78, p. 94–114, out. 2014.
HOLMBERG, K.; ANDERSSON, P.; ERDEMIR, A. Global energy consumption due to friction in passenger cars. **Tribology International**, v. 47, p. 221–234, mar. 2012.
HOLMBERG, K.; MATTHEWS, A.; RONKAINEN, H. Coatings tribology — contact mechanisms and surface design. **Tribology International**, v. 31, n. 98, p. 107–120, 1998.
HUTCHINGS, I. . **Tribology - Friction and wear of engineering materials**.

[s.l.] Butterworth-Heinemann, 1992.
IONESCU, E.; RIEDEL, R. Polymer Processing of Ceramics. In: **Ceramics and Composites Processing Methods**. [s.l.] John Wiley & Sons, Inc., 2012. p. 235–270.
JAMES, W. B. **What is sinter-hardening?** International Conference on Powder Metallurgy & Particulate Materials. **Anais**...Las Vegas: 1998
JANAKIRAMAN, N.; ALDINGER, F. Fabrication and characterization of fully dense Si-C-N ceramics from a poly(ureamethylvinyl)silazane precursor. **Journal of the European Ceramic Society**, v. 29, n. 1, p. 163–173, 2009.
JUSTUS, T. D. D. **Aplicação e caracterização de revestimento PDC resistente a oxidação em aço sinterizado**. [s.l.] Federal University of Santa Catarina, 2016.
KLAFFKE, D. et al. Tribological characterisation of siliconcarbonitride ceramics derived from preceramic polymers. **Wear**, v. 260, n. 7–8, p. 711–719, 2006.
KLEIN, A. N. et al. DC Plasma Technology Applied to Powder Metallurgy: an Overview. **Plasma Science and Technology**, v. 15, n. 1, p. 70–81, jan. 2013.
KRAUS, T. et al. cBN particle filled SiCN precursor coatings. **Advances in Applied Ceramics**, v. 108, n. 8, p. 476–482, 1 nov. 2009.
KROKE, E. et al. Silazane derived ceramics and related materials. **Materials Science and Engineering: R: Reports**, v. 26, n. 4–6, p. 97–199, abr. 2000.
LANCASTER, J. K. A review of the influence of environmental humidity and water on friction, lubrication and wear. **Tribology International**, v. 23, n. 6, p. 371–389, dez. 1990.
LIEW, L.-A. et al. Fabrication of SiCN ceramic MEMS using injectable polymer-precursor technique. **Sensors and Actuators A: Physical**, v. 89, n. 1–2, p. 64–70, 20 mar. 2001.
LIEW, L.-A. et al. Fabrication of SiCN MEMS by photopolymerization of pre-ceramic polymer. **Sensors and Actuators A: Physical**, v. 95, n. 2, p. 120–134, 2002.
LUKACS, A. Polysilazane precursors to advanced ceramics. **American Ceramic Society Bulletin**, v. 86, n. 1, p. 9301–9306, 2007.
MACHADO, R. et al. **Industrial plasma reactor for plasma assisted thermal debinding of powder injection-molded parts**WO, 2006.
MALISKA, A. M. (FEDERAL U. OF S. C. **Influência de elementos de liga e do oxigênio no processo de nitretação por plasm a em aços sinterizados**. [s.l.] Federal University of Santa Catarina, 1995.
MARTIN, J. M. et al. Friction of Hexagonal Boron Nitride in Various Environments. **Tribology Transactions**, v. 35, n. 3, p. 462–472, 1 jan. 1992.
MATWEB. **Material Property Data**. Disponível em: <http://www.matweb.com/>.
MERA, G. et al. Nanodomain Structure of Carbon-Rich Silicon Carbonitride

Polymer-Derived Ceramics. **Journal of the American Ceramic Society**, v. 93, n. 4, p. 1169–1175, 1 abr. 2010.

MOLINARI, A. et al. Low temperature ion-nitriding of Fe-Mo-C sintered steels. **J. Phys. IV France**, v. 3, n. C7, p. C7-949-C7-954, nov. 1993.

MONTGOMERY, D. C.; RUNGER, G. C. **Applied Statistics and Probability for Engineers**. 3rd. ed. [s.l.] John Wiley & Sons, Inc., 2003.

PAVANATI, H. C. et al. **Sintering carbon steel in abnormal glow discharge with simultaneous molybdenum surface enrichment**. MATERIAUX. **Anais**...Dijon: 2006

PAVANATI, H. C. et al. Ferrite stabilization induced by molybdenum enrichment in the surface of unalloyed iron sintered in an abnormal glow discharge. **Applied Surface Science**, v. 253, n. 23, p. 9105–9111, 30 set. 2007.

PEREIRA, N. C. et al. Electrochemical and microstructural studies of sintered and sintered-plasma nitrided steel containing different alloying elements. **Journal of Materials Science**, v. 30, n. 19, p. 4817–4822, 1995.

PINASCO, M. R. et al. Composition and morphology of Fe-N off-equilibrium phases in a nitrided Fe-1.5wt.%Mo sintered alloy. **Journal of Alloys and Compounds**, v. 220, n. 1–2, p. 217–224, abr. 1995.

PYE, D. **Practical Nitriding and ferritic nitrocarburizing**. Ohio: ASM International, 2003.

RICHTER, F. et al. **WO201432817 - Method for producing thermoplastic pre-ceramic polymers**WO, 2014.

RICHTER, R. et al. Organosilicon Polymers—Synthesis, Architecture, Reactivity and Applications. **Applied Organometallic Chemistry**, v. 11, n. 2, p. 71–106, 1 fev. 1997.

RIEDEL, R. et al. Silicon-Based Polymer-Derived Ceramics: Synthesis Properties and Applications-A Review. **Journal of the Ceramic Society of Japan**, v. 114, n. 1330, p. 425–444, 2006.

ROUXEL, T. Mechanical properties. In: **Polymer Derived Ceramics: From Nano-structure to Applications**. [s.l.] Destech Publishing, 2010. p. 490.

RUTZ, H. G. .; GRAHAM, A. H. .; DAVALA, A. B. . **Sinter-hardening PM steels**. International Conference on Powder Metallurgy & Particulate Materials. **Anais**...Chicago, USA: 1997

SAHA, A. et al. Characterization of Nanodomains in Polymer-Derived SiCN Ceramics Employing Multiple Techniques. **Journal of the American Ceramic Society**, v. 88, n. 1, p. 232–234, 1 jan. 2005.

SAHA, A.; RAJ, R.; WILLIAMSON, D. L. A Model for the Nanodomains in Polymer-Derived SiCO. **Journal of the American Ceramic Society**, v. 89, n. 7, p. 2188–2195, 1 jul. 2006.

SCHÜTZ, A. et al. Characterisation of novel precursor-derived ceramic coatings with glass filler particles on steel substrates. **Surface and Coatings Technology**, v. 207, p. 319–327, 25 ago. 2012.

SEIFERT, M. et al. Multiphase ceramic composites derived by reaction of Nb and SiCN precursor. **Journal of the European Ceramic Society**, v. 34, n. 8, p. 1913–1921, ago. 2014.
SEIFERT, M. et al. A novel approach to develop composite ceramics based on active filler loaded precursor employing plasma assisted pyrolysis. **Materials & Design**, v. 89, p. 893–900, 5 jan. 2016.
SIMCHI, A.; DANNINGER, H. Effects of porosity on delamination wear behaviour of sintered plain iron. **Powder Metallurgy**, v. 47, n. 1, p. 73–80, 1 jan. 2004.
SOUZA, S. A. DE. **Composição Química dos Aços**. [s.l.] Edgar Blucher, 1989.
STACHOWIAK, G. W. Solid lubrication and surface treatments. In: **Engineering Tribology**. Fourth ed. Boston: Butterworth-Heinemann, 2014.
STACHOWIAK, G. W.; BATCHELOR, A. W. Introduction. In: **Engineering Tribology**. Fourth ed. Boston: Butterworth-Heinemann, 2014. p. 1–10.
THÜMMLER, F.; OBERACKER, R. **Introduction to Powder Metallurgy**. [s.l.] Institute of Materials, 1993.
TORREY, J. D.; BORDIA, R. K. Mechanical properties of polymer-derived ceramic composite coatings on steel. **Journal of the European Ceramic Society**, v. 28, n. 1, p. 253–257, 2008a.
TORREY, J. D.; BORDIA, R. K. Processing of Polymer-Derived Ceramic Composite Coatings on Steel. **Journal of the American Ceramic Society**, v. 91, n. 1, p. 41–45, 1 jan. 2008b.
TRASS, S. et al. Structural characterisation of silicon carbonitride ceramics derived from polymeric precursors. **Journal of the European Ceramic Society**, v. 20, n. 2, p. 215–225, fev. 2000.
TRASSL, S. et al. Characterization of the Free-Carbon Phase in Si-C-N Ceramics: Part II, Comparison of Different Polysilazane Precursors. **Journal of the American Ceramic Society**, v. 85, n. 5, p. 1268–1274, 1 maio 2002.
UPADHYAYA, G. S. **Powder Metallurgy Technology**. [s.l.] Cambridge Int Science Publishing, 1997.
WACHTMAN, J. B.; HABER, R. **Ceramic films and coatings**. New Jersey: Noyes Publication, 1993.
WEINMANN, M. et al. Precursor-Derived Ceramics. In: **Handbook of Advanced Ceramics**. [s.l.] Elsevier, 2013. p. 1025–1101.
YOUSEFFI, M.; WRIGHT, C. S.; JEYACHEYA, F. M. Effect of carbon content, sintering temperature, density, and cooling rate upon properties of prealloyed Fe–1·5Mo powder. **Powder Metallurgy**, v. 43, n. 3, p. 270–274, 1 mar. 2000.
ZUM GAHR, K. H. **Microstructure and wear of materials (Tribology Series)**. Amsterdam: Elsevier Science B.V., 1987.

APPENDIX

Introduction - The Bragecrim initiative

BRAGECRIM is the acronym for the Brazilian-German collaborative research initiative in manufacturing, between CAPES and DFG, which fund and support projects in partnerships of research groups from both countries in the field of advanced manufacturing technologies. The program primary aim is to develop fundamental technological knowledge for innovative solutions to improve productivity, quality and sustainability of industrial companies from Brazil and Germany (CAPES, 2008). The exchange of knowledge is another important objective from the initiative, through work and study missions of students, researchers and professors, as schematically presented in Figure 70 and understood as a powerful mean. Over 300 researchers from numerous universities and research organizations, have been investigating key issues affecting all stages of the production cycle within its framework, which comprises materials science, industrial engineering, metrology and logistics (DFG, 2015).

Figure 70: Bragecrim participating research institutions in 2015.

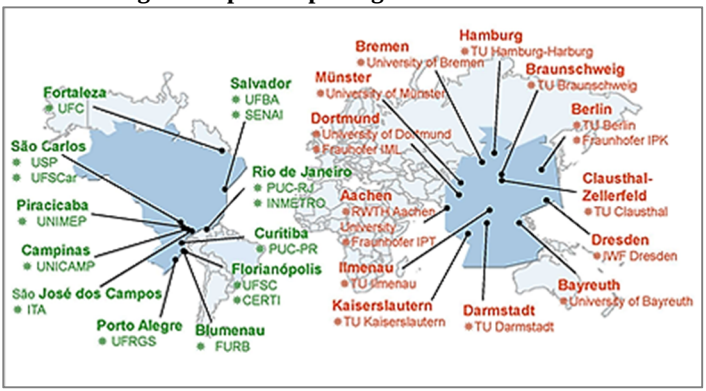

Source:(DFG, 2015)

Results and discussion – Coatings and interfaces after pyrolysis

Comparative elemental maps of coatings and interfaces after pyrolysis are presented from Figure 71 to 73 (SEM-20kV-15-16mmWD-SE).

Figure 71: Color mapping of all elements on composite S-79.

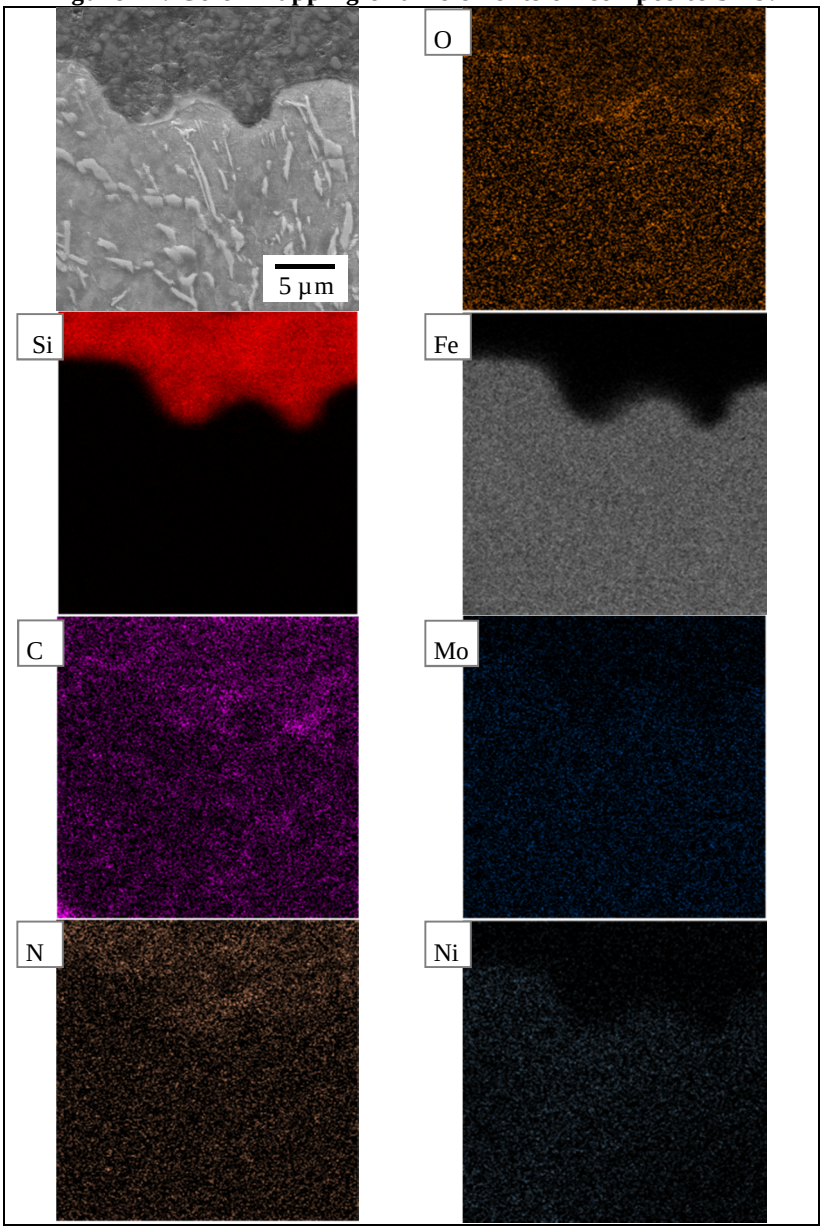

Source: Own authorship

Figure 72: Comparative of some elements on composites SN-79 and SEN-79.

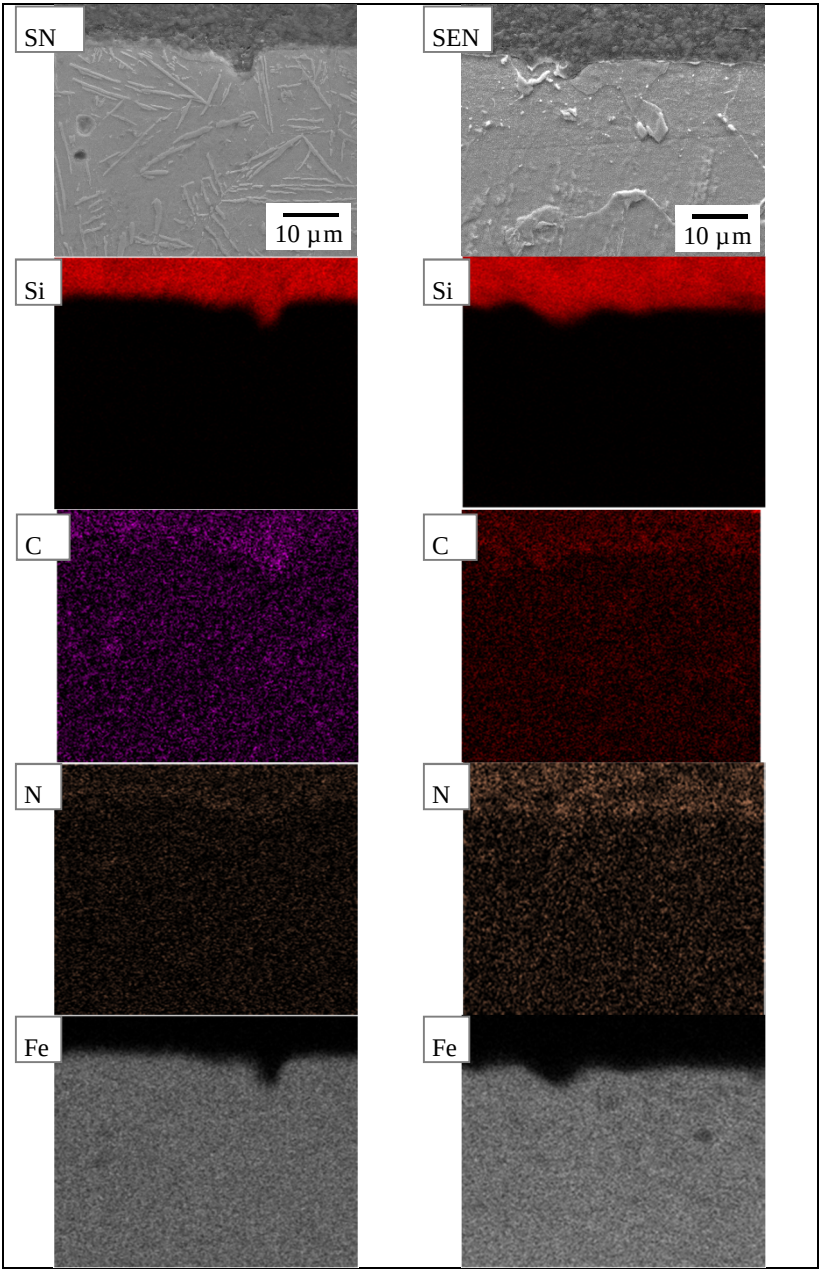

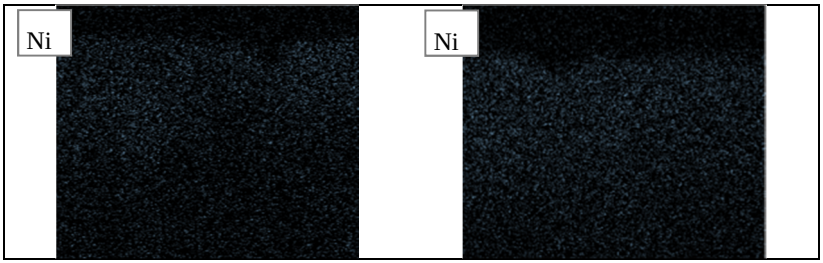

Source: Own authorship

Figure 73: Mo and O distribution on SN-79 and SEN-79 samples.

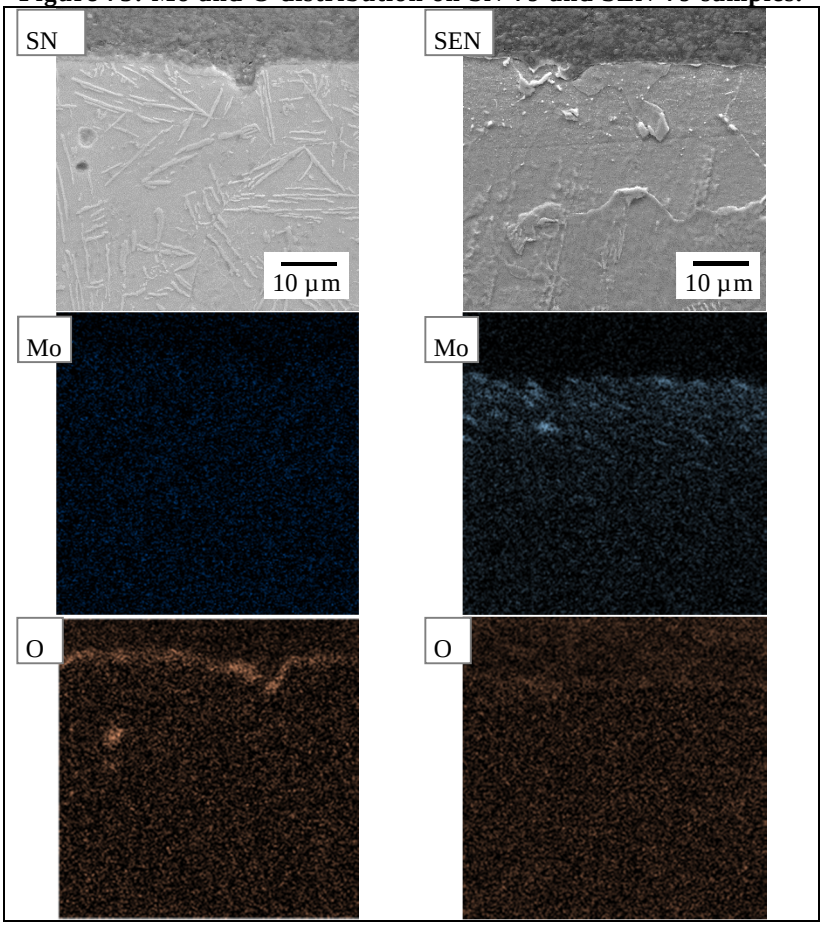

Source: Own authorship

Results and discussion – Wear tracks

The typical aspect of composites, observed under SEM, after the tribological sliding tests is presented in Figure 74.

Figure 74: Wear track comparison of coated samples, as function of filler amount and interface (SEM-15kV-12-21mmWD-SE).

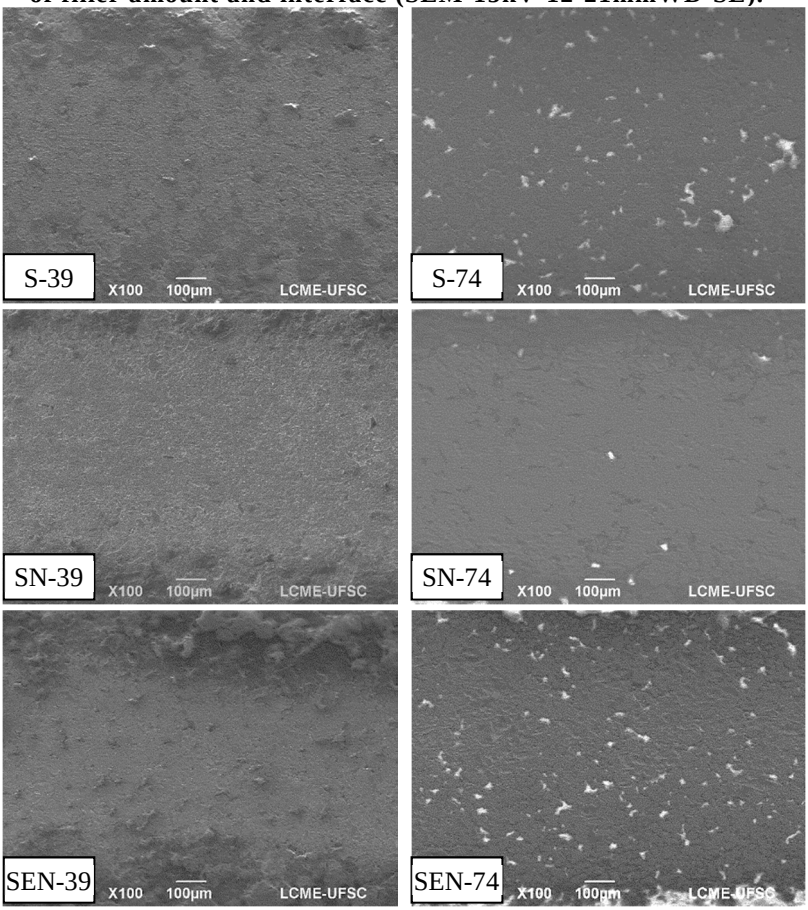

Source: Own authorship

Results and discussion – Wear tracks – elemental analysis

The chemical analyses carried on characteristic regions, using a 15kV voltage, observed in wear tracks, named A, B C and D and discussed in section 4.4.7.1, are presented in Tables 8 to 11. The EDS analyses were carried, among others, in the regions presented in Figures 66 and 67.

Table 8: Region A, in wear tracks of coated and uncoated samples.

Region A	Mass percentage					
Composite	Fe	Ni	Mo	Si	C	O
Sintered steelt	79,7	2,6	1,5	0,3	12,7	3,2
S-39	66,6	6,3	1,7	4,4	9,5	11,5
	88,5	2,4	1,7	0,4	5,9	1,1
S-74	80,7	3,6	1,2	0,5	8,8	5,2
	84,1	5,2	1,3	0,4	1,6	7,4
SN-39	89,1	-	1,4	0,6	6,5	2,4
	89,2	-	1,0	0,6	6,7	2,5
SN-74	84,0	3,3	1,3	0,5	6,0	4,9
	90,8	-	1,7	0,6	6,1	0,8
SEN-39	86,4	3,0	2,9	0,5	4,9	2,3
SEN-74	88,3	3,9	-	0,7	5,2	1,9

Source: Own authorship

Table 9: Region B, also common in wear tracks of coated and uncoated samples.

Region B	Mass percentage						
Composite	Fe	Ni	Cr	Mo	Si	C	O
Sintered steel	57,1	1,1	0,4	-	0,2	7,0	34,2
S-39	61,6	-	-	-	1,2	5,7	31,5
	59,6	-	0,7	-	1,5	9,1	29,1
S-74	47,5	-	0,8	-	1,5	16,8	33,4
	62,2	-	-	0,9	1,1	6,4	29,4
SN-39	76,9	3,9	-	1,3	0,6	7,5	9,8
	60,2	-	0,8	-	0,7	8,8	29,5
SN-74	64,2	1,6	-	-	1,1	5,6	27,5
	60,0	-	0,8	-	3,5	10,8	24,9
SEN-39	70,3	-	-	5,2	0,6	7,0	16,9
	79,3	5,6	-	1,8	0,4	8,4	4,5
SEN-74	67,3	2,7	-	3,8	0,8	8,6	16,8

	55,5	-	0,8	1,3	0,8	7,5	34,1

Source: Own authorship

Table 10: Region C, present only in wear tracks of coated samples.

Region C	Mass percentage							
Composite	Fe	Si	C	O	N	B	Zr	Al
S-39	2,3	33,5	13,7	23,9	26,6	-	-	-
	1,8	24,9	15,4	13,5	21,8	21,1	1,1	0,4
S-74	1,5	33,9	17,9	13,4	30,0	-	2,9	0,4
	1,7	35,9	9,7	12,4	29,2	7,8	2,4	0,9
SN-39	1,5	34,5	18,4	18,1	25,8	-	1,4	0,3
	1,4	27,6	19,6	23,5	24,6	-	3,3	-
SN-74	-	40,5	13,3	10,9	31,5	-	3,4	0,4
	15,2	25,9	13,9	19,7	23,0	-	2,0	0,3
SEN-39	1,9	35,7	21,5	22,7	18,2	-	-	-
	2,2	30,8	18,5	22,0	24,3	-	1,2	1,0
SEN-74	1,4	24,0	13,3	9,2	30,0	20,5	1,4	0,2
	1,2	30,0	23,0	18,9	25,8	-	0,8	0,3

Source: Own authorship

Table 11: Region D, only present in wear tracks of composites with enriched and nitrided interface (SEN).

Region D	Mass percentage					
Composite	Fe	Ni	Mo	Si	C	O
SEN-39	29,5	-	49,4	2,7	12,9	5,5
	32,2		51,5	1,7	14,6	-
SEN-74	34,6	2,3	47,3	1,0	14,8	-
	34,3	-	42,0	2,0	11,0	10,7

Source: Own authorship